Effects of Variable Energy Delivery on

Leukocyte Kinetics and Wound Healing

BY

ANDRE DANIEL PAREDES
B.S., University of California, Irvine, 2010

THESIS

Submitted as partial fulfillment of the requirements
for the degree of Doctor of Philosophy in Bioengineering
in the Graduate College of the
University of Illinois at Chicago, 2018

Chicago, Illinois

Defense Committee:

Amelia Bartholomew, Chair and Advisor
Jun Cheng
David T. Eddington
Timothy J. Koh, Kinesiology and Nutrition
Steve Mangos, Rush University

My thesis is dedicated to my grandparents Maria Cristina Olguin and Epifanio Diaz, my grandparents Maria De Jesus Fulgencio Paredes and Jose Baltazar Fulgencio, my parents Raul Paredes and Adriana Paredes, my Uncle Jesse Diaz, my Aunt Trish Diaz, and my beautiful wife Shandi Paredes, for their unconditional support and love.

ACKNOWLEDGEMENTS

First and foremost, I would like to express my sincere gratitude to my chair, advisor, and role model Dr. Amelia Bartholomew. Your work ethic, sincerity, kindness, generosity, and vision has truly been an inspiration to witness and learn from throughout my studies. You always go above and beyond what is asked of you and this thesis would not be possible without your unwavering guidance and dedication to my wellbeing and success. You are an incredible mentor, and a Godly individual, thank you.

I am also very grateful to my other incredible mentors Dr. Jun Cheng, Dr. Timothy Koh, and Dr. Steve Mangos for their patience and knowledgeable guidance. My projects would have been impossible without their belief in my abilities and extraordinarily generous allocation of time, knowledge, and resources. Their advisement allowed me to enhance my research critical thinking skills. I could not have asked for better individuals to serve as research collaborators and mentors, thank you.

I am also very grateful to Dr. David Eddington, it is an honor to have you on my committee. As well as to Susan Lee, Jessica Terrones, and Lukasz Zientara and the entire Richard and Loan Hill Department of Bioengineering for their kindness and assistance throughout my studies, thank you.

A very special thank you to Dr. William Ennis, Dr. Peter Bajcsy, and Dr. Lunaire Ford, for their generous allocation of time and knowledge. You each grew my level of understanding on various areas of expertise and helped to me to seek out other areas of investigations, thank you.

A very special thank you to my colleges and friends, Dr. Zhinan Wang, Dr. Chi Bang, Dr. Anthony Felder, Dr. Tung Hoang, and Ms. Rachana Patil, for their friendly and knowledgeable

assistance throughout my studies. Also, a very special thank you to my mentee and now colleague, Mr. David Benavidez. His dedication, grit, and countless hours of hard work on projects helped to revitalize my research spirit within the long stretches of experimentation and foreshadowing uncertainties. I am grateful to you all for your friendship and help, thank you.

Last, I would like to extend a heartfelt thank you to the higher education channels that have helped to place me in this position of success. This includes, but is not limited to, the California Minority Participation Program, Project 1000, Society of Advancement of Chicano Latino and Native American Society, Diversifying Higher Education Faculty in Illinois Program, and the International Center of Processional Development Program, thank you.

Contribution of Authors

Chapter 1 and Chapter 2 is a background of relevant studies in the context of the field and highlights the significance of my thesis. Chapter 3 and Chapter 4 represent unpublished manuscripts for which I am the primary author. David Benavidez assisted me in zebrafish experiments. Dr. Steve Mangos assisted me in zebrafish handling, approaches, and methodologies. Dr. Jun Cheng assisted me in research design of quantitative measures. My research mentor, Dr. Amelia Bartholomew contributed to the research design and refinement of both manuscripts. Chapter 5 is an interpretation of future directions and overarching conclusions of my thesis.

TABLE OF CONTENTS

CHAPTER PAGE

LIST OF TABLES

LIST OF FIGURES

FIGURE PAGE

LIST OF FIGURES (continued)

FIGURE PAGE

LIST OF ABBREVIATIONS

3D+t	three-dimensional time-lapse imaging
ATP	adenosine-triphosphate
CTF	corrected total fluorescence
CW	continuous wave
DICE	dice similarity coefficient
DHE	dihydroethidium
dpf	days post-fertilization
FOV	field of view
H_2O_2	hydrogen peroxide
IntDen	integrated density
LLLT	low level light therapy
MMP	mitochondrial membrane potential
mpeg	macrophage expressed gene
MPI	minutes post injury;
Mϕ	macrophage
NADPH	nicotinamide adenine dinucleotide phosphate
NOX	NADPH oxidase
n.s.	not significant;
$O_2^{-\cdot}$	super oxide anion
PBM	photobiomodulation
PBMT	photobiomodulation therapy
PMN	polymorphonuclear leukocytes
ROI	region of interest
ROS	reactive oxygen species
Tg	transgenic
Zirmi	**z**ebrafish **i**nflammatory **r**eactive oxygen species- and **m**acrophage kinetics- based **i**mage analysis

SUMMARY

Annually in the United States, wound and wound related complications affect millions of people and cost the healthcare system in the tens of billions of dollars. As such, chronic inflammatory wounds are a significant healthcare problem and new forms of therapy are highly sought after. Photobiomodulation therapy (PBMT) as an energy-based modality presents as an emerging paradigm-shifting approach for its clear cost, safety, and implementation advantages. Also, PBMT has been numerously reported to reduce tissue inflammation and accelerate wound closure. However, the varied responses of macrophages to oxidative stress in inflammatory diseases underscores a need to better understand how microenvironment level changes can enhance or impair wound responses. Unfortunately, precise energy parameters have not been established to optimize effects in macrophage kinetics and function within the wound tissue microenvironment**.**

To meet this need, implementation of *in vivo* model strategies capable of observing molecular real-time changes within microenvironments after variable energy treatments is required. Recently, zebrafish animal reporter-based assays have grown their feasibility to characterize inflammatory cell migration and responses to biochemical cues, such as, reactive oxygen species. Unfortunately, acquiring quantitative measures of macrophage behavior in response to oxidative stress using real-time imaging is currently beyond the scope of commercially available software solutions. This thesis describes a novel image analysis pipeline method to interrogate zebrafish wound macrophage recruitment and oxidative stress, to evaluate quantitative dose effects of PBMT on a microenvironment level.

In Chapter 1, an introduction to the scope of robust and impaired healing both in its normative and perturbed molecular conditions are presented. This in addition to a background

of current wound care interventions are acknowledged and serve as a motivation of investigating energy-based modalities of therapy.

Chapter 2 provides a framework of current published photobiomodulated cellular inflammatory and kinetic responses. This includes the concept of variable energy treatments, such as, energy fluences in PBMT and its need for a more standardized approach.

In Chapter 3, an image analysis pipeline solution is described to provide real time quantitative measures of cellular kinetics and reactive oxygen species tissue content after tissue injury. This approach, termed *Zirmi*, differs from current software solutions that may only provide qualitative, single image analysis, or cell tracking solutions. This approach demonstrated standardized space- and time-based quantitative measures of (1) fluorescent probe based oxidative stress and (2) macrophage recruitment kinetic based changes after tissue injury. The implementation of *Zirmi* image analysis pipeline performed at execution speeds as high as 10-fold faster than manual image-based approaches. Automated segmentation methods were comparable to manual methods with a DICE Similarity coefficient > 0.70.

Chapter 4 describes the effects of a dose range of fluences delivered by a HeNe laser on individual macrophage kinetics, tissue oxidative stress, and wound closure using *Zirmi*. Results showed macrophage activity could be manipulated by applied energy fluence leading to reduced levels of wound reactive oxygen species and accelerated wound closure. Particularly, this demonstrated that the zebrafish model provides a means to quantitatively compare wound macrophage behavior in response to a variety of laser treatment parameters in real time.

Future directions outlining the potential of the *in vivo* test system developed and its potential utility to the scientific community are presented in Chapter 5.

CHAPTER 1

1. INTRODUCTION

1.1. Wound Care Problem

Approximately 1-2% of the United States population will develop a chronic wound in their lifetime, designating wound care as a significant public health problem and a growing economic burden, particularly for the elderly (Gould et al. 2015). For patients covered by Medicare, a 2014 analysis reported 15% (8.2 million) experienced a wound complication with costs estimated to range from $28.1 to $96.8 billion (Nussbaum et al. 2018). Strategies aimed at accelerating wound care have targeted the alteration of the microenvironment through cytokines, growth factors, artificial scaffolds, and biologics such as stem cells or skin substitutes. However, these strategies have not demonstrated durability in solving the problem, particularly in diabetics who suffer with high rates of wound complications (Nussbaum et al. 2018). Tissue repair is a multistep process and manually orchestrating complicated modes of regulation of various cell types has proven to have limited success (Enoch, Grey, and Harding 2006). New, more cost-effective treatments are needed.

1.2. Tissue Injury, Inflammation, and Inflammatory Leucocytes

Tissue injury evokes a sequence of phases in the human body to sterilize the site of injury and reconstitute tissue and tensile strength. Once a wound is inflicted, the body, regardless of the etiology, coordinates a molecular response to enter hemostasis initiating the stages of healing: inflammation, proliferation, and remodeling (Deodhar and Rana 1997).

Following tissue injury, a complex orchestration of events is directed towards achieving hemostasis and recruiting immune cells such as macrophages and neutrophils to the site for their anti-microbial and pro-regenerative influences (**Figure 1**). As a first step, vessel injury leads to

exposed collagen, thrombin production, and coagulation to promote hemostasis and restore blood flow to the area (Minors 2007, Rong et al. 2005). Endothelial and platelet released chemical cues result in platelet activation and subsequent aggregation at the injured vessel site (Herbaczynska-Cedro, Lembowicz, and Pytel 1991). Activated platelets also produce growth factors, including transforming growth factor-β and platelet-derived growth factors, to induce vessel repair (Rajkumar et al. 2006). Fibroblasts, which participate in adventitial repair of the vessel as well, can release of reactive oxygen species, ROS, (Ardanaz and Pagano 2006) to facilitate gene expression for inflammatory cytokines, such as, interleukin-1, and downstream promotion of immune cell recruitment and activation (Siegbahn and Hammacher 1990, Wahl et al. 1987).

ROS release serves to recruit neutrophils and macrophages to the site; increased vascular permeability locally as well as other factors aid in recruitment of these cells to the wound (Scheiermann, Kunisaki, and Frenette 2013). Molecular signals are recognized by pattern recognition receptors (PRR), dependent on the etiology of tissue injury, to facilitate damage or microbial pathogen associated, DAMP or PAMP, signals to recruit leukocytes (McDonald, Pittman, Menezes, Hirota, et al. 2010, Zhang et al. 2010, Land 2015). Initially, following tissue damage ROS secreted by NADPHD oxidase (Liu et al. 2004) and dual oxidase (DUOX) can serve as a chemokine (Niethammer, Grabher, Look, and Nature 2009), a small type of cytokine. ROS, along with growth factors (Wahl et al. 1987), cAMP (Harvath, Robbins, and Russell 1991), ATP (Honda et al. 2001b) and other chemokines, are generated at optimal levels to attract leukocytes to the site of injury. In excess however, ROS can also serve as an inflammatory agent (Rajagopalan et al. 1996), along with interleukins (Baggiolini and Clark-Lewis 1992, O'Neill

and Dinarello 2000) , tumor necrosis factor (Beutler et al. 1985), matrix metalloproteinases (Thompson et al. 1995), colony stimulating factor (Inaba et al. 1992). Superoxide anion for instance, is produced endogenously throughout the adventitia, interfering with nitric oxide ability to vasodilate and progress the phases of healing accordingly (Di Wang et al. 1998). To reach tissue homeostasis, reactive oxygen species are primarily controlled by recruited leukocytes, used cyclically condone cell functional inflammatory behaviors as needed (Tarlowe et al. 2003). Therefore, ROS is an important molecular pattern, and if unregulated by leukocytes, will lead to slow and unyielding inflammatory responses (Lavine et al. 1979, Boring et al. 1997).

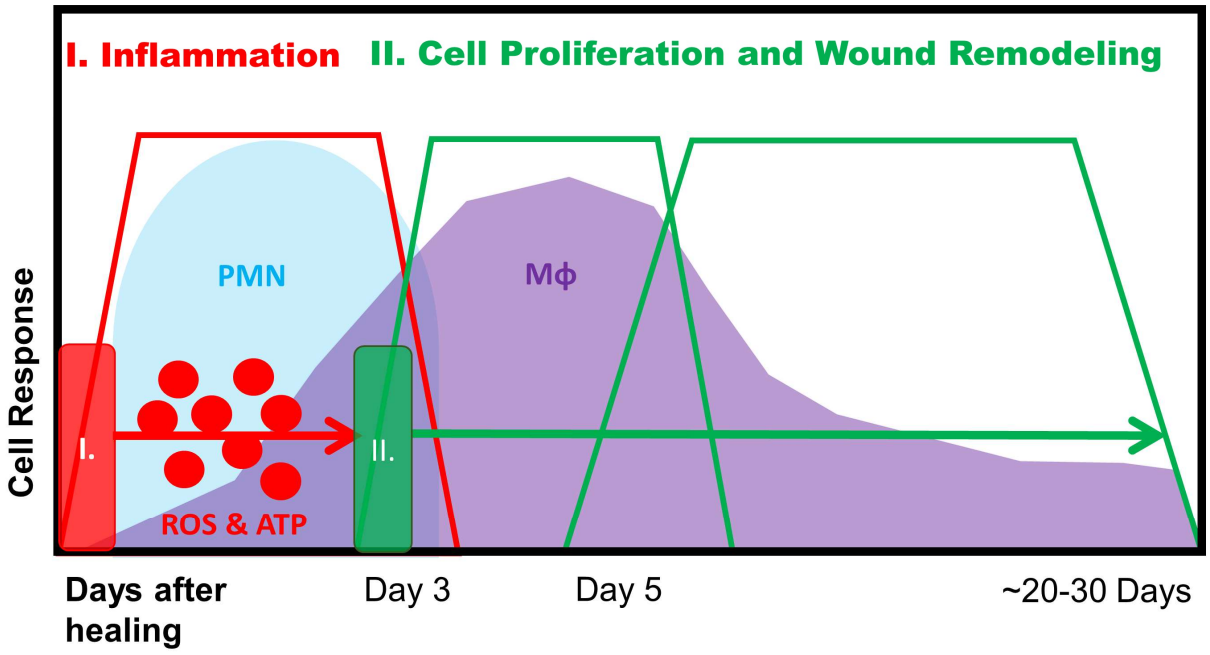

Figure 1. Robust human wound healing undergoes (I) inflammation to (II) regeneration. Within the first few days neutrophils (PMN) are the first to be recruited, primarily present throughout inflammation. Macrophages (Mϕ) recruit at a slower pace but are present throughout all phases of healing. ROS and ATP are important cytokines that affect inflammation and when balanced correctly promote an acute inflammation transition to cell proliferation and wound remodeling.

The recruitment of leukocytes, neutrophils and macrophages, commence an important protection inherent to inflammation, preventing infection (Artis et al. 2000, Roach et al. 2002, Nieminen et al. 2008, McDonald, Pittman, Menezes, and Hirota 2010). Inflammatory neutrophils and macrophages participate in cooperative defense strategies for the elimination of pathogenic and deleterious infiltrates responsible for infection (Silva, Silva, and Appelberg 1989, Novais, Santiago, and Báfica 2009). Neutrophils, as the first line of dense, arrive relatively quickly, engulfing surface labeled microbes (Colucci-Guyon et al. 2011) and sterilizing wound through respiratory bursts or degranulation, a process which involves the release of reactive oxygen species into the tissues (Rothe and Valet 1990). However, neutrophils, the most circulating leukocyte, in large quantities contributes to the slew of inflammatory buildup. The anti-microbial effects of degranulation via superoxide and hydrogen peroxide species, while desirable, can also cause damage to surrounding tissue, inducing cell death by increasing pH (Segal et al. 1981) and oxidative stress (Lamy, Mathy-Hartert, and Deby-Dupont 1996). Additionally, neutrophils undergo apoptosis following engulfment of bacteria (Kobayashi, Voyich, and Whitney 2005), further releasing intracellular contents to further progress inflammation (Grigg et al. 1991). Such debris requires clearance before the tissue injury can heal; macrophages play an important role in this clearance.

1.3. Macrophages

Macrophages follow neutrophils recruitment. Macrophages are present in all phases of healing, and play an important role regulating both inflammatory and regenerative processes (Lucas, Waisman, Ranjan, Roes, Krieg, Müller, et al. 2010). They phagocytose cellular and bacterial debris, and secrete cytokines, chemokines, and matrix proteins involved in heightening or resolving inflammatory responses.

1.3.1. Macrophage Responses to Bacteria, Necrotic and Apoptotic Cellular Debris

Inflammatory macrophages work as professional phagocytes and have a large capacity to engulf and internalize debris, cells, and microbes such as pathogens and bacteria (Flannagan, Cosío, and Grinstein 2009). Following phagocytosis, macrophages kill pathogens, microbial clearance, by the production of superoxide anions (Sasada and Johnston 1980). At the wound site, gamma interferon (Beutler et al. 1986), and endotoxins , such as, lipopolysaccharide (Doe and Henson 1978) of the bacteria cell wall, greatly stimulate macrophage pathways to increase superoxide anion production for the purpose of microbial clearance.

Internalization of necrotic cell debris also plays a role in activating macrophages. Necrotic cell debris facilitate inflammatory macrophages activation via high mobility group 1 proteins, a late mediator of endotoxin lethality, promoting macrophage recruitment and phagocytosis (Cohen et al. 2010). Further, cellular necrosis released intracellular contents promotes toll-like receptor signaling in a comparable manner to damage associated molecular patterns and lipopolysaccharide, stimulating macrophage proinflammatory responses (Andersson et al. 2000). To additionally bolster macrophage microbial clearance, macrophages engulf residual granules of reactive oxygen species left by neutrophils. Internalization of neutrophil granules play an important role in enhancing macrophage oxidative metabolism, aiding them with ROS needed to destroy microbes (Silva, Silva, and Appelberg 1989, Tan et al. 2006). Consequently, internalization of these reactive oxygen species play an important role clearing excessive oxygen species setting the stage for regeneration (Vincent et al. 2017, Novais, Santiago, and Báfica 2009).

Macrophages are also signaled by neutrophil apoptotic cell debris to aid in regeneration by a process termed efferocytosis (Kobayashi, Voyich, and Whitney 2005). Neutrophil apoptotic debris, different from necrotic cell debris, maintain high mobility group 1 firmly bound to chromatin in apoptosis (Scaffidi, Misteli, and Bianchi 2002). This apoptosis is an intrinsic process regulated within the cell by BCL2 family proteins, such as MCL-1, (Kato et al. 2006), and Src homology 2 domain-containing 5'-phosphatase (Gardai et al. 2002). Released by permeabilized cells and apoptotic neutrophils, ATP, metabolites, and other types of "eat me" signals then direct macrophages for their internalization (Nunn et al. 1996). These signals then interact with several macrophage receptors, including phosphatidylserine, complement receptor, lectins, and cluster differentiation proteins to promote macrophage recruitment (Kennedy and research 2009) and alternative activation (Lumbroso et al. 2018). Alternatively activated macrophage, via engulfment of neutrophil apoptotic intracellular materials, have been demonstrated to (1) stunt inflammatory cytokine production of interleukins, such as, colony-stimulating factor and necrosis factor, and (2) promote production of pro-healing cytokines, such as, transforming growth factor, prostaglandin and platelet-activating factor geared toward inflammatory resolution (Fadok et al. 1998). Therefore, macrophage internalization of apoptosis contribute to the alternative activation of macrophages to circumvent cyclic inflammatory tissue damage and promote tissue regeneration (Wyllie, Kerr, and Currie 1980).

Alternative macrophages timely presence are important to promote angiogenesis, collagen deposition, and wound closure (Lucas, Waisman, Ranjan, Roes, Krieg, Muller, et al. 2010). Once alternatively activated, macrophages secrete factors in the forms of proteins, growth factors, and other cytokines critical to the progression of successful tissue repair

(Mandrekar-Colucci, Karlo, and Landreth 2012). However, alternatively activated macrophage and their pivotal role in healing is not investigated in this thesis.

1.3.2. Macrophage Metabolism and Energy Demands in Normal and Abnormal Healing

Aberrant metabolism can either immunosuppress or immunoactivate to modify the susceptibility of infection or inflammatory disease (Wellen and Hotamisligil 2005). Therefore, an energy homeostasis is important for the immune response pathways to prevent inflammatory diseases, commonly associated with metabolic disorders. As a result there is growing body of evidence that demonstrates metabolic dysfunction and chronic inflammation go hand in hand (Hotamisligil 2006).

In the activated state macrophages undergo a metabolic switch, from oxidative phosphorylation to glycolysis, decreasing oxygen consumption (Keuper et al. 2017). It has been proposed that macrophage activation and corresponding increase in glycolysis could be a mechanism to rapidly generate ATP (Nascimento et al. 2005). More efficient than the tricarboxylic acid cycle in ATP generation, glycolysis can be induced quickly, enabling synthesis of ATP in response to the high demand required for increases in production of purines and pyrimidines required in biosynthesis (Vazquez et al. 2010). Activated macrophages also produce increased amounts of mitochondrial reactive oxygen species which can be used to enhance bactericidal activities (West et al. 2011). A switch to glycolytic ATP production may be a critical component for the production of reactive oxygen species production in the wound (Palsson-McDermott and O'neill 2013). Therefore, macrophages demonstrate an overarching ability to govern proliferative tasks and when dysregulated exacerbate inflammatory wound conditions (Mirza and Koh 2011). Elevated macrophage activity can accelerate wound healing responses before and after inflammation. It has classically been outlined that ROS secretion is

proportional to phagocytosis activity via NADPH oxidase. Therefore, ROS levels can be indicative of macrophage phagocytosis, inferring greater antimicrobial and antibacterial activity with an ROS increase.

1.4. Prolonged Inflammatory Responses Contribute to Impaired Wound Healing

Macrophages clearance of neutrophils is key to the resolution of acute inflammation. Neutrophil longevity is influenced by microbial induction of inflammatory cytokines, including interleukins, tumor necrotic factors, gamma interferon, colony stimulation (Colotta et al. 1992). Prolonged microbial activities can affect neutrophil mitochondrial membrane potential. This activity has been demonstrated to significantly reduce caspase-3 and capaspase-9, affecting cytokines ability to promote neutrophil longevity, stunt neutrophil apoptosis, and cycle more inflammatory behaviors (Colotta et al. 1992, Taneja et al. 2004). As a result, a dense cellular infiltrate consisting of neutrophils, macrophages, necrotic debris, and other inflammatory agents impair the site of injury, delaying healing (Khanna et al. 2010, Mirza and Koh 2011, Mittal et al. 2005, Henry and Martine 2002). Additionally, leukocytes saturate wound sites, excessive free radicals saturate the wound increasing wound oxidative stress (Jx and Nj 2014, Sen 2009, Niethammer 2016, Ushio-Fukai 2009). Therefore failure to phagocytose neutrophils in a timely manner is demonstrated to increase the longevity of neutrophils and prevent macrophage alternative activation, delaying healing and prolonging inflammation (Meszaros, Reichner, and Albina 1999).

1.4.1. The Influence of Reactive Oxygen Species on Macrophages

Redox based signaling at the site of injury plays a critical role in the progression of tissue repair (Henry, Matilde, and Fulvio 2010). As previously mentioned, tissue damage activates NOX and DUOX to generate ROS generated gradients. Next, ROS participates in a spatial-

temporal distribution to facilitate critical acute inflammatory cellular processes, such as apoptosis and recruitment (Jiang, Zhang, and Dusting 2011). To induce apoptosis, generated peroxides oxidize MAP kinase phosphatases to sustain JNK activity, well characterized in the early steps of regeneration (Ishida et al. 2010). This induction of redox based apoptosis is linked to enhancing tissue regeneration, as inhibited NOX generated ROS is shown to impair tissue apoptosis and subsequent tissue regeneration (Gauron et al. 2013). Additionally, NOX generated ROS are characterized to oxidize tyrosine kinase, Lyn, enhancing apoptosis in neutrophils (Gardai et al. 2002), thus influencing macrophage efferocytosis geared regenerative outcomes. To induce leukocyte recruitment, DUOX generated ROS have been described as forming a chemoattractant gradient (Niethammer, Grabher, Look, and Mitchison 2009). More precisely, peroxides oxidize tyrosine kinase redox sensor, Lyn, to mediate oriented leukocyte recruitment to the inflammatory foci (Yoo et al. 2011). However, acute inflammatory redox based signaling is dependent on optimal ROS threshold levels; ROS is deleterious in excess.

Excess ROS, can impair macrophages, delaying the initiation of tissue repair and regeneration. In acute inflammation, the accumulating effect of nearby cell lysing, neutrophil respiratory burst, and inflammatory macrophage activation results in increased oxygen consumption through oxidases activation. Increased oxygen consumption is linked to elevated levels of reactive oxygen species, ROS, superoxide anion ($O_2^{-\cdot}$) and H_2O_2 (Lambeth, Kawahara, and Diebold 2007). Generated ROS, in turn, supports macrophage survival and promotes the phagocytosis of short-lived, neutrophils cells (Wang et al. 2007, Brown et al. 2003), initiating a necessary microenvironment for tissue regeneration (Mirza and Koh 2011). However, in surplus, an insurmountable accumulation of necrotic debris and ROS can stagnate macrophages from phenotype switching to more regenerative alternative activations (Zhang et al.

2013). Studies now link excessive ROS based inflammatory macrophage activation to mitochondrial dysfunction (Bossche et al. 2016). These macrophages are then inhibited from their alternative abilities to dampen inflammation and promote tissue repair (Kelly and O'Neill 2015). Further, macrophage mitochondrial dysfunction is linked to NLRP3 inflammasome pathway activity, responsible for triggering pro-inflammatory responses (Zhou et al. 2010). Interesting, however, studies also show alterations to microenvironment ROS production via inducible nitric oxide synthase (iNOS), promoting alternative macrophage activation and mitochondrial respiration (Bossche et al. 2016). These representative studies demonstrate the orders of magnitude by which ROS directly and indirectly impacts the recruitment, activation, and enhancement of macrophages.

1.4.2. Impaired Wound Healing and the Dysfunctional or Absent Macrophage

The speed of wound healing is influenced by the timely presence and function of available macrophages (Ross and Odland 1968). Macrophages represent only 3% of circulating leukocytes, responsible for the clearance of residual inflammatory agents in the form of microbes, reactive oxygen species, and even neutrophils (Wetzler et al. 2000). A study examined the temporal effects of conditional macrophage depletion in mice throughout tissue repair (Lucas, Waisman, Ranjan, Roes, Krieg, Muller, et al. 2010). The study demonstrated inflammatory phase-based macrophage depletion significantly reduced granulation tissue and impaired epithelization; mid tissue repair macrophage depletion significantly increased susceptibility to hemorrhage in wound tissue; and tissue maturation phase macrophage depletion did not provide significant differences when compared to controls. Additional macrophage ablation studies corroborate macrophage stage-dependent effects. Petrie *et al.* demonstrated macrophage ablation eliminated bony-ray patterns in zebrafish following fin amputation (Petrie

et al. 2014). Mirza, DiPietro, and Koh. demonstrated eradicated macrophages reduce collagen deposition, impair angiogenesis, and overall decrease wound cell proliferation (Mirza, DiPietro, and Koh 2009). They also demonstrated an increase in proinflammatory tumor necrosis factor at the site of injury contributing to impaired healing.

Further studies correlate macrophage dysfunction to impaired healing. Studies have demonstrated isolated macrophages from diabetic mice chronic wounds to be impaired, linked to dysfunctional efferocytosis and increases in wound tissue inflammation (Khanna et al. 2010, Mirza and Koh 2011). Impaired effects were significantly associated with increases in pro-inflammatory cytokines and decreases in anti-inflammatory cytokines that could be reversed if macrophages were enabled to perform successful efferocytosis. Khanna *et al.* also found that macrophages in diabetic mice demonstrated a significant impairment in the ability to engulf apoptotic matter, ultimately contributing to elevated inflammatory wound microenvironments. Rosowski *et al.* demonstrated that in wounds with Rac2-/- macrophages, defective in basic motility to mobilize to wound regions, demonstrated a higher susceptibility to infection (Rosowski et al. 2016a). Mirza and Koh. provided evidence that wound macrophages of diabetic mice impaired activation, from pro-inflammatory to pro-healing phenotype, contributed to a pro-inflammatory wound microenvironment resembling that of a chronic wound (Mirza and Koh 2011). Results further demonstrated granulation thickness, wound closure percentage, collagen deposition vary significantly when phenotypes of macrophages are dysregulated. Additional studies have corroborated this principle linking macrophage dysregulation to elevated inflammatory expression at the wound region including interleukin-1β, matrix metalloproteases-9, Tumor necrosis factor-α, reactive oxygen species , and a dense deposit of neutrophils and cell debris prevalent in chronic wounds (Goren et al. 2009). Studies also report a correlation

between macrophage dysregulation and pulmonary carcinoma, atherosclerosis, periodontitis, chronic wounds, and other inflammatory driven diseases (Hoeksema, Stöger, and de Winther 2012, Murray and Wynn 2011, Quatromoni and Eruslanov 2012, Khanna et al. 2010). Therefore, eradication of macrophages, and dysfunctional macrophages all contribute to wounds with poorly equipped regenerative capacities.

Unfortunately, no current avenue exists for accelerating the capacity of macrophages, ensuring wound homeostasis and timely transition from inflammation to regeneration. However, metabolic dysfunction can be recovered to improve regenerative outcomes (Furukawa et al. 2017, Varga et al. 2017, Cherry and Piantadosi 2015, He et al. 2017, Hotamisligil 2006, Szeto et al. 2011). Vital to a robust scalable response in tissue repair are macrophages cellular kinetics to mobilize for featured behaviors. If the metabolic capacity of a microenvironment could be supplemented, vital governing control centers, such as macrophages, could accelerate functions to supplement the metabolic needs of regeneration.

1.5. Wound Care Interventions

1.5.1. Primary Wound Care Interventions and Skin Substitutes

Wound dressings have been applied to aid in healing and inhibit bacterial infection. Advanced forms of dressing, extend beyond providing homeostatic temperature, moist environment, and neutral pH levels (Boateng et al. 2008). Recent strategies in wound dressings focus on various synthetic polymers and target enhancements in (Dhivya, Padma, and Santhini 2015):

(1) leukocyte recruitment and support of regenerative functions
(2) epidermal migration
(3) development of granulation tissue
(4) protection against bacterial infections.

Semi permeable films, such as nylon, provide autolytic debridement while providing protection from bacteria (Moshakis et al. 1984). As such these semi permeable films are limited to epithelializing shallow wounds with low exudates. Alternatively, hydrogels provide high water content to facilitate cellular recruitment and movement to sites of injury (Jones and Vaughan 2005). Alginate dressings, a common derived biodegradable hydrogel, is reported to control microbial infection. Specifically, alginate dressings can promote macrophage activation, leading to the production of inflammatory signals, such as tumor necrotic factor (Thomas, Harding, and Moore 2000). These solutions, including other dressings such as hydrocolloid dressings, foam dressings, bioactive dressings, impregnated dressings in addition to topical agents and new and improved versions, flood the market diluting the wound care strategies (Avishai, Yeghiazaryan, and Golubnitschaja 2017).

Tissue engineered skin substitutes are naturally occurring or synthesized polymer matrixes composites designed to bypass energy requirements (Enoch, Grey, and Harding 2006). Most commonly, *in vitro* engineered skin substitutes, are employed for supplementing an injury with cells or vascularization at a greater rate than could be provided by host tissue (Black et al. 1998). New stem cell and growth factor embedded directions (Liu et al. 2008), and composite tissue transplant developments (Ameer, Mahmood, and Langer 2002) have elevated the potential of tissue engineered skin substitutes. However, skin substitutes are inherently derived from biological materials requiring an additional level of security to balance safety of patience, practicality, and clinical effectiveness (MacNeil 2007). Additionally, many engineered substitutes derived from synthetic materials present challenges as being non-biodegradable (Sun et al. 2005). For example, companies, such as Dermagraft, despite receiving positive effects in healing, are not commercially viable (Bello and Falabella 2002). Therefore, extra safety is

required for decontamination, acquiring donor cells and tissues, immune response compatibility, all of which can impede clinical cost effectiveness (Carver 1991).

1.5.2. Energy Modalities

Recent research has provided new insights in the metabolic demand of these regenerative processes. Studies have now demonstrated functional evidence of energy, in the form of ATP, responsible for inducing rapid recruitment and enhancing motility of immune cells (Sáez et al. 2017a) . Additionally, studies show metabolic dysfunction can be recovered to improve regenerative outcomes (Kalyanaraman et al. 2017).

Energy modalities include ultraviolet light C, negative pressure, electrical stimulation, ultrasound, and low-level laser irradiation (Vaghardoost et al. 2018, Ennis, Lee, and Meneses 2007). These treatments are increasing the scope of options for tissue injury reporting manipulations to inflammatory conditions and resolution (Frykberg and Banks 2015, Ennis et al. 2011). Further, they are uniquely suited to satisfy clinical safety and cost demands. However, optimization of these modalities for their effects on improving the wound microenvironment is still not defined. Knowledge of how energy manipulates the wound microenvironment presents a gap in knowledge for optimization of these therapeutics.

CHAPTER 2

2. CONCEPTUAL FRAMEWORK AND RELATED LITERATURE

As photobiology evolved in the form photobiomodulation therapy (PBMT) over the last 50 years, over 2000 scientific investigations have been conducted to substantiate its role in medicine. However, a lack standardized approaches have limited PBMT clinical effectiveness.

2.1. Photobiomodulation in Broad Clinical Practice

Photobiomodulation (PBM), via light irradiation, demonstrates a multifaceted aptitude to treat a wide range of inflammatory and tissue repair related dysfunctions. Clinical studies aimed at inflammatory conditions have demonstrating wavelengths near 632 nm , 820 nm, and 904 nm to modulate angiogenic levels, biochemical (PGE_2, TNF-alpha, IL-1beta) levels, neurophysiological levels, and other inflammatory related effects (Bjordal et al. 2006, Fabre et al. 2015, Gur et al. 2004). Clinically studies have shown photobiomodulation efficacy in the treatment of cardiac arrhythmias and ischemia (Ionin and Volkova 1989, Moshkovska 2005), increased cerebral blood flow and cognitive capabilities following traumatic brain injury (Li et al. 2015, Poiani et al. 2018), improved skeletal muscle force and reduced fatigue (de Almeida et al. 2012, Leal Junior et al. 2008), and reduction of pain in a manner similar to non-steroidal pharmaceuticals (Bjordal et al. 2006, Konstantinovic et al. 2010). From a clinical standpoint PBM offers numerous advantages: cost-effective, non-invasive, simple and pain free for the patient; potential drug equivalency for certain conditions to pharmaceutical agents and proven safety with minimal to no contraindications (Karu 2013).

2.2. Photobiomodulation in Clinical Wound Care

Photobiomodulation treatment of wounds has been described to be in the red and near infrared spectrum (600nm to 1000nm) for ideal skin penetration (0.5-2 mm) and biochemical and photophysical effects.

Studies demonstrate a PBMT aptitude to treat diabetic foot ulcers, burns, and postoperative wounds, that is currently not being met by conventional interventions (Desmet et al. 2006). A double-blind randomized clinical trial led to a decrease in diabetic ulcer size (Kaviani, Djavid, and Ataie-Fashtami 2011) using 660 nm laser (10 J/cm^2, 10mW/cm^2) treatment. Compared to placebo (n=10), patients treated with laser 6 times per week (n=13) demonstrated a significant ulcer reduction within 4 weeks of treatment. Also, 4 to 10-week follow-up evaluations demonstrated 66% of patients undergoing the laser treatment achieved complete healing, higher than the 33% seen in placebo groups. Recent clinical trials have also demonstrated significantly improved outcomes for both diabetic and non-diabetic chronic wound patients after 625 nm, 660 nm, and 850 nm light treatment. Results demonstrate that light treated ulcers (n=20) at 0.72 J/cm^2, when compared to not irradiated placebo group (n=20) significantly accelerated granulation and healing after light irradiation (Frangez et al. 2017). Also, in burn patients (n=11), 660 nm laser treatment (20 J/cm^2) combined with skin grafts led to accelerate healing (Vaghardoost et al. 2018). In post-operative healing, 660 nm treated postoperative healing reduced swelling, inflammation, and pain in patients 24 hours after surgery (Fabre et al. 2015). Further, Kazemi-Khoo evaluating laser treatment efficacy in diabetic healing demonstrated 660 nm, 650 nm, and 980 nm lasers led to improved diabetic foot ulcer healing outcomes. All three wavelengths (0.6 J/cm^2 to 6 J/cm^2) in diabetic patients (n=7) led to a reduction in ulcer size with no recorded contraindications (Kazemi-Khoo 2006). However,

studies such as these have led to a dispute in the medical community; there is no consensus on which parameters are required to stimulate relevant biological avenues to promote regeneration.

PBMT wound care has yet to standardize a clinical regiment of treatment. A meta-analysis was performed on twenty-four studies evaluating the effect of laser therapy on wound healing (Woodruff and laser surgery 2004). Results using a Cohen's d. statistic, demonstrated the mean overall effect of laser on healing was significant with the studies demonstrating augmentations in healing time, wound size, collagen synthesis, inflammation, and tensile strength. However, clinical treatment parameters used by all twenty-four studies demonstrated effective outcomes wide spectrum of wavelengths (400 nm to 1000 nm), energy fluences (0.076 J/cm^2 to 140 J/cm^2), and irradiances (1 mW/cm^2 to 1 200 mW/cm^2). Additionally, a large disparity exists in the clinical treatment strategies, ranging light exposure from 1 to 36 times in a single day and frequency a week ranging from twice per week to daily. As such, system reviews emphasize the need of more standardized modes of delivery for purposeful clinical impact (Chow and Barnsley 2005, Anders, Ketz, and Wu 2017). Wang *et al.*. reported that while clinical based laser treatments report an overwhelming potential to promote wound repair, the disparity in treatments emphasize a need for more molecular based studies (Wang et al. 2017). Therefore, to confirm the beneficial effects of photobiomodulation for clinical practice, more mechanistic and molecularly stimulated avenues need to be investigated.

2.3. PBMT Effect on Mitochondria

A series of studies have indicated that electromagnetic waves in the visible and NIR light spectrum interact with the cellular respiration chain (Kato 1981, Karu 1987). Studies of isolated rat mitochondria provided evidence that mitochondria were affected by monochromatic visible 632 nm light (Passarella et al. 1983). In isolated rat liver mitochondria treatment with the 632

nm laser (5 J/cm^2) has been reported to increase mitochondrial membrane potential and ATP (Passarella, Casamassima, and Molinari 1984). Additional *ex vivo* studies demonstrated enhanced ATP synthesis with exposure to a 632 nm wavelength delivering 5 J/cm^2 (Passarella et al. 1988, Karu, Pyatibrat, and Kalendo 1995). Yu *et al.*, alternatively demonstrated 660 nm (10 mW/cm^2) increased oxygen consumption (0.6 J/cm^2 and 1.2 J/cm^2) and energy charge (1.8 J/cm^2 and 2.4 J/cm^2) in isolated rat mitochondria (Yu et al. 1997). Yu *et al.*. further demonstrated that the electron chain components complex I, III, and IV affects membrane potential after respective red laser treatment. These findings provided a foundation of data indicating that mitochondria played a role mechanistically in photobiomodulation as a chromophore (**Figure 2)**.

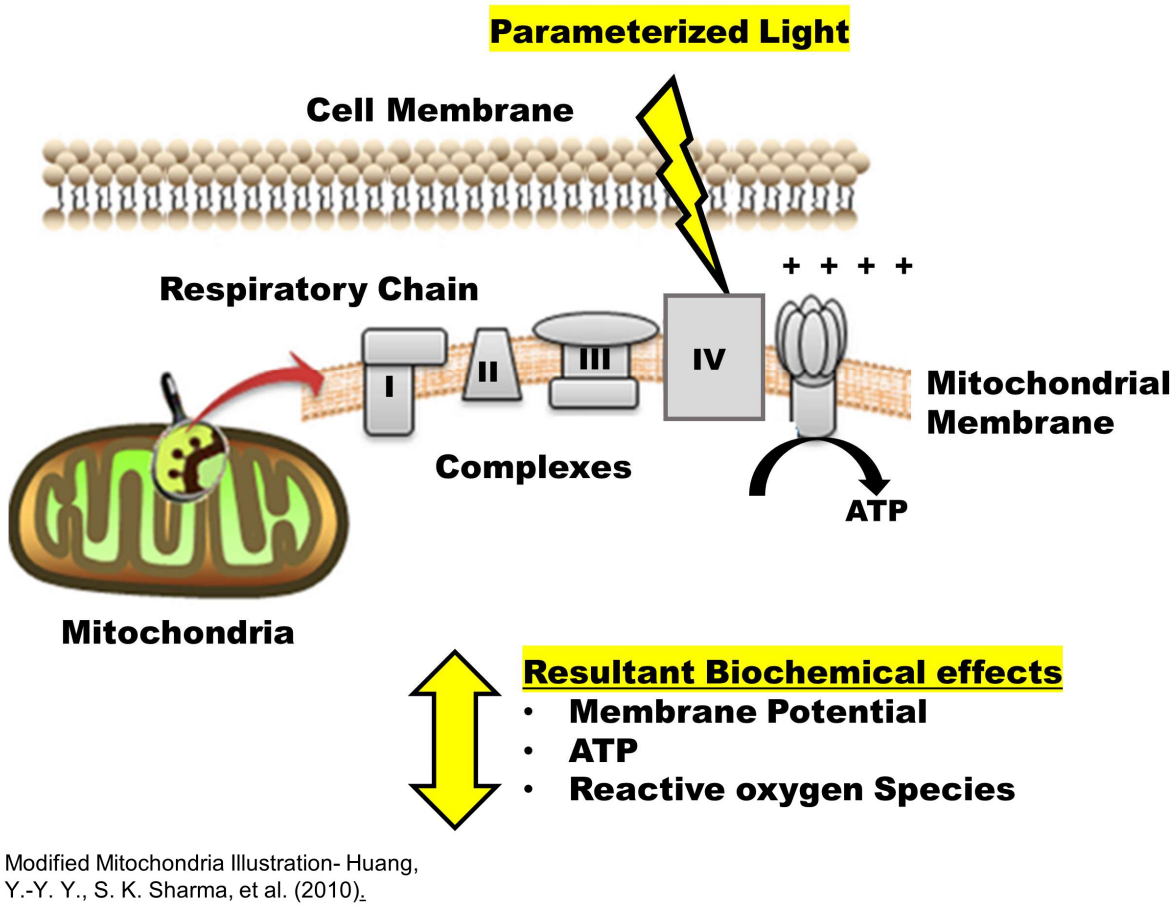

Figure 2. Parameterized light affects mitochondrial activity modulating membrane potential and ATP and ROS via activation of complexes: complex I, NADH dehydrogenase; complex II, succinate dehydrogenase; complex III, cytochrome bc complex; IV cytochrome c oxidase.

The mitochondria electron transport chain complexes are now widely accepted as chromophores. A study using male Winstar rats, demonstrated increased activities of respiratory chain complex I, II, III, and IV, after 904 nm treatment (5 J/cm^2) (Silveira, da Silva, et al. 2009). Cytochrome c oxidase, complex IV, is known as playing a central role in the bioenergetics of a cell. Isolated cytochrome C oxidase (CCO) were measured for conformational change activity, inferring electron transfer. Results demonstrated an increase in its conformational change commonly after 632 nm treatment (2 J/cm^2 and 10 mW/cm^2) implicating

cytochrome c oxidase as a mitochondrial photoacceptor (Pastore 2000). Karu *et al.* described an action spectrum using HeLa cells, identifying cytochrome C oxidase as a primary mitochondrial photoacceptor (Karu, Pyatibrat, and Afanasyeva 2004). Karu *et al.* further provided evidence that the action spectrum was believed to be a result of the heme core within the complex, with a single band at 619 nm and a compound band in the NIR region with a maximum peak at 820 nm (Karu et al. 2005). As a result, the now recognized term, photobiomodulation, was defined as a form of non-ionizing and non-thermal light therapy involving endogenous chromophores to elicit a "photophysical and photochemical event at various biological scales" (Anders, Ketz, and Wu 2017).

2.4. PBMT Effects on ROS

Photobiomodulation has been reported to affect ROS production, however, the effects have differed depending on the fluence applied *ex vivo*. ROS is a byproduct of mitochondrial cellular respiration (Zorov, Juhaszova, and Sollott 2006); as electrons are transferred within multi-subunit complexes, such as NADH dehydrogenase, superoxide radicals are generated (Lee et al. 2011) . The motif is believed to play a role in PBMT, enhancing electron transfer and increasing intracellular ROS. Kushibiki *et al.* assayed ROS production via 2'-7' dichlorodihydrofluorescein diacetate ROS probe after 405 nm (100 mW/cm^2) in a variety of cells including mouse preadipocytes, prechondrocytes, myoblasts, mesenchymal stromal cells, fibroblasts, and macrophages (Kushibiki et al. 2013). Results demonstrated enhanced ROS production after 405nm treatment in all cell types. Another study demonstrated 980 nm (1 5700 mW/cm^2) laser elevated ROS production assessed by 2'-7' dichlorodihydrofluorescein diacetate in a dose dependent manner in osteoblasts. Highest energy fluence (78.75 J/cm^2) demonstrated highest ROS production and lowest energy fluences (1.57 J/cm^2 and 7.87 J/cm^2) demonstrated

lowest ROS production (Migliario et al. 2014). Results also indicated all fluences had significantly elevated ROS production when compared to non-treated control, but 10 J/cm^2 correlated to the most enhanced cellular proliferation of all groups. Another study demonstrated 810 nm laser (3 J/cm^2 and 20 mW/cm^2) affected cortical neurons mitochondrial membrane potential, assayed with tetramethyrhodamine, and ROS generation, assayed with Mito-sox (Huang et al. 2013). Chen *et al.* demonstrated 810 nm increased reactive oxygen species and ATP synthesis in a dose dependent manner on murine fibroblasts (Chen, Arany, and Huang 2009). Low fluence (0.003 J/cm^2) demonstrated no significant increase in ATP synthesis while higher fluences (0.03 and 0.3 J/cm^2) increased ATP synthesis by 10% and 60%, respectively and correlated to increases in mitochondrial ROS. Results also demonstrated ROS production after 0.3 J/cm^2 were correlated to nuclear factor kappa B activation, regulating various inflammatory and cell survival pathways. In neurons, 810 nm laser, demonstrated a significantly increased ROS production and mitochondrial membrane potential. However, results also demonstrated in oxidative stressed cells, 810 nm treated neurons had an even more significant increase on mitochondrial membrane potential (30%) but reduced ROS presence. More recent studies have corroborated near infrared laser effects on neurons, demonstrating controlled mitochondrial ROS generation after 750, 810, and 950 nm (200 mW/cm^2) treatment to protect from global brain ischemia conditions (Sanderson et al. 2018). Large quantities of mitochondrial ROS generation by the electron transfer of cytochrome C is known to trigger apoptosis (Giorgio et al. 2005). Wu *et al.* evaluated 633 nm high fluences (120 J/cm^2) at an irradiance of 200 W/cm^2 effects on human lung adenocarcinoma ROS production and apoptosis (Wu et al. 2009). Results demonstrated high fluence 633 nm laser treatment induced excessive levels of intracellular ROS

and apoptosis. These experiments indicate PBMT can manipulate ROS production within a target cell *ex vivo*.

2.5. PBMT Unknown Effects

The primary mechanism of light action on the mitochondrial photoacceptor may not provide a full explanation of the mechanisms elicited by photobiomodulation; several different light facilitated parameters contribute to similar and opposing biological effects. Optimization of these photobiomodulations for their effects on improving the wound microenvironment is still not defined. This gap in knowledge primarily rests on fundamental gaps in mechanisms elicited following energy-based treatments. If there was a more sensitive marker for photobiomodulation effects, the treatment may become more standardized. PBMT needs a standardized approach for parameters, including wavelength, fluence, irradiance, and pulsing modality (Tunér and Hode 1998)

2.5.1. Effect of Light Wavelength

Photobiomodulation effects have been reported in variety of wavelengths, eliciting debate on which wavelength to use for therapies; generally, increased wavelengths are believed to be more penetrant (Ash et al. 2017). Light as an electromagnetic form of radiation has been well defined to positively correlate with absorption, Beer's Law (Kocsis, Herman, and Eke 2006). One study measured the optical properties of several different cell types, including cartilage, muscle, skin, tumor, and myocardium with wavelengths ranging from 630 nm to 1064 nm using replicated parameters and measurement equipment (Beek et al. 1997). They determined 630 nm light had the largest differences in optical properties, suggesting that differences may be explained by inherent biological variations of the tissue. Other studies have added that tissue constituents affect wavelength diffusivity (Gemert and Jacques 1989). Kim *et al.* measured 635

nm and 850 nm light diffusivity via optical fiber sensor in porcine skin with varying differences in water content (Kim, Shin, and Jeong 2015). Results demonstrated that both wavelengths under the same energy fluence propagated energy fluence differently based on the wavelength optical properties of water. Further, measured fluence rate inside skin was dependent on the tissue water content. These studies shed light on the varying effects within *in vitro* studies in varying wavelengths.

Varying wavelengths have been demonstrated to alter photobiomodulation effects. In human adipose derived stem cells 415 nm, 540nm, 660 nm, and 810 nm at 3 J/cm^2 were compared to determine the effects of wavelength dependent photobiomodulation (Wu et al. 2010). Cellular responses were evaluated including: cell proliferation, mitochondrial membrane potential, ATP production, ROS generation, Calcium concentration, and pH levels. Cell proliferation, ATP production, ROS generation, and mitochondrial membrane potential were increased after 660 nm and 810 nm wavelengths. In contrast, 415 and 540 nm demonstrated decreased cell proliferation and ATP levels which coincided with greater levels of ROS generation and mitochondrial membrane potential.

Alternative studies have also demonstrated similar effects in varying wavelengths. One study demonstrated a difference in the absorption wavelength of the mitochondrial electron chain resulting in enhanced ATP synthesis on isolated rat liver mitochondria at 515 nm, (Morimoto et al. 1994), when previous studies demonstrated elevated ATP synthesis near 630 nm, 820 nm, and 904 nm. NIH-3T3 fibroblasts treated with 904 nm laser demonstrated significant increases in proliferation and procollagen synthesis (Pereira et al. 2002). In embryonic skin fibroblasts 810 nm demonstrated increased activation of NF-kB in addition to increases in mitochondrial reactive oxygen species and ATP levels when compared to non-irradiated controls (Chen et al.

2011). Human foreskin fibroblasts demonstrated an increase in proliferation after 630 nm treatment compared to non-irradiated controls (Hsieh et al. 2012). Another study used human skin fibroblasts, Hu02, to assess 660 nm light bioenergetics and subsequent responses (Naderi et al. 2017). Hu02 cells treated with 660nm demonstrated a significant increase in reactive oxygen species generation, cell proliferation doubling time, and cell viability. These studies demonstrate a wide variance of wavelengths applied *in vitro*; *in vivo* applications may require more investigation for optimization based on cell/tissue type.

2.5.2. Effect of Energy Flux

Multiple photobiomodulation effects have been reported in similar or same wavelengths eliciting debate on an energy quantity for treatment. A common unit of energy for light is joules, J, equivalent to kg m^2 s^{-2}. Joules are equivalent to Watts, W, or kg m^2 s^{-3} multiplied by the time of exposure in seconds. Light energy fluence and irradiance are both parameters used to control energy deliverance in treatment, incorporating both J and W. Light energy fluence, commonly reported as J/cm^2, can be simplified as the number of photons (N) or number of energy passing through a target area (A). This energy fluence (E), can be described by Equation 1:

$$E = \frac{dN}{dA} \quad (1)$$

Additionally, the radiant flux of light energy or light irradiance (I) is derived by time of irradiation in seconds (T) of joules per target unit area. Therefore, light irradiance, W/m^2, can be described by Equation 2:

$$I = \frac{dN}{dA\,dT} \quad (2)$$

In vitro studies (**TABLE I)**: Van Breugal and Dop Bar demonstrated that 632.8 nm at kept constant at 180 mJ at variant powers (0.55 mW to 5.98 mW) for irradiation time (30 seconds to 330 seconds) on human fibroblasts demonstrated significant changes in cell proliferation (van Breugel and Bär 1992). Stimulatory effects were maximized at lower irradiation times and irradiance, whereas inhibitory effects were maximized at high laser powers. **TABLE I** demonstrates the wide range of delivered energies to cultured cells. It is surprising to see that there is a 6- to 10-fold range of energy fluences in which beneficial effects have been described. Even more variable is the irradiance which ranges from 0.68 mW/cm^2 to 530 mW/cm^2. Such wide variances make it difficult to define parameters which can provide reproducible and consistent results.

TABLE I. PBMT ENHANCED CELLULAR PROCESSES WITH VARIABLE DOSING

Light Source (wavelength)	**Irradiation**	**Fluence**	**Cell Model**	**Photobiomodulation effect**	**Reference**
Laser (660nm & 780nm)	1 W/cm^2	6 J/cm^2	Human Neutrophils (PMN)	Increased ROS generation and oxidative burst effect against Candida albicans cells (fungi)	Cerdeira *et al.* (2016) J Biophotonics
GaAslAs (808nm)	(0.37 to 0.566) W/cm^2	(11.3 to 17) J/cm^2	HOF fibroblasts & NOKSI keratinocytes	Increased ROS generation to toxic levels. Protective catalase activity differs in cell type	Engel at el. (2016) J Biophotonics
LED (470nm & 660nm)	50 mW/cm^2	30 J/cm^2	C2C12 myoblasts, NIH/3T3 fibroblasts, BIR10 keratinocytes	Modulated proliferation and apoptosis. Increased migration kinetic (scratch wound)	Teuschi *et al.*(2015) Dermatological Surg
Lasers (660nm & 780nm)	(10.3 and 375) mW/cm^2	(2.6 and 7.5) J/cm^2	J774 macrophages	Modulated COX-2 activity & IL-6 mRNA. Reduced TNF-a & iNOS mRNA expression	Fernandes *et al.* (2015) J Photochem and Photobio
Laser (652nm, 806nm) vs LED (637nm, 901nm)	(5.57 and 1.30) mW/cm^2	(10.02 and 2.334) J/cm^2	A549, U20S, and PtK2 epithelial cells	Increased Migration (Scratch Wound), Proliferation	Spliter & Berns (2014) J Biomedical Optics
GaAs diode (915nm) CW and Pulsed (100 Hz)	166.7 mW/cm^2	(5, 14, and 45) J/cm^2	Human Dermal Fibroblasts	Modulated mitochondrial potential (MMP) & ROS generation	Belletti *et al.*. (2014) Lasers Med Sci
Laser (660nm)	75 mW/cm^2	4.5 J/cm^2	U937 (alveolar macrophages)	restored DEX effect. Decreased IL-8 & TNF and HDAC(more gene activation) via PKA via inhibition of PI3K.	Souza & Aimbire *et al.* (2014) J Photochem and Photobio
HeNe (632.8nm)	530 mW/cm^2	1,589 J/cm^2	BV2 murine microglial (resident brain macrophages)	Increased viability and phagocytosis. Reduced LPS cytokine expression, NO expression via tyrosine kinases Src and Syk.	Song, Zhou, and Chen (2012) J Neuroinflammation
HeNe (632.8nm)	10.22 mW/cm^2	5 J/cm^2	WS1 Diabetic human skin fibroblasts	Increased migration, viability, proliferation, and collagen production	Ayuk & DTech & Abrahamse (2012) Diab Tech & Therapy
HeNe (632.8nm)	12.74 mW/cm^2	(1 and 2) J/cm^2	RAW 264.7 (murine macrophages)	Increased Phagocytosis via Src activity	Lu *et al.*. (2011) Biophoton Immu Resp
Laser (660nm)	17.9 mW/cm^2	4.5 J/cm^2	AMJ2-C11 (rat alveolar macrophages)	Reduced MIP-2 mRNA and ROS generation and NF-kB after LPS stimulation. Potentiated after NAC	Lima *et al.* (2010) Photomed Laser Surg

Nd:YAG (1064nm) Laser (830nm) HeNe (632.8nm)	(22, 6, and 12.7) mW/cm^2	5 J/cm^2	WS1 Diabetic human skin fibroblasts	Increased migration, viability and proliferation. Modulated ATP production	Houreld & Dtech & Abrahamse (2010) Diab Tech & Therapy
Nd:YAG (1064nm) Laser (830nm) HeNe (632.8nm)	(2.07, 5.95, and 12.73) mW/cm^2	5 J/cm^2	HSF human skin fibroblasts	Modulated mRNA IL-6, bFGF and Proliferation	Hawkins *et al.* (2007) Photomed Laser Surg
HeNe (632.8nm)	3 mW/cm^2	(0.5 to 16) J/cm^2	HSF human skin fibroblasts	Increased Migration (Scratch Wound), Proliferation, bFGF mRNA	Hawkins *et al.* (2006) Photomed Laser Surg
Laser (830nm)	316.7 mW/cm^2	(9.5 and 19) J/cm^2	Human Neutrophils (PMN)	Reduced opsonized PMN ROS generation via Luminol	Fujimaki *et al.* (2003) J Clin Laser Med Surg
HeNe (632.8nm)	0.68 mW/cm^2	(0.01 to 0.03) J/cm^2	Spleen Phagocytes	Increased Respiratory burst of Phagocytotic Cells via Luminol	Karu *et al.* (1989) Lasers Surg Med

In vivo studies (**TABLE II)**: AL-Watban *et al.* evaluated wound healing in diabetic rats using different energy fluences (5, 10, 20, and 30 J/cm^2) and wavelengths (532 nm to 980 nm) (Al-Watban, Zhang, and Andres 2007). Results demonstrated percentage of relative healing were most optimal at 633 nm delivered at 10 J/cm^2, establishing differences in efficiencies not only by wavelength but also by energy fluence. Other reports have shown 685 nm, 830nm, at energy fluences 20 J/cm^2 and 50 J/cm^2 to have increased collagen production on cutaneous wounds in the dorsum of Wistar rat (Mendez et al. 2004). With 20 J/cm^2 treatments demonstrating more collagen production than 50 J/cm^2. Another study evaluated wound tensile strength in rats after 635 nm and 670 nm with an energy fluence of 5 J/cm^2 but variant irradiances (4 mW/cm^2, 15 mW/cm^2) (Vasilenko et al. 2010). This study demonstrated significantly improved healing with both 635 nm at 15 mW/cm^2 and 670 nm at 4 mW/cm^2. Erdle *et al.* evaluated 670 nm effects on a mouse burn injury model at the same energy fluence (3.6 J/cm^2) but with low, medium and high irradiances (1.6, 8, and 40 mW/cm^2, respectively)

(Erdle et al. 2008). All irradiances increased percent healing of injuries on day 2. Low irradiance increased 4-fold better when compared to untreated controls, and 1.5-fold better than high irradiances. Alternatively, a study evaluating healing in splinted wounds of diabetic mice after 660 nm treatment (4.7 J/cm^2 to 6.3 J/cm^2) at variant irradiances (58 mW/cm^2 to 313 mW/cm^2) found little differences (Peplow et al. 2011). Results demonstrated that each irradiance had enhanced reepithelization and granulation tissue when compared to nonirradiated control, but not each other. Conflicting results by energy flux in *in vivo* studies underscores the need for a reproducible model in which each parameter can be studied *in vivo* to identify optimal parameters for clinical translation.

TABLE II. PBMT IMPROVED REGENERATIVE OUTCOMES IN ANIMALS WITH VARIABLE DOSING

Light Source (wavelength)	**Irradiation**	**Fluence**	**Animal Wound Model**	**Photobiomodulation effect**	**Reference**
Laser (660nm)	11.3 mW/cm^2	(1,5, 10) J/cm^2	Male Sprague-Dawley Rats	Increased Collagen Deposition, rupture strength and stiffness. Reduced Mφ -(3 & 7 days)	Suzuki & Takakuda (2016) Lasers Med Sci
GaAl (904nm)	400 mW/cm^2	(3 and 5) J/cm^2	Male Wistar Rat	Reduced nonenzymic oxidative stress and IL-6 and IL-10 production (mRNA)-Reduced inflammatory response (2,12,24 h)	Silveira *et al.* (2016) Free Radic Res
GaAlAs (830nm) CW and Pulsed (50 Hz)	(2 500 and 1 2500) mW/cm^2	4 J/cm^2	Male Wistar Rat	Reduced TNF-a, IL-1B inflammatory cytokines. Increased TGF-B1. Modulated Nitric Oxide (1,4,8,15 days)	Guerra *et al.* (2016) Lasers Med Sci
Laser (808nm) CW and Pulsed	1 276 W/cm^2	6.38 J/cm^2	Male Wistar Rats	Increased Healing rate, granulation, epithelization and wound reduction (3, 7 14 days)	Tabakoglu *et al.* (2016) Lasers in Surg Med
Laser (890nm) Pulsed (80 Hz)	1 mW/cm^2	0.2 J/cm^2	induced diabetic Wistar rats	Increased Diabetic fibroblasts, macrophages-and increase bFGF gene (angiogenesis) in all rats (4,7,15 days)	Sharifian *et al.*. (2014) Lasers Med Sci
Pulsed Laser (890nm, 80 Hz)	1.08 mW/cm2	(0.03 and 0.2) J/cm^2	STZ (bacteria) induced diabetic Wistar Rats	30 days after STZ injections used Biometrics to establish load and stress of wounds. LLLT decreased maximum load and stress in non-diabetic. Increased Elastic Modulus max load and stress in LLLT diabetic injuries. (All tensiometrical examination 45 days after STZ injection)	Dadpay *et al.* (2012) J PhotoChem and PhotoBio
Laser (HeNe 632nm)	4.02 mW/cm^2	(0.5 to 2) J/cm^2	Mice	Increased collagen deposits, fibroblasts granulation tissue reduced leukocytes	Prabhu *et al.*. (2012) J Biophotonics
Laser (890 nm) Pulsed (50 Hz)	Not described	Not described	Rabbits	Increased wound closure and fibroblasts presence. Reduced mononuclear infiltration via Histopathology-(3,7,14 days)	Hussein *et al.*. (2011) N. Am J Med Sci
Laser (660nm)	375 mW/cm^2	67.5 J/cm^2	Male BALB/c mice	Reduced Neutrophil influx from BALF and Reduced TNF-a mRNA and cAMP expression in alveolar macrophages (3 hours)	Lima *et al.* (2011) Lasers Med Sci
Laser (660nm)	(58 to 313) mW/cm^2	(4.7 to 6.3) J/cm^2	Diabetic mice	Increased epithelization, granulation and collagen deposit(14 days)	Peplow *et al.* (2011) Lasers in Surg Med

LED GaAlAs (660nm)	9 mW/cm^2	(10 to 32.4) J/cm^2	Holtzman Rats	modulated aerobic metabolic capacity in temporalis muscle via Cytochrome C oxidase (CCO).	Hayworth *et al.*. (2010) J Photochem and Photobio
GaAlAs (780nm) CW and Pulsed (2 336 Hz)	9.91 mW/cm^2	2 J/cm^2	Male Sprague-Dawley Rats	Increased fibroblasts and blood vessel formation. Reduced macrophages -(4,7, &15 days)	Bayat *et al.*. (2010) Photomed Laser Surg
AsGa (904nm)	Not described	5 J/cm^2	Male Wistar Rats	Increased ETC Complexes I,II,III and IV activity support hypothesis ATP increase -(5 days) - Reduced wound size (2007)	Silveira *et al.*. (2009) J Photochem and Photobio
Laser (diode 532, 633, 810, 980 nm)	(15.56 to 22.22) mW/cm^2	(5 to 30) J/cm^2	induced diabetic Male Sprague-Dawley Rats	LLLT group significantly had a faster healing time in diabetic rats. (3 weeks)	Al-Watban *et al.*. (2007) Photomed Laser Surg
HeNe (632.8nm)	588.2 mW/cm^2	10 J/cm^2	induced diabetic male Wistar Rats	Increased granulation and epithelization. Reduced mononuclear infiltration and inflammatory cell density (4,7,15 days)	Rebelo *et al.* (2006) Photomed Laser Surg
HeNe (632.8nm)	(139 and 281) mW/cm^2	(2.09 and 4.21) J/cm^2	Sprague Dawley Rats	Increased tensile strength, collagen deposition, reduced mononuclear cell infiltration (1 ,3, 5 days)	Yasukawa *et al.* (2006) Laboratory Animal Science
GaAs (904nm)	0.149 mW/cm^2	5 J/cm^2	Male Wistar Rats	In Induced muscle trauma Reduced ROS generation, iNOS, and NF-kB activation. Increased collagen deposition (12 hours, 7 ,14 days)	Rizzi *et al.* (2006) Lasers Surg Med
Lasers (685nm & 830nm)	Not described	(20 and 50) J/cm^2	Male adult Wistar Rats	Increased fibroblasts, collagen deposition, re-epithelization. Reduced mononuclear cell infiltration via Histopathology (7 days)	Mendez *et al.* (2004) J Clin Laser Med Surg
Laser (830nm)	79 mW/cm^2	5 J/cm^2	Female diabetic mice	Increased wound tensile strength in all mice via Tensiometer(4 or 7 days)	Stadler *et al.*.(2001) Lasers Surg Med

2.5.3. Effect of Pulsing Modality

Photobiomodulation effects have been reported in variety of laser operating states, eliciting debate on whether continuous wavelengths or pulsed lasers should be used for photobiomodulation effects. Pulsing in light sources is controlled by pulse width measured in seconds and pulse repetition rate (frequency) measured in Hertz, Hz. Molecularly, pulsed and continuous wavelength lasers have been demonstrated to elicit varying effects on the mitochondria.

Effects on Mitochondria: A study of mitochondria in fibroblasts evaluated 915 nm laser pulsed (100 Hz) and continuous at 5, 15, and 45 J/cm^2 responses in the mitochondrial membrane potential via tetramethyrhodamine methyl ester molecular probes (Belletti et al. 2015). This molecular probe emitted fluorescence proportional to the amplitude of the mitochondrial membrane potential and was measured over time. The 915 nm treated fibroblasts demonstrated decrease in potential in both pulsed and continuous modalities at high fluences, 45 J/cm^2. At lower fluences, 5 J/cm^2 pulsed modality decreased mitochondrial membrane potential, while continuous wavelength laser increased mitochondrial membrane potential. While optical properties of biological tissue are thought to have better light diffusivity with pulsing, these studies do not demonstrate a clear-cut direction regarding the role of pulsed vs constant source energy. There are still mechanistic effects that are not completely understood.

Effects of pulsed vs continuous on inflammation and tissue healing: Overall, continuous administration may provide an advantage over pulsed administration for reduction of inflammation and tissue regeneration. Mantineo *et al.* evaluated the effect of different power irradiation parameters (10, 20, 30, 40, and 50 mW) with continuous (830 nm and 980nm) and pulsed laser (830 nm) on inflammation induced in gastrocnemius muscles of rats by measuring

peripheral blood cytokine levels and histologic examination of the muscle(Mantineo, Pinheiro, and Morgado 2014). Treatment was applied daily for five sessions. Continuous state irradiation treatment at 830 nm demonstrated the greatest decrements in inflammatory cytokine production and inflammatory cell infiltrate in the muscle. A study investigated the effects of a pulsed continuous wave lasers at 635 nm (1.0 J/cm^2) at 100, 200, 300, 400, and 500 Hz in the role of healing in rats (Al-Watban and Zhang 2004). This study demonstrated continuous wave without pulse had the most efficacious healing closely followed by 100 Hz; both demonstrated nearly a 3-fold improvement in percentage of relative healing over 500 Hz treated wounds. Gigo-Benato evaluated Wistar rat nerve regeneration in continuous 808 nm laser versus 905 pulsed laser (Gigo-Benato et al. 2004). Results demonstrated continuous wave laser at 808 nm to have better nerve regeneration, but also demonstrated combined treatment of both continuous and pulsed to have the most effective nerve regeneration. A clinical study evaluated the treatment of episiotomies in woman with pulsed or continuous wave laser at 670 nm (10, 25 and 50 Hz). Results demonstrated pulsed laser enhanced wound repair more than continuous wavelength (Kymplová, Navrátil, and Knížek 2003).

Effects of super pulsed lasers and body temperature on energy absorption: Other parameters can affect the degree of energy absorbed when pulsed. Super pulsed lasers provide 100-200 nanosecond pulses at high power (50,000 mW); this delivery is believed to provide more light diffusivity through tissue. Joensen *et al.* compared 810nm, 200mW continuous wave energy to super pulsed 904 nm laser (60 mW) for effects on rat skin flaps which were harvested and then irradiated (Joensen et al. 2012). Results demonstrated super pulsed 904 nm laser were significantly more penetrated through skin than 810 nm continuous wave lasers, even when at lower output powers.

Energy absorption can also be influenced by temperature. Yeo *et al.* evaluated 660 nm at frequencies of 1, 10, 25, and 50 Hz peak intensity studying the effects of frequency, temperature, and glycerol injection in a soft tissue model (Yeo et al. 2011) . Results demonstrated an increased absorption with cooling, with a 1.5-fold increase in intensity at 10^{o} than 40^{o}. Further, a 1.8-fold increase was seen in 10 Hz than continuous wave laser treatment. Injection of glycerol also increased photon density within the tissue. When combined, all three were better in energy delivery than each alone. These results punctuate the large number of variables which affect therapeutic delivery of energy to tissues and the need for reproducible models which can study each parameter alone and in combination *in vivo*.

2.6. PBMT Cellular Effects on Macrophages

2.6.1. PBMT Effects on Macrophage Inflammatory Responses

In the 1980's preliminary studies were first conducted to on immune cells to better navigate clinical outcomes in healing. Karu *et al.*, in an effort to corroborate Ender Mester red laser effects, investigated 632.8 nm irradiation (0.01 J/cm^2 to 0.03 J/cm^2) on primary rat spleen phagocytes (Karu et al. 1989). Results demonstrated phagocytes significantly increased respiratory bursts 2-fold, both in presence and non-presence of bacteria, measured via chemiluminescence. Dube *et al.* used mice peritoneal macrophages to demonstrate 632.8 nm significant increases in lysozyme and cathepsin activity, in addition to, increased phagocytosis of yeast cells (Dube, Bansal, and Gupta 2003). This study also measured changes in macrophage morphology, as sign of cellular activation and differentiation. A significant increase in cell size and spreading was seen after 632.8 nm laser treatment, indicting activation.

Recent *in vitro* studies have begun to characterize phenotypical changes in macrophages in response to PBMT. Fernandez *et al.* investigated the capacity of 660 nm and 780 nm

photobiomodulation to affect the activation state of macrophages J774 cell line at both 2.6 J/cm^2 and 7.5 J/cm^2 fluence (Fernandes et al. 2015). Fernandez *et al.* demonstrated both wavelengths promoted the transition of macrophages from an inflammatory state to an anti-inflammatory state, measured via ELISA. Both lasers significantly reduced TNFα and iNOS expressions, with 660 nm providing an additional uptake of IL-6 expression and production. Overall, it appears that PBMT effects on macrophages *ex vivo* enhance bacterial phagocytosis, increase respiratory burst, enhance activation, and possibly hasten the transition from pro-inflammatory to pro-regenerative macrophage functions.

2.6.2. Macrophage Induced Fibroblast Proliferation Following PBMT

One preliminary study investigated 660 nm, 820 nm, 870 nm, and 880 nm pro-healing alternative activation on macrophage-like cell line, U-937 (Young et al. 1989). This study demonstrated U-937 treated with wavelengths 660 nm and 820 nm had a significantly improved proliferative effect on 3T3 fibroblasts. In contrast, 870 nm demonstrated minimal stimulation and 880 nm had inhibitory effects on fibroblast proliferation. These findings align with mitochondrial absorption bands detected at 619 and 820 (Karu et al. 2005). Bolton *et al.*. further determined the effects of light sources ranging from 400-2000 nm on U-937 macrophages. Bolton *et al.* corroborated Young *et al.* findings demonstrating macrophages, after PBMT, contributed to enhanced fibroblast proliferation (Bolton, Dyson, and Young 1992). Bolton further went on to demonstrate similar significant findings with 660 nm (2.4 J/cm^2 to 9.6 J/cm^2) on U-937 macrophage enhanced fibroblast proliferation, with 7.2 J/cm^2 demonstrating the most significant effects (Bolton, Young, and Dyson 2004). An additional study similarly investigated U-937 macrophage-like cells effects on fibroblast proliferation after 820 nm varying pulsing frequency

(Rajaratnam, Bolton, and Dyson 1994). Varying pulses demonstrated significant differences in fibroblast proliferation from each other and from non-irradiated controls.

These findings provide strong evidence for the effect of photobiomodulation on some macrophage activities, but due to the nature of being *ex vivo*, these studies in isolation limit *in vivo* understandings. The behavior of macrophages in response to a wound microenvironment is not defined. Insights on macrophage wound recruitment kinetics and overall effect on wound closure require a method to mark and track macrophages *in vivo* and compare responses between wounded and non-wounded conditions.

CHAPTER 3

3. AN AUTOMATED QUANTITATIVE IMAGE ANALYSIS PIPELINE OF *IN VIVO* OXIDATIVE STRESS AND MACROPHAGE KINETICS

3.1. Background and Rationale

The varied responses of macrophages to oxidative stress in health and disease underscores a need to better understand how tissue level changes of oxidative stress can enhance or impair injury responses. Zebrafish can be bred to express fluorescent transgenic inflammatory cells such as macrophages, to be imaged in a whole organism approach in real time due to their translucent phenotypical characteristics (Baker 2010). The conservation between zebrafish and human pathways has been verified extensively, supporting image-based analysis as an ideal strategy to characterize biological phenomena comprehensively to gain insights into human inflammatory responses (Forn-Cuní et al. 2017). Currently, no analysis pipeline exists to leverage the zebrafish *in vivo* visualization advantage that has promulgated to high impact inflammatory discoveries concerning leukocyte recruitment and oxidative stress after injury (Niethammer, Grabher, Look, and Mitchison 2009).

Unfortunately, many relevant image processing strategies do not provide transferable analysis pipeline solutions, introducing non-standard data formats prohibitive of broad implementation (Svensson, Medyukhina, Belyaev, Al-Zaben, et al. 2017). A recent survey of automated processing strategies within zebrafish image data, implore image analysis software's to be transparent, user-friendly, and readily available (Mikut et al. 2013). The motivation for this work is to provide a readily available quantitative analysis pipeline of zebrafish-based inflammatory oxidative stress and macrophage kinetics in parallel over time (

Figure *3*).

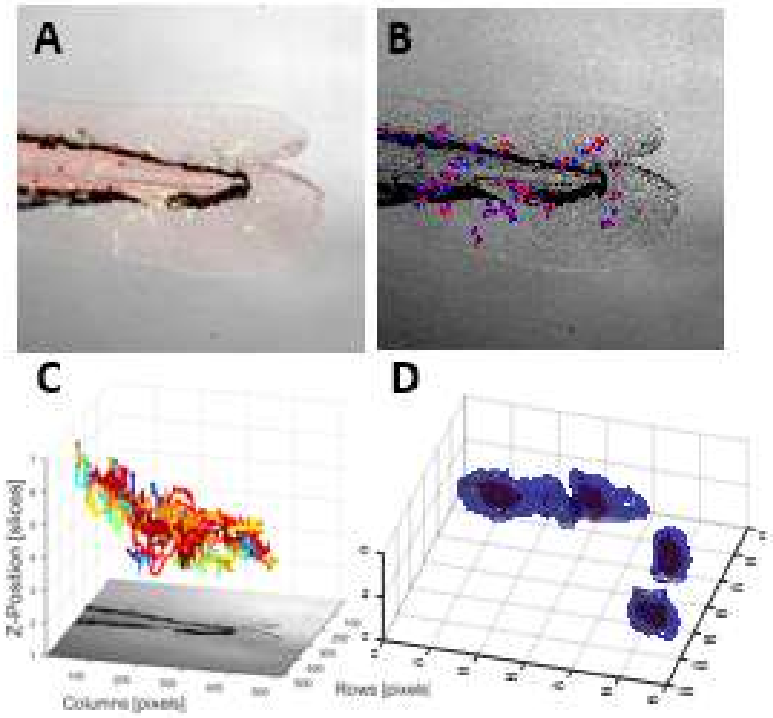

Figure 3. ROS loaded Transgenic Wounded Larval Zebrafish Images. Zebrafish wound (A) at 10x magnification shows fluorescent macrophages (B) color mapping, to detect low threshold (blue) and high threshold (red) pixel intensity in (C) 3D with total travel path vector displacement of (D)macrophages

In vivo visualization of real-time inflammatory oxidative stress responses to biochemical cues such as reactive oxygen species (ROS) are possible. However, quantitative ROS detection over time is still underdeveloped, limited by qualitative or *ex vivo* static endpoints (Mugoni, Camporeale, and Santoro 2014b, Owusu-Ansah, Yavari, and Banerjee 2008). The use of *in vivo* ROS probes could theoretically provide information on oxidative stress in real time after injury in zebrafish. However, new forms of *in vivo* quantitative analysis require new custom non-generic processing pipelines of image-based analysis, which current available commercial software do not meet (Mikut et al. 2013, Koopman et al. 2006, Walker et al. 2012, Pase, Nowell, and Lieschke 2012).

Cell tracking image processing algorithms and software, in contrast, are more developed. Many imaging tools and software such as ImageJ®, Fiji®, Volocity®, Metamorph® and even Photoshop® have been used to map morphological behavior of cells in zebrafish injuries (Schindelin et al. 2012, Schneider, Rasband, and Eliceiri 2012, Hall et al. 2009, Gray et al. 2011). However, published zebrafish tracking software strategies have yielded discrete analysis on only relatively few fish (1-3 fish), short time segments, large sampling frequencies (3-10 minutes), and/or relatively small populations of cells (1-10 cells per fish). This gap may be explained by the complicated demand of manual modes of tracking and/or data management required to comprehensively format time-based changes. As a result, the added complexity and breadth of data analytics required is prohibitive of analysis. Quantitative analysis of time-based changes of both ROS and cell tracking outcome measures in parallel requires a standardized analysis pipeline.

*Zirmi (***Z**ebrafish **i**nflammatory **r**eactive oxygen species- and **m**acrophage kinetics- based **i**mage analysis) software was developed to facilitate an image analysis pipeline to quantitatively derive fluorescence intensity and cell tracking measures of oxidative stress and cellular kinetics, respectively. This software, on the MATLAB platform, (1) automates image processing and (2) quantitative strategies (3) to manage and export data in user-friendly and reproducible formats, (4) leveraging existing image processing opensource software tools. A main advantage of using the *Zirmi* analysis pipeline is that it builds upon established, automated, and readily available algorithms. *PhagoSight* pre-processing and keyhole tracking algorithms (Reyes-Aldasoro, Akerman, and Tozer 2008) were incorporated to avoid parallel developments. Another advantage of *Zirmi* analysis is that it introduces user-customizable modes of selecting regions and cell tracks for standardized formats of quantitative measures. Lastly, *Zirmi* provides user-

friendly data management which is available open-source and can be readily amended to improve throughput and accessibility issues. We tested this analysis pipeline, according to wide-spread zebrafish preparation and imaging strategies, to acquire standardized quantitative data measures of oxidative stress and cell kinetics based on severity of wounding. Our study demonstrates that the *Zirmi* analysis pipeline solution facilitates gains in time, reproducibility, and data measures that support oxidative stress and cell kinetic quantitative evaluations.

3.2. Material and Methods

3.2.1. Zebrafish Assay Preparation

The *Tg(mpeg:dendra2)* zebrafish line, in which the promoter *mpeg* was used to drive *dendra2* expression in macrophages (Ellett et al. 2011), was purchased through ZIRC (Cat.#ZL10389). Housing, water quality and spawning were performed according to standard protocols (Mugoni, Camporeale, and Santoro 2014a, Renaud, Herbomel, and Kissa 2011). E3 embryo media was reconstituted in distilled water for a 1X Solution (5 mM NaCl, 0.17 mM KCl, 0.33 mM $CaCl_2$, 0.33 mM $MgSO_4$) with 0.05 % methylene blue for standard use with larval zebrafish for incubation at 28 ºC in 100mm glass dishes. As per AVMA guidelines, larvae were anesthetized using buffered Tricaine, 3-amino benzoic acidethylester at certain time points as described below (Sigma,168 mg/L, adjusted to pH 7.0 using $NaHCO_3$). Immediately following experimental procedures, larvae were humanely euthanatized first with 400 mg/mL tricaine solution and then 10 % sodium hypochlorite solution as per 2013 AVMA guidelines. All procedures and animal conditions described herein were approved by the Animal Care Committee at the University of Illinois at Chicago.

(a) *Fish Selection*: Naturally dechorionated larvae at 3 dpf (days post-fertilization) were placed in 75mm glass dishes with 5mL of E3 media. Animals that did not meet uniformity in

wound size, distance from notochord, or demonstrated small breaks or nicks in the embryonic outline were euthanatized and not included in the experiments (

(b) **Figure *4*A**).

(c) *ROS Probe Loading*: Dihydroethidium (DHE, Sigma) dye was reconstituted in 1ml of anhydrous dimethyl sulfoxide (DMSO, Sigma-Aldrich) at 10mM and stored in aliquots. Zebrafish larvae, 3 dpf in groups of 8- 15, were transferred to a 35 mm diameter glass bottom dish (MATEK) and loaded (Mugoni, Camporeale, and Santoro 2014b) with 35 uM DHE solution in 1X Dulbecco's Phosphate buffer solution and incubated for 40 minutes in the absence of light, then transferred to a separate 75 mm glass dish, and washed with pre-warmed E3 media to remove excess DHE (

(d) **Figure *4*B**).

(e) Mounting and Wound Placement: After ROS loading, larvae zebrafish were anesthetized (168 mg/L, Tricaine), immobilized (1% low melting point agarose solution for lateral mounting), and underwent single caudal fin incisions, initiated approximately 50 μm to 100 μm from notochord and extended to the end of the caudal fin via 28-gauge sterile needle **(**

(f) **Figure *4*C)**. Animals which did not meet uniformity in wound size (320 ± 50 μm), distance from notochord, or demonstrated small breaks or nicks in the embryonic outline were euthanatized and not included in the subsequent stages of study (

(g) **Figure *4*D**).

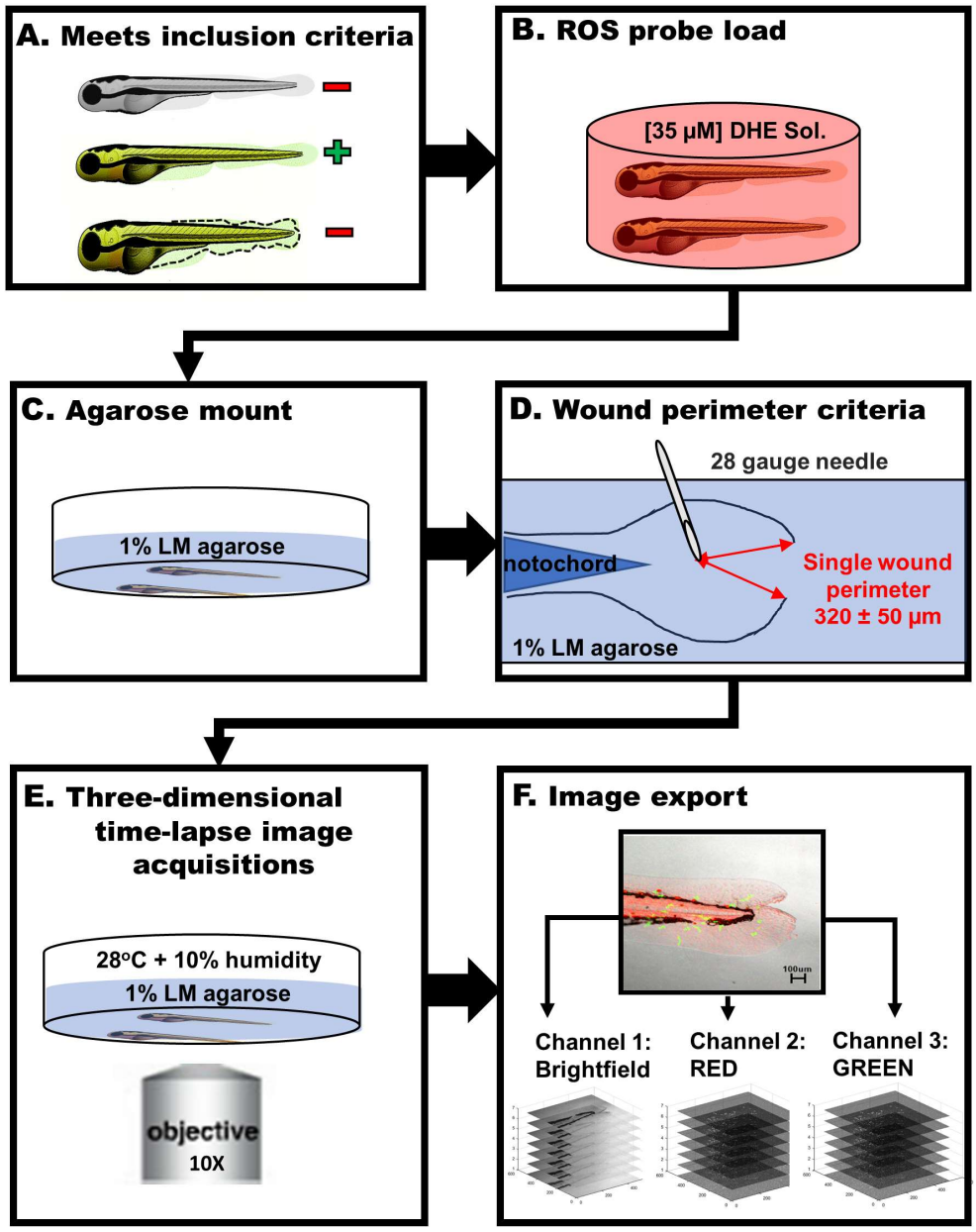

Figure 4. Zebrafish image-based assay workflow schematic. **A.** Zebrafish larvae selected for image-based assay had to meet an inclusion criterion based on physiological and fluorescence quality. **B.** Fish selected were loaded with reactive oxygen species probe solution, Dihydroethidium [35 µM], that was optimized according to microscope setup. **C.** Fish were then mounting laterally in 1% Low melting temperature agarose as flat as possible. **D.** Once mounted fish were subjected specific injury resulting in "V" shaped wound perimeter (red) with a sterile 28-gauge needle to create a wound perimeter, **E.** Minutes post injury, fish were placed in a controlled 28°C temperature environment with 10% humidity and imaged in three-dimensional and time-lapse (3D +t) manner at 10X magnification to capture cell migration. Greyscale 3D+t digital images were exported into directories by channel: Brightfield, RED, and GREEN.

3.2.2. Imaging

A Zeiss LSM 510 confocal microscope was used with a NA 0.75/10X objective to image the zebrafish in time-lapse conditions. Two fluorescent channels (ch) were filtered with excitations 488 nm for dendra2 and 561 nm for ethidium were targeted at 0.80 and 0.08 mW respectively through ZEN® software. Three-dimensional time-lapse (3D+t) images were taken in 60 second intervals from 25 to up to 130 minutes' post injury (MPI). The lateral pixel resolution was 1.64 µm and the image dimensions were 512 x 512 pixels. Using microscope programed automation, up to 8 fish were imaged per session with at least one non-wound for group baseline comparative analysis. Z-stacks were comprised of 7 frames with 10 µm spacing along the Z axis. The typical larval zebrafish 3 dpf caudal fin demonstrated a depth approaching 100 µm in thickness while the typical larval zebrafish leukocyte demonstrated a depth ranging from 10-20 µm. Fluorescent macrophages were detected with various optical sections, overcoming the limitations of the NA 0.75/10X objective depth of focus of ~10 µm. Zebrafish Larvae were maintained on an enclosed microscope stage which maintained uniform conditions of 24ºC and 10% Humidity (

Figure *4*E). Greyscale images with 16 bits per pixel (BPP) were acquired and exported in TIFF file format from ZEN® software (

Figure *4*F). The TIFF files were stored within a unique experiment labeled directory. Raw images were exported to channel labeled folders: grayscale z-stack bright field (channel 1:BF); Texas Red fluorescent z-stack 561 nm (channel2: RED); GFP fluorescent z-stack 488 nm (channel 3: GREEN).

3.2.3. Overview of Software

Zebrafish **i**nflammatory **r**eactive oxygen species- and **m**acrophage kinetics- based **i**mage analysis, *Zirmi*, software was developed to enable a pipeline for automated batch image processing and quantitative comparative analysis. The analysis software consisted of four modules: module 1, raw data formatting and standardization (**Figure 5A-C**); module 2, image-based fluorescence probe quantitation (**Figure 5D-F**); module 3, image-based cell fluorescence spatial and temporal migration kinetics(**Figure 5G-I**); module 4, data management and consolidation into Excel (**Figure 5J-K)**. Additionally, supportive figures can be automatically exported to PowerPoint via *Zirmi* when applicable.

Module 1: Three-dimensional time-lapse data format

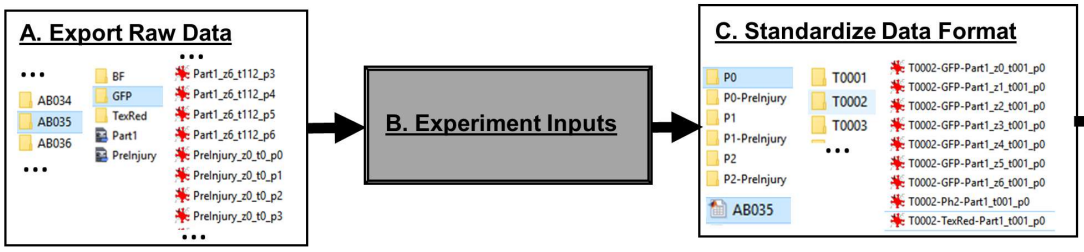

Module 2: Three-dimensional time-lapse fluorescent probe quantitation

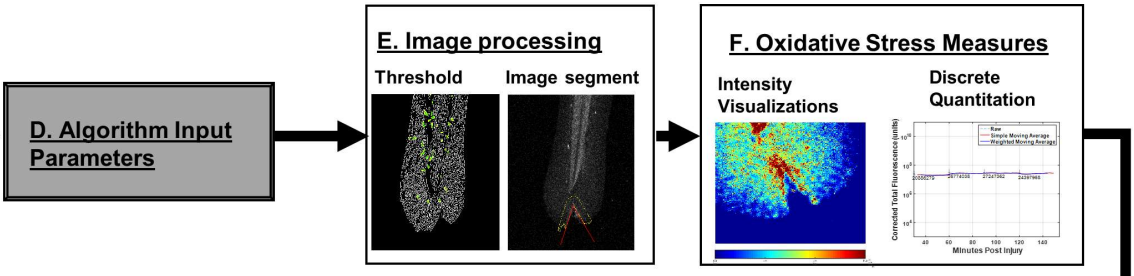

Module 3: Three-dimensional time-lapse cell trajectory kinetics quantitation

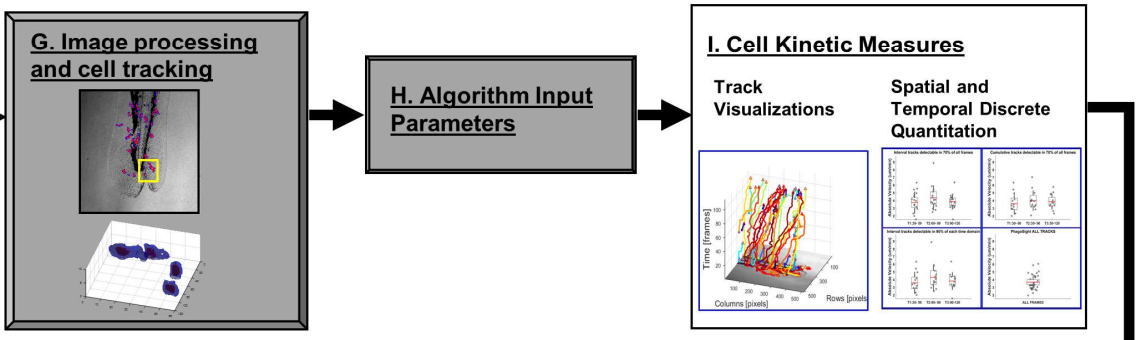

Module 4: Database management

J. Amendable Excel (.xls) oxidative stress measures (CTF) over time

MPI	AB036_P0	AB036_P1	AB036_P2
30	3212655	3212654.565	6019816
60	3400921	3400920.522	5673592
90	3322539	3322539.153	5782952
120	3484150	3484149.642	5684056

K. Amendable Excel (.xls) cell Kinetics measures over time database

WorC	Name	sec per Frame	MPI	AbsVel um/min	Staticity (0 to 1)	Meander (0 to 1)	SD AbsVel
2W	AB035_P0	60	28	2.42681	0.48573	0.386097	1.6013924
W	AB035_P1	60	28	4.36859	0.46132	0.315245	2.2574483
C	AB035_P2	60	28	1.32621	0.31725	0.234459	1.2690029

Figure 5. *Zirmi* software image analysis pipeline schematic. *Zirmi* software progresses raw data through 4 modules in an automated fashion. In module 1, three dimensional time-lapse raw digital images (**A**) and experiment relevant inputs (**B**) are standardized into directories to facilitate throughput processing (**C**). Next, module 2 takes user-input parameters (**D**) to specify image processing algorithms (**E**) for image-based discrete oxidative stress measures over time (**F**). In module 3, *PhagoSight* algorithms are ran from formatted directories for throughput cell tracking (**G**). User-input parameters (**H**) are then used to customize algorithms to control outcomes and visual tools for context (**I**). Lastly, in module 4 the information gathered from the previous three modules are consolidated into Excel databases that are automatically updated as more raw data is analyzed through the analysis pipeline (**J, K**).

3.2.4. MATLAB Implementation

The *Zirmi* Software was developed in MATLAB R2015a. To streamline user inputs a graphical user interfaces were created to facilitate global access across modules. These user inputs were stored into databases within uniquely generated. mat files that were amendable. Once stored user inputs were used to standardize heterogeneous imaging as well as provide custom algorithm parameters (**TABLE VII, Appendix A**). The following imaging inputs were requested and used to standardize outcome measures: minutes post injury (MPI), sampling frequency (minutes per frame), image lateral resolution (pixels per micron), z-stack resolution (microns per stack), and bits per pixel.

(a) Fluorescent probe image analysis steps*:* (1) RED composite digital images were created by fusing all respective 2D sections together, scaling the intensities of each image jointly; (2) employ median Gaussian filter to remove Poisson noise present in confocal imaging due to a statistical variation in the number of detected photons; (3) define **parameter 1 (**pixel threshold) to image segment fish tissue; (4) employ morphological filters, using a kernel with radius of 20 pixels, to erode spurious pixels; (5) define **parameter 2** (ROI) by outlining wound margin in BF image; (6) employ **parameter 3** (μm), the radial distance extended from the wound margin, to define wound ROI area, inclusive of only fish tissue via image

segmentation algorithms; (8) define **parameter 4** (ROI), background region(s) are selected at users discretion for $\mathbf{B(t)}$ average background fluorescence intensity determinations per time point, "t"; (9) employ background subtraction, where $\mathbf{X(t)}$ is the wound ROI based pixel intensity average at time point "t", with the following equation:

$$\boldsymbol{\Delta X = X(t) - B(t)} \qquad (3)$$

(10) calculate Integrated Density ($\boldsymbol{IntDen}(t)$) with wound ROI area ($\boldsymbol{A(t)}$) with the following equation:

$$\boldsymbol{IntDen}(t) = \boldsymbol{A(t) * X(t)} \qquad (4)$$

(b) Fluorescent cell image analysis steps: (1) employ *PhagoSight*, a detailed description of this method can be found at (http:/*PhagoSight*.org) (Henry et al. 2013), to avoid erroneous and manual tracking → Set GREEN image stack as 0 to 7 and BF as 8-9 → Set low and high threshold to optimize cell-to-cell segmentation and attenuate noise verified by visualization tools → Set minimum cell size surface area as 80 pixels^2 → save uniquely generated keyhole tracking file, 'handles' into standard directories → use visualization tools for quality control to verify distinguished tracks and eliminate collisions and artifacts; (2) For consistency, instantaneous speed, distance between tracks, net distance, max distance, and meandering index were algorithmically derived according to literature (Svensson, Medyukhina, Belyaev, Al-Zaben, et al. 2017); Pixel coordinate based centroid positions <**x**,**y**,**z**> from '*handles.nodeNetwork*' struct array, used for spatial referencing of successfully tracked macrophage ('*Mp'*) at different time frames ('*t')* , were placed in a matrix array or ***P(t);*** to determine absolute velocities, the Euclid distance between original [$\mathbf{x_o,y_o,z_o}$] and subsequent

[x_1,y_1,z_1] centroid positions in a z-stack were computed per ***P(t)*.** Only single frame successive centroid position per macrophages were used and placed in cell array $R_p(t)$; . (3) tracks were further standardized to minimize strenuous proofing with amendable parameter conditions to customize algorithms to user needs with the following parameters→ **parameter 5** (%), cell track inclusion criteria based on percent of distinguishable centroid position relative to frames → **parameter 6** (μm), maximum distance traveled by cell to be considered static: To determine a quantifiable metric for the time macrophages spent not moving or moving slow, Stasis $K_p(t)$ was determined; Stasis threshold was set to approximately 10% of macrophage surface diameter, equal to 0.9 μm (**parameter B,** user customizable):

$$\boldsymbol{Kp(t)} = \begin{Bmatrix} 1, & \boldsymbol{Rp(t)} > parameter\ 6 \\ 0, & parameter\ 6 \leq \boldsymbol{Rp(t)} \end{Bmatrix} \qquad (5)$$

Therefore, the following formula was used to compute, Static Ratio, L_p per cell track in *'n'* frames:

$$\boldsymbol{Lp} = \frac{[\sum_{t=1}^{n} \boldsymbol{Kp(t)}\,]}{n} \qquad (6)$$

→ **parameter 7** (centroid position, S_o**),** epicenter of the wound gap or position of interest → **parameter 8** (centroid position, N_o,) notochord tip or position of interest, used to define S_1 spatial domain → **parameter 9** (μm), radial distance used to define spatial domains S_2, S_3 and S_4; (4) derive direction based kinetic from parameters → macrophage centroid positions were oriented with respect to S_o, for discrete oriented net Euclid vector distances (μm) to wound determinations → Forward Migration Index (FMI) quantified the discrete movements toward wound assigned 1 or 0 and takes the ratio between the progress in the "wound"

direction by a cell and the total distance → Forward to Backward Index (FBI) (1 to -1), quantified as (Forward movements – Backward movements / Total movements).

3.2.5. Statistical Analysis

Statistical analysis of the data was performed by paired and unpaired Student T test for parametric data via Microsoft Excel. Wilcoxon signed-rank test was used to test the hypothesis of zero median for the difference between paired samples via MATLAB®. Differences were considered significant at $p<0.05$.

3.3. Results

3.3.1. Module 1: Data Formatting of Standardized Three-dimensional Time-lapse Imaging

The main goal of this software was to automate time-based quantitative measures of the changes in oxidative stress (channel 1 fluorescence) and macrophage (channel 2 fluorescence) kinetics within thousands of images per fish. A central limitation in throughput image analysis arises from inadvertent three-dimensional time-lapse (3D+t) imaging disturbances and unavoidable heterogeneity of batch-to-batch image acquisitions. To circumvent compromising data and time, assays are attuned to strict standardizations (

Figure *4*). Voided from imaging analysis are fish absent of fluorescence and fish experiencing inadvertent nicks or breaches in tissue leading to an inflammatory response. Reactive oxygen species probe loading, and prolonged imaging preparation are performed in agreement with accepted and published experimental strategies (Mugoni, Camporeale, and Santoro 2014b, Owusu-Ansah, Yavari, and Banerjee 2008). Injury margins are created by V-shaped incisions within the caudal fin and consistent in location and wound perimeter size. Digital greyscale images are formatted by channel (GREEN, RED, and BF) and archived into subdirectories according to batch, position of acquisition sequence (P0, P1, P2…etc.), and frame

(T0001, T0002, T0003…etc.). Ultimately, to permit an automated analysis pipeline (**Figure 5**), respective subdirectory contains images distinguishable by channel with all stacked images respective to that batch, position, and time frame. Lastly (.mat) files are created with user-inputs (**TABLE VII, Appendix A**) to standardize future data measures regardless of heterogeneity of imaging.

3.3.2. Module 2: Fluorescent Probe Image Analysis

The second module we tackled was to automate discrete image-based oxidative stress determinations of injuries (**Figure 6A-6E**) for comparative analysis. To obtain absolute quantitation capable of comparative analysis, unwounded (baseline) caudal fins needed to first have an automated approach. Region of interests (ROI's) pixel areas, $\boldsymbol{A_o(t)}$, were determined by using 40, 10-pixel diameter, circles placed within unwounded caudal fin (**Figure 6G**), extending beyond the notochord. This enabled stochastic determinations of fluorescent intensity baseline values, to calculate Integrated Density, see methods. To calculate unwounded fin's Corrected Total Fluorescence, CTF, background intensity values, $\mathbf{B(t)}$, were used in the following equation:

$$\boldsymbol{CTF_o(t)} = (\boldsymbol{IntDen(t)}\ of\ Unwounded\ fin) - (\boldsymbol{A_o(t)} * \boldsymbol{B(t)}) \quad (7)$$

Next, for wounded fins, wound size and erroneous manual tracing biases needed to be eliminated. To circumvent manual tracing errors, V-shaped wounds were leveraged to accurately determine intensity values of interest. For larval zebrafish 3 days post fertilization a 65 μm extended perimeter (yellow) surrounding the wound margin (red) (**Figure 6H-6I)** was used to form a robust wound area $\boldsymbol{A(t)}$ over the course of time, '**t**'. Next to circumvent area size-based bias, correction was employed through Integrated Density correction, through established

literature (McCloy et al. 2014). In this manner, the following equation was used to automate Corrected Total Fluorescence, $\boldsymbol{CTF(t)}$, quantitative measures with user-defined check points for manual reselecting of ROI if necessary over the course of time, '**t**',

$$\boldsymbol{CTF(t) = IntDen(t) - (A(t) * X_o(t))} \quad (8)$$

where $\boldsymbol{X_o(t)}$ is the background subtracted fluorescent intensity of baseline over time, '**t**'. This standardized method of selecting wound region provided automated CTF measures on a time-lapse frame-by-frame basis. *Zirmi* pipeline further permitted ROI adjustments on a frame-by-frame basis whenever necessary to remain precise regardless small fin shifting. Measurable V-shape wounds with simple ROS probe strategies provided a uniform method for imaging analysis to standardize oxidative stress measures. **Figure 6** visualizations are automatically displayed in MATLAB and exportable, at user's discretion, to facilitate contextual understandings and to correct ROI's in a meaningful way.

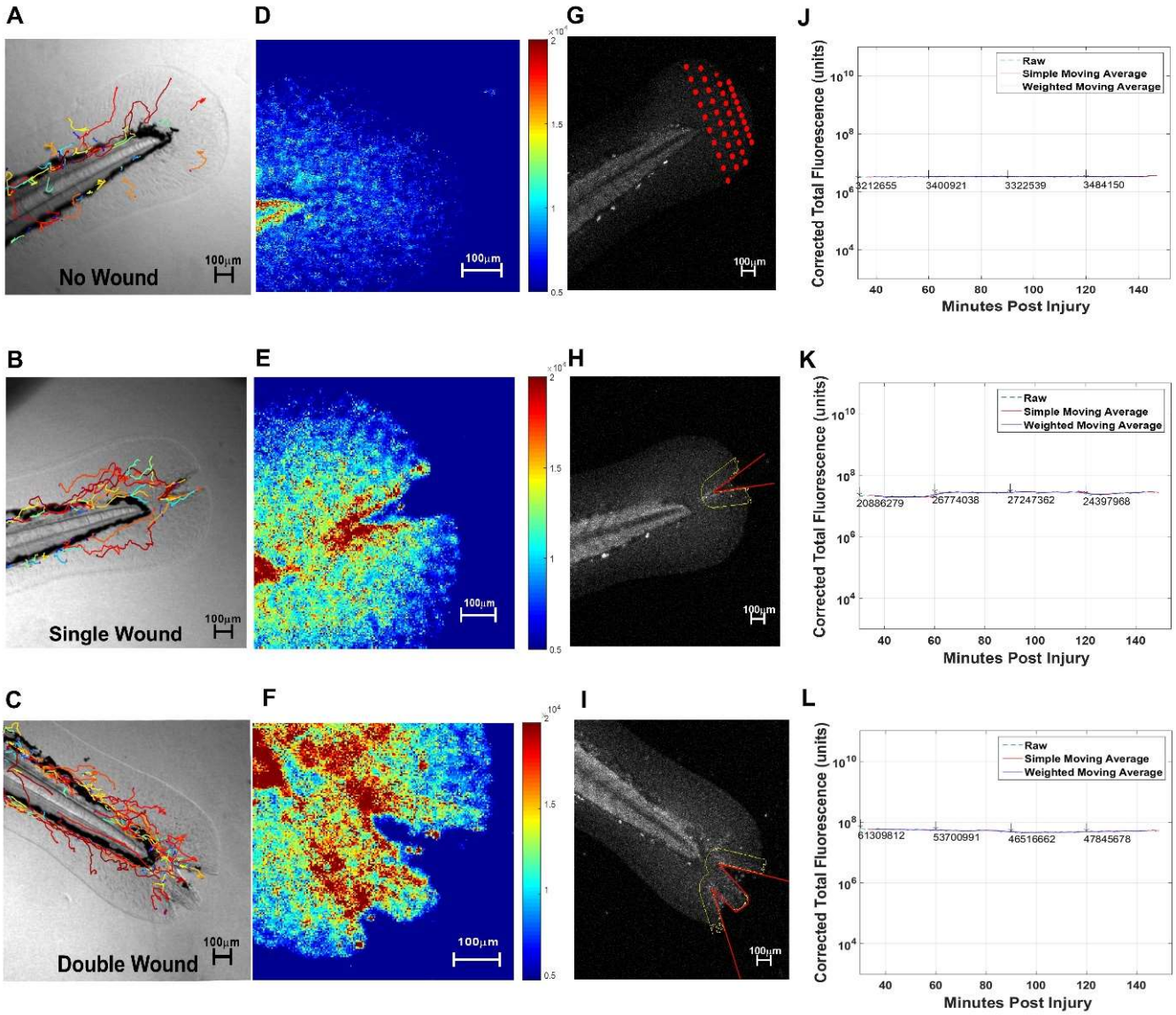

Figure 6. *Zirmi* module 2 - reactive oxygen species probe image analysis. Macrophage migration patterns of unwounded control zebrafish (**A**), single wound (**B**), and double wound (**C**) can be detected in parallel with caudal fin oxidative stress (**D,E,F**). 40 discrete 10 µm diameter circles in unwounded fins are used for capture background fluorescence regions of interest, ROIs (**G**). For wounded fins a uniform user-defined distance (yellow line - 65 µm) from wound perimeter (red line) was used to define wound ROI (**H,I**). Using these ROIs, the Corrected Total Fluorescence was discretely determined in an automated manner overtime per fin injury type (**J,K,L**) to form databases and visualization tools that could be exported to Excel and PowerPoint, respectively

3.3.3. Module 3: Fluorescent Cell Kinetic Image-based Spatial and Temporal Quantitation

The third module of our image analysis pipeline was directed toward user-friendly throughput and uniform cell tracking for more granular cellular kinetic measures. However, tracks are user intensive and require several rounds of visual proofs to extract information worthy of comparative analysis. To tackle this obstacle a robust keyhole modeling solution, via *PhagoSight ,* was implemented to determine macrophage centroid (3D+t) positions (

Figure 7A, 7B) regardless of image-set size. Further, to overcome constraints of single cumulative measures in one spatial or temporal domain (Svensson, Medyukhina, Belyaev, Al-Zaben, et al. 2017), *Zirmi* adapted customizable algorithm parameters (**TABLE VII, Appendix A**). User-defined parameters permitted streamline proofing and quality control selection of tracks based on time and space. As a results, quantitative data measures incorporated descriptive metric outcomes, such as average speed, meandering index, and net distance toward wound, to provide a simple and well accepted mode of evaluating persistence and direction (Svensson, Medyukhina, Belyaev, Al-Zaben, et al. 2017). Alternative inferential measures require assumptions, such as, isotropic or ergodic conditions, relying heavily on finding the right representation of data which can bottleneck reproducibility and minimize utility of image data (Loosley et al. 2015). *Zirmi* adaptation of simple measures permitted automated elimination of confounders; if a cell centroid position was not identifiable at any frame then measures were equally absent from discrete and averaged data sets. This provided another dimension to proofing and selecting tracks, minimizing assumptions and saving time. To standardize track selection, a track selection criterion was implemented to group tracks and respective measures according at user's convenience. First, track that met a user-defined percent of distinguishable

centroid positions were selected. This eliminated enabled relatively equal impact of measures from track to track; temporally shorter tracks can skew quantitative evaluations. Second, tracks could be grouped according to time domains [T_1 = 30-59 MPI; T_2 = 60-89 MPI ; T_3 = 30-60 MPI ; T_1 = 30-60 MPI ; T_1 = 30-60 MPI] (

Figure *7*B, 7C). And thirdly, tracks could be grouped according to spatial domains [S_1,S_2, S_3, S_4,] originating from S_o (

Figure *7*D, 7E), as defined in Methods . Using *Zirmi,* customizable parameters permit permutations of spatial and temporal domains, for more granular or cumulative derivations for comparative analysis. Measures are grouped according to these track selection criteria on a single fish basis, provided significant changes when compared than all-inclusive averages (**TABLE VIII, Appendix A)**.

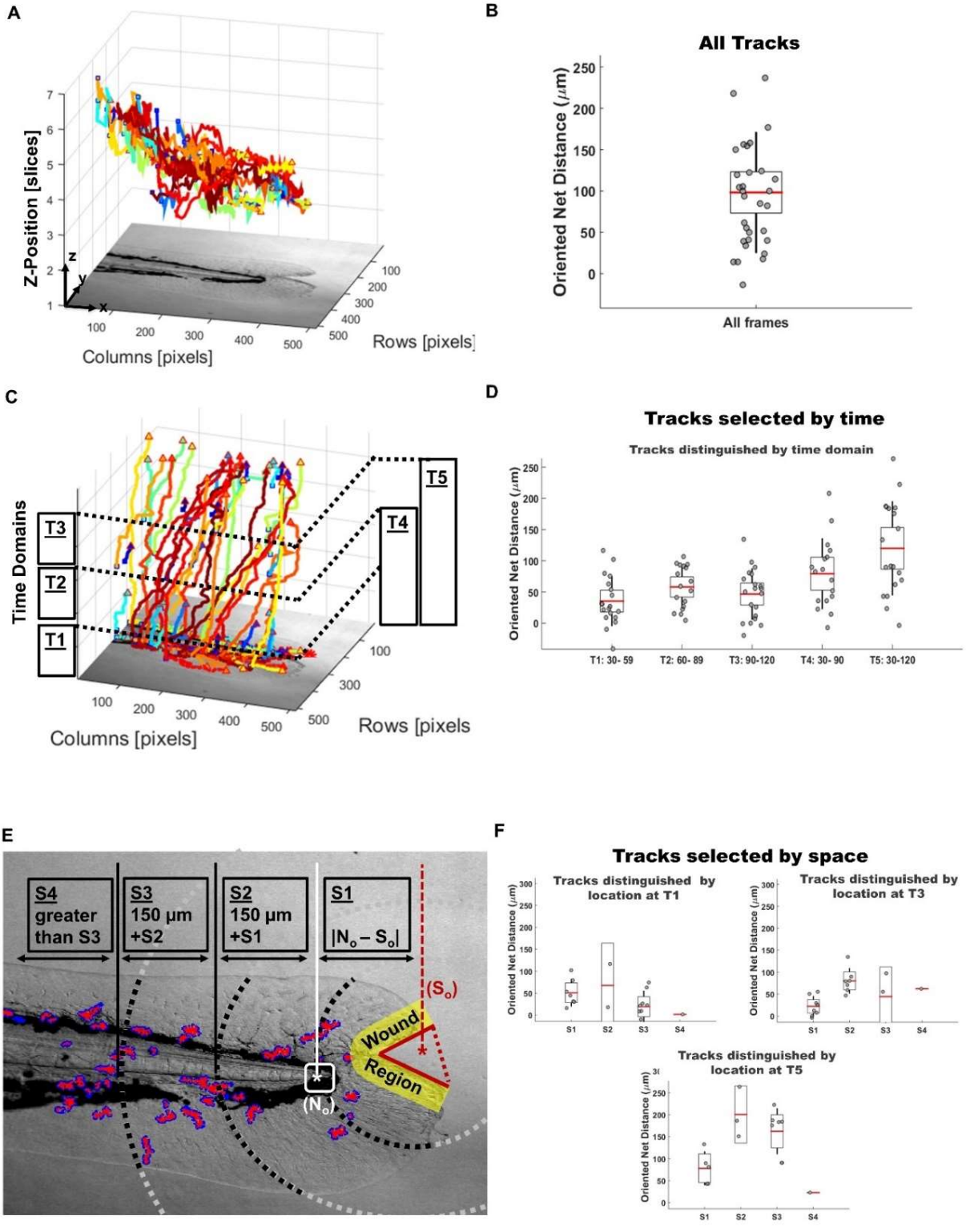
A
Z-Position [slices]
Columns [pixels]
Rows [pixels]
B
All Tracks
Oriented Net Distance (μm)
All frames
C
Time Domains
T1
T2
T3
T4
T5
Columns [pixels]
Rows [pixels
D
Tracks selected by time
Tracks distinguished by time domain
Oriented Net Distance (μm)
T1: 30- 59
T2: 60- 89
T3: 90-120
T4: 30- 90
T5: 30-120
E
S4 greater than S3
S3 150 μm +S2
S2 150 μm +S1
S1 |N_o – S_o|
(S_o)
Wound Region
(N_o)
F
Tracks selected by space
Tracks distinguished by location at T1
Tracks distinguished by location at T3
Tracks distinguished by location at T5
Oriented Net Distance (μm)
S1
S2
S3
S4

Figure 7. *Zirmi* module 3 –cell migration image analysis. Macrophage discrete positions in the tail were tracked via *PhagoSight* keyhole modeling in a three-dimensional and time-lapse manner (**A**) to derive all cell tracks inclusive of all frames (**B**). With discrete position information, tracks were then parsed by time domains (**C**) to derive time-based changes (**D**). Selection of tracks by space was done by outlining the wound perimeter (red solid line) to get the wound epicenter (red asterisk) by which the user can use to segment by wound region (yellow) and additional space domains S1 (via white asterisk), and S2, S3, S4 (**E**). With these selection criteria tracks could be grouped by time and space (**F**) on outcome measures ranging from speed, meandering index, static ratio, net distances, and direction. Selected tracks were plotted on MATLAB (**B,D,F**) exportable to PowerPoint and discrete values exportable to Excel.

3.3.4. Validation and Speed

A spatial overlap index, Dice Similarity coefficient (DICE), was used to measure reproducibility between manual and automated methods of segmentation of cells, fish tissue, and wound region over a 90-frame single wound imaging-set. DICE has been adopted to validate various image segmentations of clinical relevancy and a value > 0.7 is considered to be effective overlap (Zou et al. 2004).

$$\mathbf{DICE} = 2 * \frac{|\boldsymbol{X} \cap \boldsymbol{Y}|}{|\boldsymbol{X}| + |\boldsymbol{Y}|} \quad (9)$$

DICE reproducibility validation metric ranged from 0, no spatial overlap to 1, complete overlap. We observed *Zirmi* incorporated automated image processing methods to be as effective as manual image processing strategies with up to 10-fold increase in speed execution (**TABLE III**). Manual methods were created in MATLAB scripts using available generic single imaging processing workflows **(SCRIPT 1, Appendix B)**. However, manual image processing strategies of a reproducible "V"-shaped wound, as performed in *Zirmi* (**SCRIPT 2, Appendix B)**, was difficult and highly prone to user error. Therefore, execution speeds of manual methods for wound region represented the time it would take to perform manual wound tracings at users best judgment (**SCRIPT 3, Appendix B)** compared to *Zirmi* automated strategy. To this effect the

DICE measure of the wound region represented the *Zirmi* method's first wound region spatial overlay to all respective future *Zirmi* time point wound region image segmentations.

TABLE III. ACCURACY VERIFICATION AND EXECUTION TIME OF *ZIRMI* IMAGE ANALYSIS PIPELINE

	Accuracy verification	***Zirmi* execution speed**	
Time-lapse image segmentation	***DICE***	***Time [s] Automatic***	***Time [s] Manual***
Module 2 -Wound Region	0.84. ± 0.07	160 ± 16	2 020 ± 157
Module 2 -Caudal Fin Tissue	0.90 ± 0.18	122 ± 10	5 110 ± 233
Module 3 - Macrophages	0.78 ± 0.2	977 ± 512	3 740 ± 912
***DICE**, Dice similarity coefficient*			

3.3.5. Module 4: Representative Experiment For Database Comparative Analysis

Finally, to test the assembly and utility of the *Zirmi* modular analysis pipeline we compared differences in macrophage migration and oxidative stress, in parallel, based on wound severity; no current analysis pipeline exists (**TABLE IV)**. Test experiment data was gathered from *Tg(mpeg-dendra2)* zebrafish 3 dpf with three caudal fin wound severity conditions: unwounded (n=4); single wound with a wound perimeter averaging a total length of 320 ± 10 µm, (n=4); and doubly wounded with a wound perimeter, 544 ± 59 µm (n=4, $p<0.0001$) 1.7-fold larger than single wound perimeters. Imaging was performed with 90 frames (60 seconds sampling frequency), with 3 different channels (RED,GREEN, and BF) at 7 optical sections per frame (10 µm apart) resulting in 1890 images just in a single fish to analyze in an automated manner. Raw data was ran through Module 1, 2, 3 and 4 consolidating databases of fish based

on wound severity to Excel for comparative analysis. To facilitate standard uniform measures, wound regions were selected with a 65-um radial distance from the wound perimeter (**Figure 6D-6F**). Track selection consisted of 30-minute based time domains (

Figure *7*B), with cell centroid positions detectable within 70% of frames. Tracks were oriented toward the epicenter of the wound gap (selected as $S_{o,}$

Figure *7*E). In baseline unwound fish, the most distal position of the caudal fin was selected as S_o. Briefly, we observed severity of wounding to be associated with quantitatively higher levels of ROS and more rapidly responding macrophages as demonstrated by increased velocities, decreased static activity, and increased recruitment to the wound sites over time **(**

TABLE V) **(Figure 12, Appendix A)**. A 2- to 3-fold increase in ROS from unwounded (0.9 ± 0.2 x10^7) to singly wounded (2.2 ± 0.5 x10^7) caudal fin averages, and an additional 2- to 3-fold increase from singly wounded to doubly wounded (5.4 ± 0.4 x10^7) caudal fins cumulatively over time. In doubly wounded caudal fins, velocity was significantly higher than singly wounded or unwounded fins ($p=0.006$). Static movements, defined as 0.9 μm or less, were measurably more prominent in uninjured caudal, when compared to singly wounded fins. Overall, significant differences observed between interval and cumulative analysis emphasized the dynamic changes that can be easily detected in macrophage kinetics by track selection criteria and Corrected Total Fluorescence values.

TABLE IV. ADVANCES IN REAL-TIME QUANTITATIVE SIMULTANEOUS CELL TRACKING AND ROS IMAGING

First author	Cell tracking method	Quantifiable cell tracking	Automated cell tracking	ROS imaging	Quantifiable *in vivo* ROS measure	Automated ROS measure
Koopman (2006)	not available	not available	not available	Single cell *ex vivo*, flow cytometric; real time unavailable	not available	not available (single timepoint measures)
Owusu-Anshah (2008)	not available	not available	not available	Dihydroethidium (DHE) fluorescent probe for real time live tissue imaging in *Drosophila*	not available	not available (single qualitative measures)
Hall (2009)	Image J	no solution provided (requires additional software)	time-lapse cell tracking; additional tools required for visual proofing	not available	not available	not available
Pase (2012)	not available	not available	not available	Metamorph fluorescent HyPer H_2O_2 imaging	HyPer fluorescent intensity ratio measure	not available
Walker (2012)	not available	not available	not available	no image-based solution available; relies on fluorescent microplate reading; cannot detect wound region	ARQiv microplate whole fish detection	high throughput
Henry (2013)	*PhagoSight,* MATLAB	quantitative with data checking feature	Opensource, package; automated method for cell tracking and single time domain data measures;	not available	not available	not available

Mugoni (2014)	not available	not available	not available	Single cell *ex vivo* fluorescent probe based	not available (flow cytometric based)	not available; (single timepoint measures)
Wang (2016)	single image-based cell counts	not available	not available	Not available; PCR based	not available	not available
Zhang (2016)	not available	not available	not available	Single cell and whole fish fluorescent-probe based imaging	fluorescent-intensity – method not provided	not available; (single timepoint measures)
Jelcic (2017)	not available	not available	not available	Real-time image-based measures of HyPer within zebrafish wounds	corrected HyPer fluorescent intensity ratio-based measures	Image J, MATLAB, and Python methods used for specific automation

3.4. Discussion and Conclusions

The decision to create an opensource image analysis pipeline, *Zirmi*, was based on a lack of readily available and customizable software solutions capable of automating quantitative assessment of fluorescence outcome measures within the zebrafish model. *Zirmi* prompted user-friendly interfaces to customize algorithm parameters by which users could specify or balance the quality of measures relevant to their investigative purposes. To demonstrate utility to *Zirmi* image analysis pipeline wounding severity and oxidative stress were investigated. Results add to previous studies defining early wound macrophage recruitment (Ellett et al. 2011, Hall et al. 2009, Li et al. 2012b, Gray et al. 2011). These findings emphasize the importance of standardized automated analysis pipelines for experimental conditions, such as wound size, for accurate evaluations of oxidative stress and macrophage migration.

TABLE V. COMPARISON OF GROUP ZEBRAFISH AVERAGE ROS GENERATION & AVERAGE MACROPHAGE SPEED, STATIC RATIO, AND WOUND RECRUITMENT

Time frame (minutes)	*Zirmi* 30-59	*Zirmi* 60-89	*Zirmi* 90-120	*Zirmi 45*	*Zirmi 60*	*Zirmi* 90	*Zirmi* 120
	Velocity [µm/min]	***Velocity [µm/min]***	***Velocity [µm/min]***	***Mϕ # at Wound***	***Mϕ# at Wound***	***Mϕ# at Wound***	***Mϕ# at Wound***
No Wound (NW)	3.07 ± 0.06	2.88 ± 0.40	2.70 ± 0.40	N/A	N/A	N/A	N/A
Single Wound (SW)	3.65 ± 0.4	4.04 ± 0.14	4.27 ± 0.48	2 ± 1	4 ±1	5 ± 1	6 ± 1
Double Wound (DW)	4.43 ± 0.35	4.21 ± 0.20	4.12 ± 0.21	4 ± 1	6 ± 2	7 ± 1	8 ± 1
	P values						
NW vs SW	** p=0.049*	***p=0.003*	***p=0.006*	*N/A*	*N/A*	*N/A*	*N/A*
NW vs DW	***p=0.003*	** p=0.005*	***p=0.001*	*N/A*	*N/A*	*N/A*	*N/A*
SW vs DW	**p=0.02*	*n.s. p=0.2*	*n.s. p=0.3*	**p=0.03*	*n.s. p=0.06*	**p=0.04*	**p=0.04*
	Static Ratio (0 to 1)	***Static Ratio (0 to 1)***	***Static Ratio (0 to 1)***	***CTF 10^6***	***CTF 10^6***	***CTF 10^6***	***CTF 10^6***
No Wound (NW)	0.60 ± 0.21	0.59 ± 0.20	0.61 ± 0.19	0.91 ± 0.27	0.90 ± 0.21	0.9 ± 0.24	0.94 ± 0.2
Single Wound (SW)	0.32 ± 0.1	0.23 ± 0.08	0.25 ± 0.04	2.34 ± 0.72	2.17 ± 0.53	2.13 ± 0.4	2.15 ± 0.2
Double Wound (DW)	0.18 ± 0.07	0.20 ± 0.07	0.24 ± 0.07	5.92 ± 0.32	5.58 ± 0.4	5.22 ± 0.5	5.0 ± 0.28
	P values						
NW vs SW	**p=0.01*	** p=0.01*	**p=0.01*	**p=0.03*	**p=0.02*	*** p=0.004*	*** p=0.001*
NW vs DW	** p=0.01*	** p=0.01*	** p=0.02*	**** p<0.0001*	**** p<0.0001*	**** p<0.0001*	*N/A*
SW vs DW	**p=0.04*	*n.s. p=0.3*	*n.s. p=0.4*	**p=0.04*	***p=0.001*	**** p=0.0001*	**** p<0.0001*

Mϕ, Macrophage; #, number; CTF, Corrected Total Fluorescence; N/A, Not applicable; n.s., Not Significant. Unpaired T-Test (*p<0.05,* *p<0.01, ***p<0.001, n.s. > 0.05)

To develop an automated process, we defined attributes of the wound for a standardized approach. We used a V-shaped incision within the caudal fin which differed from other caudal fin wounding methods, in which amputations were applied orthogonally to the notochord line. V-shape wounds provided a reproducible and measurable injury that imaging processing tools could use to standardize both wound oxidative stress and cell kinetic-based outcome measures. In our hands, we observed caudal fin amputations to result in a large single wound line which made tracking and localizing cells within the wound proximity problematic; wound orientation was too broad and cell clustering was increased making it difficult to algorithmically separate and track cells (data not shown). Another standardization was the definition of the wound perimeter. We observed that a larger wound margin consistently demonstrated a significantly larger inflammatory response with increased oxidative stress and increased macrophage activity. To allow automated comparisons between experiments, wound perimeters were defined; we believe that these boundaries set automatically can improve the accuracy of quantitative measures in oxidative stress and macrophage migration. Other standardizations include the use of non-wounded areas of the fish to serve as standardized background calculations for the detection of ROS.

The selection of DHE as a probe for ROS was based on prior reports of reliability with quantitative measures in other applications (Mugoni, Camporeale, and Santoro 2014b, Owusu-Ansah, Yavari, and Banerjee 2008). Our automated approach enables quantitative real time measurements, which is an advantage over existing methods that have been accomplished *ex vivo,* either through proteomic assays (Mugoni, Camporeale, and Santoro 2014b), flow cytometry (Owusu-Ansah, Yavari, and Banerjee 2008), or through HyPer genetically encoded peroxide levels (Niethammer, Grabher, Look, and Mitchison 2009). Jelcic *et al.*, have reported

image-based software approach, incorporating multiple software's, to elegantly quantify hydrogen peroxide reaction-diffusion kinetics in zebrafish (Jelcic et al. 2017). This method provides a unique and sensitive means to measure H_2O_2 diffusion in real time using a radiometric biosensor. Our simplicity of method, which also quantifies ROS in real time, differs in that its method is designed to work with higher throughputs and is formatted to work with cell tracking. We observed Corrected Total Fluorescent values to be comparable across fish showing consistent, uniform, reproducible wound attributes. CTF allowed for comparative analysis of fish with differing wound severity. To address confounding areas of expression, we applied user proofing and manual tracing. To address the detection of DHE within the notochord as a potential confounder of wound ROS content in a standardized fashion, uniform wound distances of 65 um were defined as the limits of wound boundaries. In future applications, as fluorescent probes continue to improve in specificity (Zhang et al. 2016), we expect simple *Zirmi* opensource image-based quantitative methods to become even more effective.

Established *PhagoSight*, pre-processing and keyhole algorithms, were integrated into *Zirmi* workflow to leverage current powerful existing solutions and to avoid parallel developments. *PhagoSight* keyhole modeling algorithms can provide data on the most probable landing position of a macrophage in a time-ordered set of coordinate points (Reyes-Aldasoro, Akerman, and Tozer 2008). This software has advanced the field in providing single measures in one space or time domain (Svensson, Medyukhina, Belyaev, Al-Zaben, et al. 2017). Such analytics are user intensive and may require several rounds of visual proofs for comparative analysis. To increase throughput, we have extended this knowledge base, adding standardized methods for automated capabilities. *Zirmi* software eliminates uncertainties from computations if not proofed and corrected by user. Alternative more inferential measures of migration

persistence and direction bias can be used, such as, mean squared displacement, turning angle distribution and tangent to tangent correlation and, persistent random walks as a tool for understanding the migration system of populations of cells (Liepe et al. 2016). These measures make inferential determinations implicitly dependent on the sampling interval, therefore, they are not reproducible without equivalent sampling intervals across every analysis and high fidelity of cell positions (Loosley et al. 2015). The advantage of *Zirmi* is that incorporates a user-friendly workflow to eliminate confounding effects of heterogenous batch imaging conditions, such as varying sampling acquisition.

Custom made non-generic image solutions are needed to answer specific biological questions in the zebrafish whole organism model that that are reliable (Mikut et al. 2013). The contribution of this work to the field is its ability to automatically process three-dimensional time-lapse images with amendable parameters for standardized quantitative measures. This enabled standardized quantitative evaluations of both oxidative stress and macrophage migration after injury over time. Defining early events of macrophage activity and their degree of response to ROS can provide critical insights for the development of wound therapeutics. Future studies will incorporate this method to define simultaneous changes in ROS and macrophage metrics, and to what extent these parameters are perturbed in normal and dysfunctional wound healing conditions.

CHAPTER 4

4. THE EFFECT OF FLUENCE ON MACROPHAGE KINTECS, OXIDATIVE STRESS, AND WOUND CLOSURE USING REAL-TIME *IN VIVO* IMAGING

4.1. Background and Rationale

Resolution of the inflammatory phase of wound repair is highly dependent on the recruitment and function of macrophages and removal of excessive oxidative stress (Ross and Odland 1968) . Excessive recruitment or prolonged retention, results in a persistent pro-inflammatory state leading to deficient wound healing. In diseased states, macrophage dysfunction can result in the failure to adequately remove neutrophils, which produce a large number of free radicals and corresponding oxidative stress within the wound (Ushio-Fukai 2009). Early neutrophilic recruitment and respiratory burst activity result in increased oxygen consumption through NADPH-oxidase (NOX), generating reactive oxygen species, ROS, superoxide anion ($O_2^{-\cdot}$) and peroxide, H_2O_2. NOX, in turn supports macrophage survival and promotes the phagocytosis of short-lived, neutrophils (Wang et al. 2007), initiating a necessary microenvironment for tissue regeneration. Excess ROS may impair macrophages, delaying the initiation of tissue repair and regeneration while low threshold levels may also impair wound healing due to insufficient levels to initiate macrophage phenotype switching to the more regenerative alternatively activated macrophages (Zhang et al. 2013). As a result, macrophages have a multifaceted role in mitigating oxidative stress and governing proliferative tasks critical to healing make them a sought after target for therapeutic intervention (Silva 2011, Koh and DiPietro 2015).

Photobiomodulation (PBM), most commonly delivered by red laser light near the 635 nm wavelength, has been reported to enhance cardinal functions such as phagocytosis and secretion

of chemical cues, crucial to oxidative stress clearance (Wynn, Chawla, and Pollard 2013, Silva 2011, Koh and DiPietro 2015, Chawla, Nguyen, and Goh 2011, Young et al. 1989, Karu et al. 1989, Lu et al. 2011, Souza et al. 2014, Fernandes et al. 2015). Further, some studies have suggested red laser light treatment promotes inflammatory resolution and wound closure (de Medeiros et al. 2017, Suzuki and Takakuda 2016, Figurová et al. 2016, Houreld 2014, Dawood and Salman 2013). Extension of *in vitro* studies to clinical trial has been promising (Kazemi-Khoo 2006, Houreld and Foot 2005, Heidari et al. 2017, Vaghardoost et al. 2018), however guidelines defining laser treatment settings of wavelength and duration are not yet established (Tchanque-Fossuo et al. 2016) . The wide range of fluencies studied both *ex vivo* (1 J/cm^2 to 30 J/cm^2) and *in vivo* to enhance macrophage function suggests a need for real time monitoring of macrophage response as well as their biochemical cues. Without such granular and *in vivo* contextual analyses, a consensus in defining precise parameters for low level red laser may lack precision and reproducibility (Wang et al. 2017, Tunér 2015).

The motivation for our work was to establish an *in vivo* model to interrogate the effects of a range of fluences on real time measures of macrophage kinetics and tissue oxidative stress and to correlate such effects with the pace of wound closure. The zebrafish model presents powerful transgenic phenotypes to facilitate *in vivo* real-time characterization of macrophage recruitment and oxidative stress after injury (Renshaw and Trede 2012, Ellett et al. 2011, Hall et al. 2009, Cvejic et al. 2008, Walters et al. 2010, Niethammer, Grabher, Look, and Mitchison 2009, Yoo et al. 2011). Insights on leukocyte migration behavior and reactive oxygen species generation at zebrafish wound sites have yielded high impact discoveries, providing novel insights translatable to mammalian systems (Lisse, King, and Rieger 2016, Niethammer, Grabher, Look, and Mitchison 2009, Oliveira et al. 2015, Robertson and Holmes 2014, Yoo et al. 2011). To track

individual macrophage trajectories following tissue injury, zebrafish, transgenic for a fluorescent macrophage marker, *Tg(mpeg-dendra2),* underwent dihydroethidium (DHE), loading to enable simultaneous fluorescent detection of macrophage movement and tissue levels of oxidative stress throughout long time-lapse imaging. Fish were injured at the caudal fin and treated with red 635 nm, 5 mW output power, at a treatment dose range supported by the literature (Huang et al. 2010, Hawkins, Houreld, and Abrahamse 2005, Hamblin 2017) (control), 3, 9, 18 J/cm^2. This model enabled studies of the effects of fluence from a constant wave source on macrophage responses and tissue oxidative stress in *real-time*. This powerful model will enable additional comparative studies on laser settings including wavelength, mode of delivery (intermittent vs constant) in a quantitative manner, providing greater precision in defining therapeutic settings.

4.2. Material and Methods

4.2.1. Zebrafish assay Preparation & Imaging

Zebrafish housing, experiment selection, wounding, and DHE probe loading were performed in accordance to methods described in **Chapter 3, Section 3.2.1 Zebrafish assay preparation.** Three-dimensional time lapse confocal imaging was performed in accordance to methods described in **Chapter 3, Section 3.2.2. Imaging.**

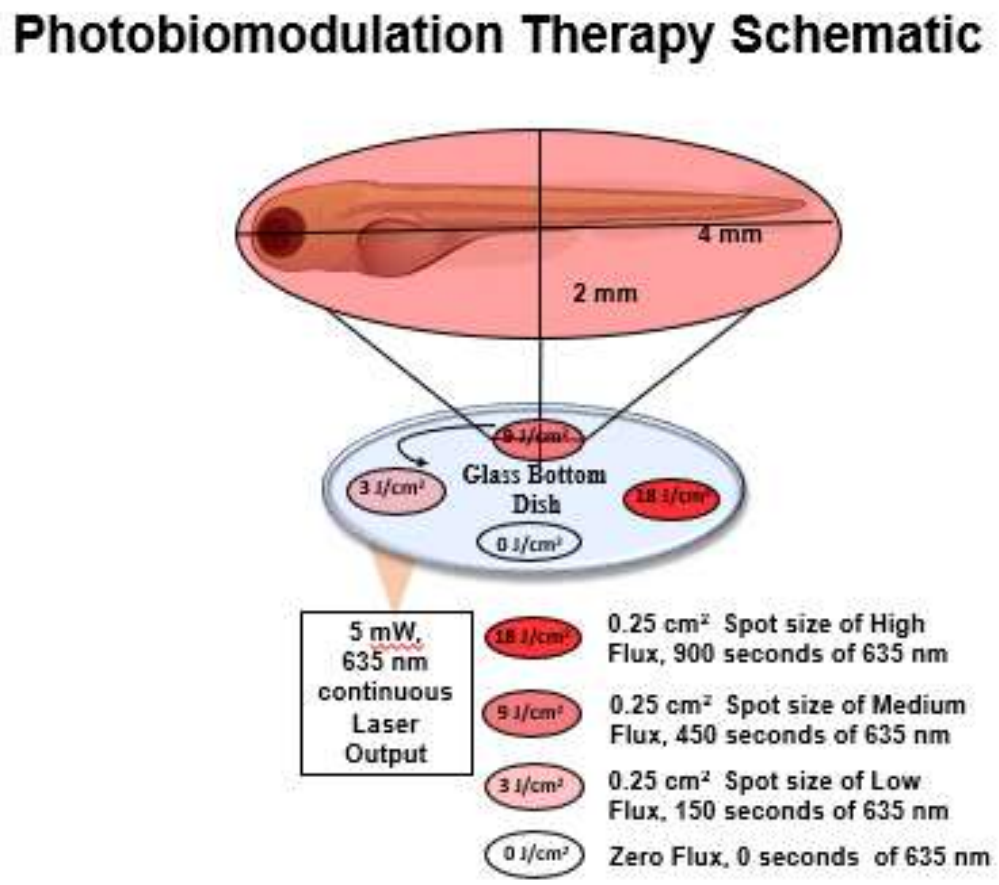

Figure 8. Photobiomodulation Therapy Schematic shows laser treatment schematic with a continuous laser of635 nm wavelength at 5mW output power. Laser is applied directly to the glass of 35 mm glass bottom dish to treat Fish. The entirety of the fish with a spot size of 0.25 cm^2 is treated with either 150, 450, or 900 seconds of irradiation for an energy fluence of 3, 9, and 18 J/cm^2, respectively.

4.2.2. Laser Irradiation for Time-lapse Imaging

Photobiomodulation laser treatment was administered through laser irradiation via a research grade 5mW (laser Power Source box: Zerona Medical Laser, Mode #: EML-2245; Erchonia Corporation, McKinney, Tx) emitting 635 nm continuous wave. Laser spot was elliptical at 0.25 cm^2 (4 mm x 2 mm) at delivery site **(**

Figure *8*). Laser dosing was quantified in energy fluency (unit Joules/cm^2) equivalent, **TABLE VI**. Larvae were randomly assigned 5 treatment groups; baseline no laser no injury, no laser control 0 J/cm^2 with injury, 3 J/cm^2 laser dose with injury, 9 J/cm^2 laser dose with injury, and 18 J/cm^2 laser dose with injury. Laser irradiation was initiated 5-15 minutes post injury.

TABLE VI. LASER TREATMENT PARAMETERS AT TARGET

Treatment groups by Energy fluence (J/cm^2)	**0 J/cm^2**	**3 J/cm^2**	**9 J /cm^2**	**18 J /cm^2**
Beam spot size (cm^2)	n/a	0.25 cm^2	0.25 cm^2	0.25 cm^2
Irradiance (mW/cm^2)	0 mW/cm^2	20 mW/cm^2	20 mW/cm^2	20 mW/cm^2
Radiant energy (J)	0 J	0.75 J	2.25 J	4.5 J
Number of points irradiated	n/a	1	1	1
Number of treatment sessions	0	1	1	1

4.2.3. Analysis of Time-lapse Images

All time-lapse images were analyzed using open source *Zirmi* software in MATLAB R2015a, as described previously in **Chapter 3**. Quantifying cells kinetic, measures were based on centroid positions, not whole cell morphology. Therefore, detailed morphological changes could were not distinguishable with the current analysis. Macrophage centroid positions were tracked using *PhagoSight* software's keyhole algorithm and visualization tools for proofing (Henry et al. 2013). Subsequently, *Zirmi* software was used to select macrophage tracks that

matched a selection criterion or of distinguishable centroid positions in over 70 % of all frames. Additionally, error prone tracks of macrophages near wound region were eliminated from analysis if they aggregated together. Macrophage migration was analyzed between (30 to 120) minutes post injury. Time intervals were defined as T1 [30 to 60 minutes post injury], T2 [30 to 90 minutes post injury], and, an overview time interval, T3 [30 to 120 minutes post injury]. To analyze the extracted data more efficiently wound regions were normalized, orienting positions with respect to the epicenter or Zero Position (S_o) of the wound margin for discrete distance to wound determinations. Baseline unwound fish, most distal position of the caudal fin was selected as the Zero Position. Centroid positions of zebrafish macrophages were used to compute spatial-temporal metrics of macrophage tracks respective to wound including: absolute velocity (μm/min), quantified as the average of each discrete movement per frame; static ratio (1 to 0), quantified as 1 when all movements per track exceeding as displacement 0.9 μm; meandering index (1 to 0), quantified as the vector distance length from start to finish over the discrete sum of distances traveled; wound oriented distance traveled (μm), quantified as Euclid vector distance from macrophage centroid to $S_{o;}$ forward movements (1 or 0) with positive net displaced wound oriented distances quantified as 1. Additionally, *Zirmi* software was used to manually trace wound region to isolate background subtracted DHE mean fluorescent intensity values approximately 65 μm radially extended from the wound margin.

4.2.4. Fin Regeneration Assay

Fish were mounted laterally in glass bottom dishes and imaged using a ZEISS inverted epi-fluorescent microscope in the first 60 minutes post injury. Immediately after, fish were treated with laser 0 (n=8), 3 (n=12), 9 (n=9), and 18 (n=10) J/cm^2 doses. After treatment, fish were maintained at 28^o C in E3 media and, 24 hours after injury, anesthetized and imaged again.

Total wound closure was reported as percent of wound closure. The wound perimeter was measured using ImageJ (NIH) for 1 hour and 24 hour fins per fish. Percent Closure (**R%**) was an evaluation of 24 hour wound closure defined as:

$$\boldsymbol{R\% = 100\ x\ \frac{1\ hour\ wound\ perimeter - 24\ hour\ wound\ perimeter}{1\ hour\ wound\ perimeter}} \qquad (10)$$

4.2.5. Statistical Analysis

In each group the means, standard deviation, and 95% confidence intervals of macrophage metrics, corrected fluorescent values, percent regeneration was calculated. Statistical Analysis was performed in GraphPad Prism and Microsoft Excel. Linear correlations were performed to derive Pearson r coefficients. P values were used for testing the hypothesis that there is no relationship between observed phenomenon (null hypothesis). P smaller than the significance level (0.05) was considered significant.

4.3. Results

4.3.1. Laser Dose Response of Oxidative Stress After Wounding

Control (

Figure *9*A) untreated fish demonstrated higher pixel (red) intensity values around the margin of injury ((

Figure *9*B) than red laser treated 3 J/cm^2 ((

Figure *9*C, 9D). DHE mean intensity values used to calculate geometric means and 95% confidence intervals at 60 and 120 minutes post injury of control (n=21) and dose groups 3 J/cm^2 (n=11), 9 J/cm^2 (n=8), and 18 J/cm^2 (n=8) ((

Figure 9E). At 60 minutes post injury a dose trend was noted as 3 J/cm^2 exhibited an overall 29 % ROS reduction in wound region (11 013.4 ± 2 000.59, p=0.03) compared to control fish (13 599.55 ± 1 563.5). In contrast, 9 J/cm^2 exhibited values were near control (14 108.78 ± 2 456.05, p=n.s.) and 18 J/cm^2 exhibited an overall 19% increase in ROS values (16 337.55 ± 2 893.64, p=n.s) at near wound region compared to control. At 120 minutes post injury, the 3 J/cm^2 treated group remained improved over control group, (p=0.01, significantly lower ROS than control), whereas the 9 J/cm^2 treated group had no significant effect (p=n.s.), and the 18 J/cm^2 group showed significantly increased ROS(p=0.02). At 120 minutes post injury, a more significant dose response was noted as 3 J/cm^2 oxidative stress (10 190.45 ± 1 674.98) was significantly 26% less than 9 J/cm^2 (13 753 ± 2 527.06, p=0.02), and was significantly 37% less overall than 18 J/cm^2 (16 161.02 ± 2 416.72, p <0.001).

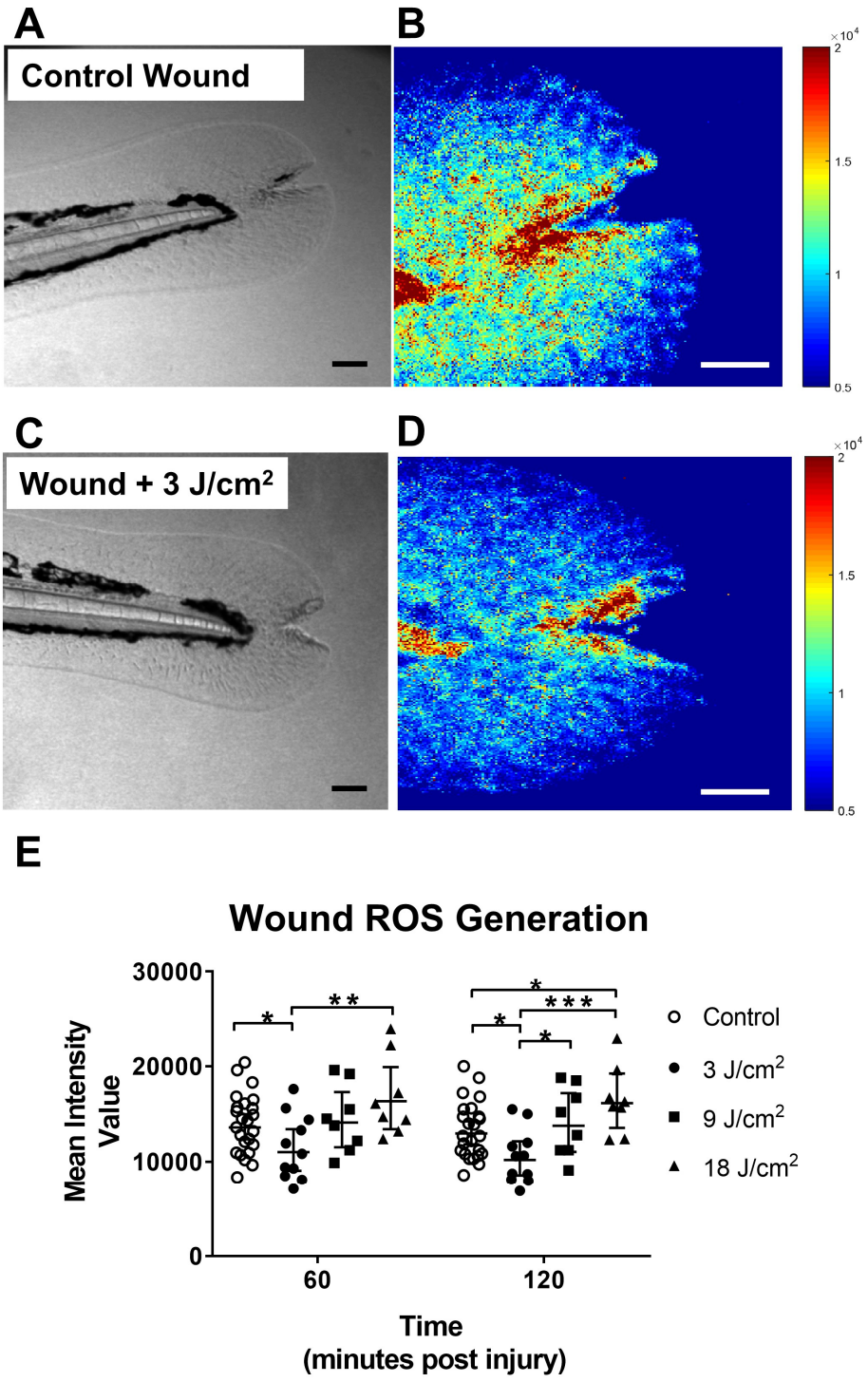

Figure 9. Laser effects oxidative stress. A and B display bright field image of fish after 60 minutes post injury of a wounded untreated control and of a wounded and treated fish with 3 J/cm^2, respectively. Figure C and D display a color-map of the ROS probe (DHE) intensity; red hue indicating saturated DHE and blue hue indicated absence of DHE . Fish of untreated wounds

0 J/cm^2 (n=21) were compared with laser treated wounds: 3 J/cm^2 (n=11) and 9 J/cm^2 (n=8), 18 J/cm^2 (n=8). E displays group overall geometric mean ± 95% confidence intervals of DHE mean intensity values at 60 and 120 minutes post injury. Student T-tests *($p < 0.05$), **($p < 0.01$), ***($p<0.001$) were performed in Microsoft Excel.

4.3.2. Laser Dosing Exhibits Different Levels of Macrophage Kinetics in Response to Wounding

We investigated experimental fish groups, 0 (n=19; 227 macrophages tacked, 3 (n=12; 196 macrophages tracked), 9 (n=10; 96 macrophages tracked), and 18 (n=8; 118 macrophages tracked) J/cm^2 at the same three temporal groups [T_1, T_2, T_3] to see if laser doses would influence macrophage kinetic behavior. When compared to control, 3 J/cm^2 macrophages overall demonstrated significantly more wound biased directed migration (

Figure *10*A, 10B). Speed (

Figure *10*C), and meandering index (

Figure *10*D) were used for determining persistent travel. Overall, cumulatively, 3 J/cm^2 macrophages exhibited significantly faster speeds (T_3: 4.5 ± 0.7 vs 3.9 ± 0.5 μm/min, p=0.01), and more "straightness" or higher meandering index (T_3: 0.44 ± 0.09 vs 0.37 ± 0.09, p=0.04) when compared to non-treated control fish. Higher Static ratio (

Figure *10*E), was used to provide more insight on the pattern of travel, to provide insights on "pausing" and henceforth efficiency in travel. Compared to controls (T_3: 0.177 ± 0.05, p=0.03) 3J/cm^2 exhibited significantly less "pausing "overall (T_3: 0.135 ± 0.04, p=0.03), while 9 J/cm^2 (T_3: 0.139 ± 0.04, p=0.1) and 18 J/cm^2 (T_3: 0.154 ± 0.02, p=0.25) were only slightly less than control in a dose dependent manner. However, persistence through speed, meandering index, and static ratio does not demonstrate a migration bias, it merely reflects a consistent direction orientation. Therefore, vector distances from macrophage centroid positions

to the centroid position of the wound gap were used to compare cells orientation to the site of injury. Higher net distances traveled toward wound were used to indicate a preferential wound travel behavior, or migration bias (

Figure *10*F). Laser demonstrated a significantly higher net distances toward wound in 3 J/cm^2 overall (T_3: 125 ± 50 μm) when compared to 9 J/cm^2 (T_3: 92 ± 52 μm, p=0.8) and compared to non-treated fish (T_3: 89 ± 38 μm, p=0.02). 18 J/cm^2 demonstrated an overall decrease in macrophage wound oriented net distances (T_3: 75 ± 38, p=0.2).

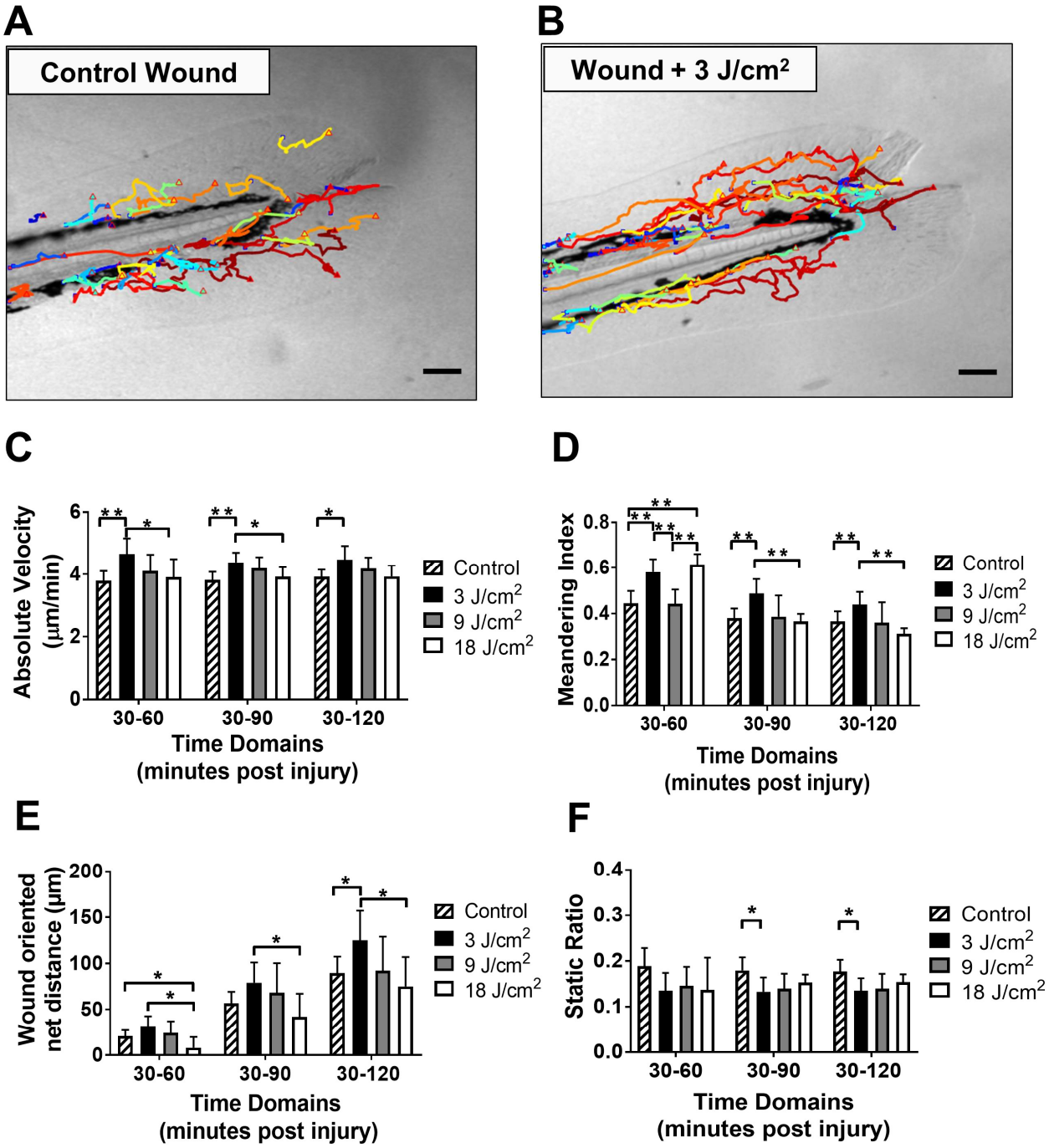

Figure 10. Wound recruited macrophages of 0, 3, 9, 18 J/cm^2 treatment groups of fish (n=20, 12, 10, and 8 respectively) were tracked using software analysis. Representative control fish (A) and 3 J/cm^2 (B) are shown with trajectories with the highest total distances hued as dark red and lowest values hued as dark blue. Quantitative measures of were algorithmically derived at T1 (30 to 60 minutes post injury), T2 (30-90 minutes post injury), and T2 (30-120 minutes post

injury) temporal domains post injury with means and 95% CIs for each independent group measure. Macrophage measures of absolute velocity (C), meandering index (D) were determined to evaluate persistence. Wound oriented net distance traveled (E) and static ratio (F) were determined to evaluate wound bias efficiency. Statistical differences were computed with Student t-tests *($p < 0.05$), **($p < 0.01$) in Graphpad® Prism.

4.3.3. Laser Dose Response of 24 Hour Wound Closure

To examine 24 hour regenerative capacity of the caudal fin, wounds were measured 1 hour (**Figure 11A, 11B**) and 24 hours post injury (**Figure 11C, 11D**). Single wounds were induced and grouped according to laser treatment: Control 0 J/cm^2 wound margin 343 ± 102 μm (n=8), 3 J/cm^2 wound margin 309 ± 64 μm (n=12), 9 J/cm^2 wound margin 318 ± 81 μm μm (n=9), 18 J/cm^2 wound margin 318 ± 88 μm (n=10). Percent wound closure (Geometric mean ± 95% confidence interval) of unirradiated controls (38 ± 8 %) were compared to treated groups: 3 J/cm^2 (51 ± 12 %, p=0.02), 9 J/cm^2 (48 ± 11%, p=0.04), and 18 J/cm^2 (45 ± 12%, p=n.s.) (**Figure 11E**). Treated fish exhibited accelerated wound closure outcomes 24 hours post injury in a dose trend manner as doses exhibited by 13%, 10%, and 7% increases from 3, 9, and 18 J/cm^2, respectively. To ensure 1 hour wound margin size did not influence 24 hour wound size outcomes, a linear regression was performed indicating no correlation to 1 hour wound size and 24 wound size per group: control (r=0.22, p=n.s.), 3 J/cm^2 (r=0.14, p=n.s.), 9 J/cm^2 (r=0.37, p=n.s.), and 18 J/cm^2 (r=0.09, p=n.s.) J/cm^2. These results indicate that less than 9 J/cm^2 doses may be an ideal therapeutic range for zebrafish caudal fin accelerated wound closure.

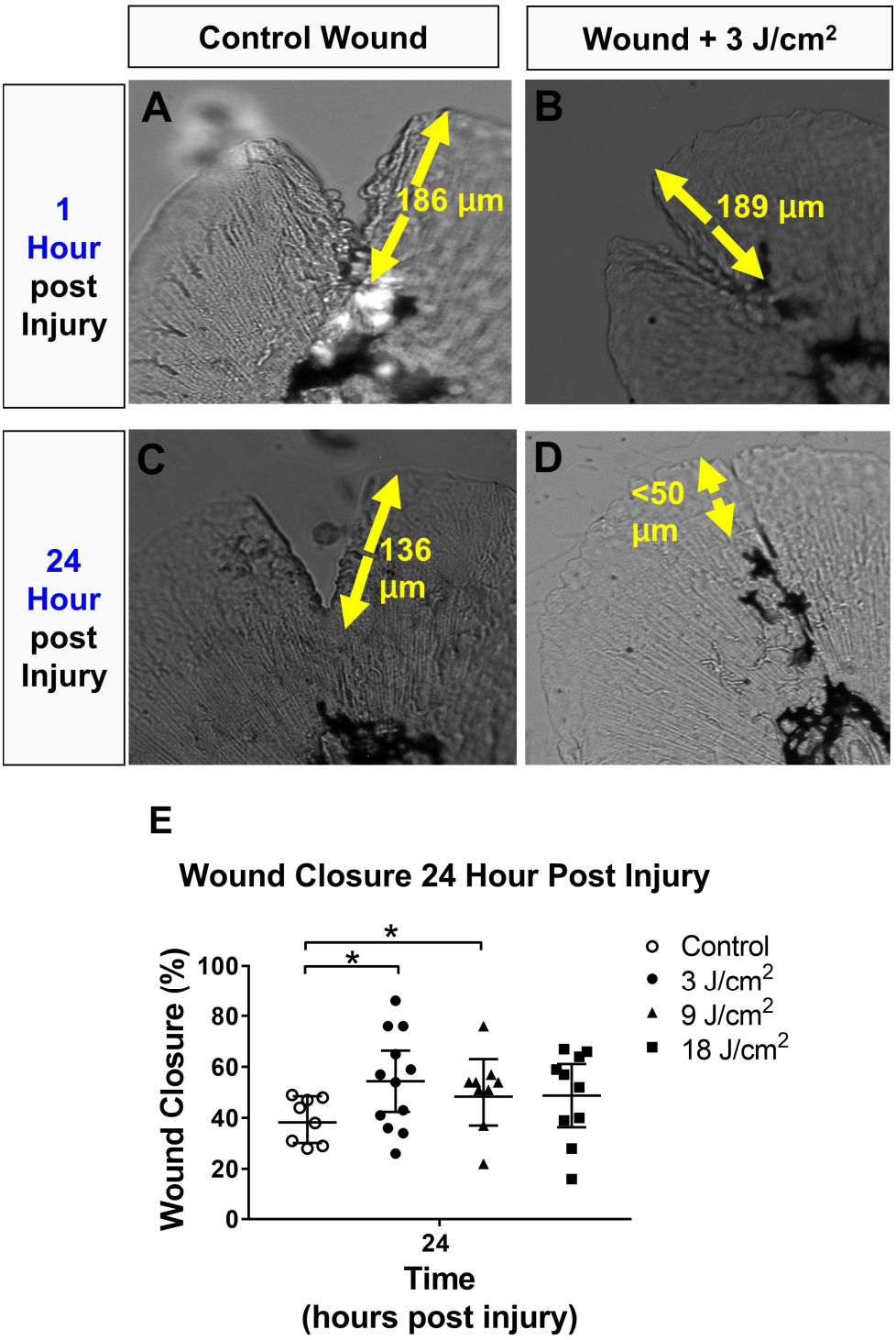

Figure 11. Laser effects on fin wound closure. A and B show caudal fin wound region 1 hour post wounding. Figures C and D display the wound region 24 hours post wounding, untreated and treated with (3 J/cm^2) laser, respectively. Figure E displays the geometric mean ± 95% confidence interval of percent wound closure from 1 hour to 24 hours post wound of untreated

control group (n=8) and 3, 9, and 18 J/cm^2 laser treated groups (n=12, 9, and 10 respectively). Student T-tests *($p < 0.05$) were performed in Microsoft Excel and wound measurements were performed in ImageJ.

4.4. Discussion and Conclusions

Results from the present study demonstrate a dose response, present in speed, meandering index, static ratio, and distance traveled toward wound by wound macrophages in response to fluence. A dose of 3 J/cm^2 was identified as eliciting the most persistent and wound oriented trajectory. The 3 J/cm^2 dose *in vivo* effect included elevated macrophage speeds, meandering index values, with a resultant contribution in more "straightness" in migration and less "pausing" when compared to either non-treated or treated groups. In contrast, a dose of 18 J/cm^2 resulted in slower macrophage responses. The 9 J/cm^2 cell kinetic measures consistently fell between both high and low energy fluences. Fluence elicited a dose dependent effect on wound reactive oxygen species content and wound closure. The magnitude of reactive oxygen species within the wound and wound closure rate are relevant to clinical parameters when monitoring wound therapeutics, providing support for this model as means to interrogate multiple parameters of laser treatment settings in an *in vivo* setting.

Our findings agree with recent *in vitro* studies in which laser treatment has been reported to promote a pro-healing macrophage response. In these studies, enhanced phagocytosis of various types of macrophages with red (600-700) nm laser with low energy fluences (2 to 20) J/cm^2 (Karu et al. 1989, Lu et al. 2011). Lu *et al.*. reported 670 energy fluence of 9 J/cm^2 led to protection from retinal degeneration by decreasing pro-inflammatory cytokine expression and thus the reduction of polarized macrophages. A wavelength of 670 nm delivering 9 J/cm^2 has led to mitigation of oxidative damage (Albarracin et al. 2013). Song *et al.* reported red 632.8 nm laser treatment of 20 J/cm^2 enhanced phagocytic function of microglia in an *ex vivo* transwell

culture system and suppressed pro-inflammatory cytokine TNF-α and nitric oxide expressions (Song, Zhou, and Chen 2012). We observed 18J/cm^2 with a 635 nm wavelength *in vivo* to lead to undesirable increases in reactive oxygen species; differences in response may be explained as tissue specific. Souza *et al.* reported red laser 660 nm at 4.5 J/cm^2 reduced pro-inflammatory activation of alveolar macrophages, commonly tied to reactive oxygen species generation (Souza et al. 2014). El Kabany at Korraa reported 632.8 nm laser treated phagocytes (1 to 5) J/cm^2 *in vitro*, enhanced percent phagocytosis, respiratory burst production, and Arginase I mRNA production in a dose-dependent manner (El Kabany and Korraa 2008). Fernandes demonstrated that J774 macrophages could be oriented from a classically activated pro-inflammatory state, M1, to an alternatively active, M2, pro-healing state with red 660 nm or 780 nm laser 7.5 J/cm^2 and 2.6 J/cm^2, respectively(Fernandes et al. 2015). Souza demonstrated both lasers could reduce TNF-α, iNOS expression and TNF-α and COX-2 production, however, 660 nm also resulted in an up-regulation of IL-6 expression. While the majority of reports favor a range of 3- 20 J/cm2 to be beneficial to reduction of macrophage inflammatory behavior and improved regenerative responses, it is possible that other fluencies may be required depending on tissue target; Song *et al.* demonstrated an associated increase in alternative activated macrophages and recovery of rat spinal cord injury after 810 nm wavelength laser with 150 mW output power and 0.3/cm^2 light spot suggesting fluences far greater than those described above(Song et al. 2017). These findings punctuate a need to establish precise parameters for tissue specific responses.

Based on the large data sets involved in time lapse imaging, this study focused on macrophage initial recruitment; selection of the quantitative measures of migration was important for quantifying an elicited effect on cellular kinetics. Our study outlines macrophage kinetics speeds, 3 μm/min to 6 μm/min average, and meandering index, 0.4 to 0.6, that falls

within the, range previous zebrafish literature (Ellett et al. 2011, Li et al. 2012a). However, the time post injury is important in considering an average macrophage migration behavior. Initial recruitment (30 to 60) minutes post injury demonstrate elevated speeds and less meandering for all zebrafish groups. These values lessen as time progresses. Red laser treated zebrafish do not appear to experience supernatural kinetic behavior, with speeds, for instance, that exceed the range of macrophage ranges previously reported. Further, 3 J/cm^2 macrophage static ratios were significantly correlated to respective speeds ($r = -0.56$, $p < 0.01$, data not shown). To this effect, red laser treated macrophages at 3 J/cm^2 demonstrated move movement, shown by decreased static ratio, implicating macrophages were simply more active rather than traveling at abnormally faster speeds frame-by-frame. It is well accepted that speed and meandering index can be used for determining persistence, also defined as period by which a cell moves in the same direction (Svensson, Medyukhina, Belyaev, Al-Zaben, et al. 2017). The 3 J/cm^2 treated group demonstrated elevated speed and meandering index values, contributing to more "straightness" in migration when compared to both non-treated or treated groups. Additional, measures demonstrated a preferential wound migration bias with less "stopping" and lower static ratios when compared wound than the untreated controls. Therefore 3 J/cm^2 macrophages demonstrate persistent or efficient wound oriented tracks, as they demonstrated considerably higher net distances toward wound and higher meandering index values (Svensson, Medyukhina, Belyaev, Al-Zaben, et al. 2017). Such vigorous movement is likely to utilize greater energy; recently, reports have highlighted the role of enhanced levels of ATP, as a means of stimulating changes in speed and migration behaviors of immune cells (Kotwal and Chien 2017, Kelly and O'Neill 2015, Sáez et al. 2017b). Since laser treatment has been linked to enhanced ATP production (de Oliveira et al. 2014, Anders, Ketz, and Wu 2017, Karu 2010, Hawkins and

Abrahamse 2006), it is possible that increased available ATP spurred increased macrophage activity (Kotwal, Sarojini, and Chien 2015). These migrations based descriptive measures help to shape a more complete characterization of red laser effect within the wound microenvironment.

Our work is in agreement with prior reports in which red laser treatment (1 J/cm^2 to 60 J/cm^2) enhanced wound closure with a reduction of oxidative stress via elimination of inflammatory cellular infiltrates such as neutrophils and apoptotic or necrotic debris (de Medeiros et al. 2017, de Lima et al. 2016). Therefore, it is possible that increased macrophage cellular kinetics may play a direct role in the reduction of oxidative stress by hastening the pace neutrophil clearance. The minimization of stops along the way and speed in which macrophages traveled to the wound, support this notion. Alternatively, it is well accepted that the mitochondria, while an important source of energy, in inflammatory conditions are rendered hyperactive leading to excessive superoxide anion production. Therefore, this excessive production of ROS is a putative mechanism of a dysregulated wound microenvironment contributing to prolonged inflammation. Sanderson *et al.* provides evidence of a near-infrared laser (810 nm, > 100 J/cm^2) effect on photoacceptor, cytochrome oxidase c , to reduce mitochondrial membrane potential, reducing its hyperactivation and excessive superoxide anion levels within cranial ischemia reperfusion injuries in rats (Sanderson et al. 2018). Photoacceptor, cytochrome oxidase c , is a well-accepted target red laser with previous studies demonstrating 632.8 nm wavelengths (low fluences, such as, 2 J/cm^2 and 5 J/cm^2) modulating mitochondrial membrane potential and generation of reactive oxygen species (Karu et al. 2008, Pastore 2000, Silveira, Silva, et al. 2009). In contrast, red laser photobiomodulation is largely implicated in increasing mitochondrial membrane potential to increase ATP production and

redox signaling (Hamblin 2018). These contradicting findings may be explained by the biphasic nature of the effects of laser therapy, photobiomodulation, a query that might be addressed in future studies using the zebrafish *in vivo* model.

Previous zebrafish research has indicated that a hydrogen peroxide burst is prevalent in zebrafish within the first 20 minutes after injury, responsible for a chemotactic gradient correlated to leukocyte recruitment (Niethammer, Grabher, Look, and Mitchison 2009). Therefore, we probed deleterious superoxide anion, via Dihydroethidium (DHE), to focus on oxidative stress. We recognize DHE as one of many tools to probe oxidative stress. Its utility when compared to genetic models is its simplicity and reliability for *in vivo* detection of oxidative species (Mugoni, Camporeale, and Santoro 2014a). DHE has been effectively used to probe oxidative stress in zebrafish , validating the assay using KCN, a known inhibitor of superoxide dismutase (Nazarewicz, Bikineyeva, and Dikalov 2013). Notably, for an optimized ROS signal, the notochord and surrounding cavity was avoided due to high probe signal capable of confounding normalized measurements. Potential confounders of this method could also include potential off target binding with nitrogen-based species. Such binding is believed to be minimal and can be regulated, as recent report indicates fluorescence detection, preferential to reactive oxygen species enabling the possibility of ROS quantification in real time (Nazarewicz, Bikineyeva, and Dikalov 2013). Based on methods described in **Chapter 3** previous literature, we selected DHE for oxidative stress determinations.

CHAPTER 5

5. FUTURE DIRECTIONS AND CONCLUSIONS

5.1. PBMT and Dose Parameters

The zebrafish wound model provides a means to identify laser effects on macrophage and potentially, neutrophil kinetics *in vivo* and correlate these effects with the pace of wound healing. Future studies can advance the field by performing a series of comparative studies to demonstrate the effect of power, wavelength (violet, 405nm, green 535nm, red, 600-660nm, near infrared 800-850nm, etc..) and comparative of pulsed versus constant delivery of identical total Joules delivered. Further, the utility of singular vs combinatorial wavelength therapy can be identified. Such foundational studies undertaken *in vivo* can provide the mechanistic underpinnings for the development of clinical therapeutics.

5.2. PBMT and ATP

Photobiomodulation has been well characterized to augment isolated mitochondrial ATP production (Passarella *et al*. 1988) and intracellular ATP levels. PBMT ability to increase wound microenvironment ATP levels wound may demonstrate a functional link to increased phagocyte recruitment kinetics and may serve to accelerate a physiologic process. Upon tissue injury, infected and dying cells release ATP extracellularly into the wound microenvironment (Idzko, Ferrari, and Eltzschig 2014). This extracellular ATP serves as a danger signal to phagocytes, such as macrophages, directly interacting with specific purinergic G protein-coupled receptors to affect motility (Honda et al. 2001a). A recent *in vitro* study demonstrated 500 μM extracellular ATP levels in phagocyte media led to quantifiably faster phagocyte speeds, increased cytosolic calcium levels, and increased intracellular ATP levels (Sáez et al. 2017b).

Further, when extracellular Pannex1 and $P2X_7$ receptor were inhibited, membrane permeability and intracellular ATP and calcium levels decreased leading to decreased phagocyte speeds. Intracellular ATP is known for stimulating pathways involved in elevating cytosolic calcium levels, well characterized to intracellularly drive motility in phagocytes (Shumilina, Huber, and Lang 2011). Therefore, these studies suggest that that extracellular ATP levels boost motility by permeating into the cells to activate ATP dependent cytosolic calcium increases required for motility. Future studies can build upon this knowledge by evaluating therapeutic levels of photobiomodulation for its ability to generate intracellular ATP for quantifiably faster phagocyte speeds *in vitro*. Evaluations of intracellular calcium levels would help to corroborate a mechanistic avenue for PBMT to enhance phagocyte motility. Additional comparisons between extracellular ATP exposure to PBMT of intracellular ATP production and motility measures would further aid in assessing therapeutic effectiveness. High performance liquid chromatography is capable of assessing ATP metabolites in fish tissue (Lin, Cormier, and Torsella 1996) and would enable this determination. Evaluating ATP levels if *in vitro* in relation to macrophage motility will provide more information on PBMT ability to modulate ATP for enhanced cellular kinetics.

PBMT ability to increase ATP levels and microenvironment metabolism may further serve to regulate epigenetic modifiers such as histone modifications, DNA methylation and microRNA pathways (Sassone-Corsi 2013). Transcription silencing and activation at specific residues have influence on histone post translational modifications, such as acetylation and methylation. Therefore metabolites such as acetyl coenzyme A (acetyl-CoA), and ATP, can affect epigenetic modifiers to regulate gene expression (Wellen *et al*. 2009, Imai and Guarente 2010). Recognized epigenetic modifiers include HAT(histone acetyltransferases),

HDAC(histone deacetylases), HMTS(histone methyltransferases) , KDMs (lysine demethylases) , kinases, and phosphatases are dependent on localized concentrations of metabolites constituting the basis for a malleable epigenome (Sassone-Corsi 2013, Katada, Imhof, and Sassone-Corsi 2012). If specific PBM generated metabolites significantly influence epigenetic modifiers, this could serve as an additional traceable response of PBMT anti-inflammatory cell expressions.

5.3. PBMT and Neutrophils

We propose to apply the same parameters to study the effect of 635nm irradiation on enhanced neutrophil migration kinetics *in vivo* as these effects are not known. Neutrophils and macrophages are well characterized to participate in cooperative inflammatory behaviors (Silva 2011), such as, cross-talk for cyclical recruitment (Filippo *et al*. 2013). In zebrafish, transgenic strategies have permitted real time monitoring of neutrophils (Keightley *et al*. 2014). Current zebrafish research has made unprecedented characterizations in neutrophil kinetics, demonstrating neutrophil retrograde migration behavior (Mathias *et al*. 2006) and redox based tyrosine kinase regulated recruitment (Yoo et al. 2011) of initial hydrogen peroxide bursts after tissue injury (Niethammer, Grabher, Look, and Mitchison 2009). Rosowske *et al.* demonstrated impaired motility in neutrophils, via Rac2 deficient neutrophil transgenic fish, resulted in fewer recruited macrophages and neutrophils to the site of injury (Rosowski et al. 2016b). Results further correlated fewer recruited neutrophils with higher susceptibility to infection, ultimately increasing percent mortality. Zebrafish studies also demonstrate neutrophil early recruitment leads to removal of debris and microbes (Li et al. 2012a), and reduces initial ROS levels following tissue injury (Pase *et al*. 2012). These findings suggest that kinetics of neutrophil migration behavior to the site of injury is important to the reduction of ROS and acceleration of

healing. Examination of fluence on neutrophil can help define a therapeutic protocol to optimize both macrophage and neutrophil kinetics for acceleration of wound healing.

In addition to accelerated neutrophil migration, neutrophil removal via macrophage phagocytosis may also be affected by 635nm laser therapy. Removal of wound neutrophils is required for resolution of acute inflammation and the progression of wound healing. Known macrophage dysfunction results in the failure to adequately remove neutrophils an leads to the production of a large number of free radicals and corresponding oxidative stress within the wound (Ushio-Fukai 2009). Excessive oxidative stress delays wound healing. The zebrafish animal model is a useful tool to observe neutrophil recruitment and persistence (Miller *et al*. 2003, Matsumoto 2003). Future studies could involve examination of neutrophil clearance rate, histologic measures of macrophage phagocytosis, and a correlation between wound ROS and neutrophil numbers. Studies to define expression of known molecules (i.e., CD36, CD61, TNF-alpha) involved in macrophage clearance of neutrophils can also be undertaken to identify whether laser treatment facilitates neutrophil clearance by these mechanisms (Savill et al. 1992, Meszaros, Reichner, and Albina 2000).

5.4. Ischemia Reperfusion Injury

Ischemia reperfusion injury contributes to the extent of morbidity and mortality in myocardial infarction, ischemic stroke, and acute kidney injury. For organ transplantation, ischemia reperfusion injury limits preservation times, increases transplant rejection, and decreases graft survival. In ischemia reperfusion injuries, a prolonged lack of adequate blood flow, or ischemia, inhibits oxygen supply to the site of injury, hinders metabolic capacity and exacerbates the accumulation of oxidative stress (Rodríguez *et al*. 2007). Ischemia may also lead to an irreversible pattern of mitochondrial dysfunction, (Buja 2005). Reducing ischemia

reperfusion damage could have widespread impact on morbidity and mortality of several different conditions.

Photobiomodulation therapy has been shown to minimize tissue damage after ischemia reperfusion injury in thoracic organs and the brain. In animal hearts, photobiomodulation therapy with red and infrared (600 to 900 nm) wavelengths (8, >20 mW/cm^2, >10 J/cm^2) have demonstrated significantly increased levels of ATP as well as decreased infarct size, decreased myocardium inflammation, and decreased mortality (Oron, Yaakobi, Oron, Hayam, *et al*. 2001, Oron, Yaakobi, Oron, Mordechovitz, *et al*. 2001, Quirk *et al*. 2014). In brain, treatment with near infrared lasers (700 to 1000 nm) have led to improved protection from ischemic reperfusion conditions, modulating cytochrome c oxidase and reducing oxidative stress (Sanderson *et al*. 2018). In lungs, treatment with 660 nm (67.5 J/cm^2, 375 mW/cm^2) led to reduction of inflammatory neutrophil influx and inflammatory cytokine levels such as TNF-alpha levels when compared to non-irradiated controls. While there appears to be efficacy in thoracic organs and the brain, to date, the effect on organs located within the abdomen has not been determined and present a gap of knowledge in the field. After mechanistic studies can identify optimal laser wavelengths, power, and mode of pulsing effects on neutrophil and macrophage kinetics, these insights can be applied for the mitigation of ischemia reperfusion injury.

5.5. Conclusions

Photobiomodulation therapy has reported both beneficial and non-beneficial effects on regenerating tissues and wounds (Al-Watban, Zhang, and Andres 2007, Byrnes, Barna, and Chenault 2004, Moon *et al*. 2014, Doroty *et al*. 2010, Lima *et al*. 2010). The field has a wide variety of reports with broad ranges in wavelength, fluence, power, and frequency and these variabilities make it difficult to compare outcomes and standardize therapy for optimal clinical

outcomes. Because this therapeutic has no known side effects, it has great potential. Its optimization rests on defining the laser parameters that optimize the regenerating microenvironment. This report outlines a quantitative *in vivo* means to identify and track a cellular element critically involved in changing the quality and pace of wound healing. Using this platform, new insights regarding macrophage velocity, meandering, and stasis were gained. These initial findings demonstrate the mechanistic effect of 635 nm wavelength on augmenting speed and directionality of macrophage responses to the wound. This newly established analysis of zebrafish model and associated software platform provides a foundation for a pipeline of investigations. Investigations examining each parameter of PBMT on macrophage and ROS behavior individually and in concert with each other in zebrafish is novel. These investigations provide a potential of more thorough investigations on the degree and speed of wound closure after PBMT, with potential future implications for the successful treatment of myocardial infarction, ischemic stroke, and the preservation and survival of transplanted organs.

CITED LITERATURE

Al-Watban, F.A.H., X.Y. Zhang, and B.L. Andres. 2007. "Low-level laser therapy enhances wound healing in diabetic rats: a comparison of different lasers." *Photomedicine and Laser Surgery* 25 (2):72-77.

Al-Watban, Farouk A., and X. Y. Zhang. 2004. "The comparison of effects between pulsed and CW lasers on wound healing." *Journal of clinical laser medicine & surgery* 22 (1):15-18. doi: 10.1089/104454704773660921.

Albarracin, Rizalyn, Riccardo Natoli, Matthew Rutar, Krisztina Valter, and Jan Provis. 2013. "670 nm light mitigates oxygen-induced degeneration in C57BL/6J mouse retina." *BMC Neuroscience* 14 (1):125. doi: 10.1186/1471-2202-14-125.

Ameer, GA, TA Mahmood, and R Langer. 2002. "A biodegradable composite scaffold for cell transplantation." *Journal of Orthopaedic Research* 20 (1):16-19.

Anders, Juanita J., Ann Ketz, and Xingjia Wu. 2017. "Basic Principles of Photobiomodulation and Its Effects at the Cellular, Tissue, and System Levels." *Laser Therapy in Veterinary Medicine: Photobiomodulation*.

Andersson, Ulf, Haichao Wang, Karin Palmblad, Ann-Charlotte Aveberger, Ona Bloom, Helena Erlandsson-Harris, Alfred Janson, Riikka Kokkola, Minghuang Zhang, and Huan Yang. 2000. "High mobility group 1 protein (HMG-1) stimulates proinflammatory cytokine synthesis in human monocytes." *Journal of Experimental Medicine* 192 (4):565-570.

Ardanaz, Noelia, and Patrick J Pagano. 2006. "Hydrogen peroxide as a paracrine vascular mediator: regulation and signaling leading to dysfunction." *Experimental biology and medicine* 231 (3):237-251.

Artis, David, Neil E Humphreys, Christopher S Potten, Norbert Wagner, Werner Müller, Jacqueline R McDermott, Richard K Grencis, and Kathryn J Else. 2000. "β7 integrin-deficient mice: delayed leukocyte recruitment and attenuated protective immunity in the small intestine during enteric helminth infection." *European journal of immunology* 30 (6):1656-1664.

Ash, Caerwyn, Michael Dubec, Kelvin Donne, and Tim Bashford. 2017. "Effect of wavelength and beam width on penetration in light-tissue interaction using computational methods." *Lasers in medical science* 32 (8):1909-1918.

Avishai, Eden, Kristina Yeghiazaryan, and Olga Golubnitschaja. 2017. "Impaired wound healing: facts and hypotheses for multi-professional considerations in predictive, preventive and personalised medicine." *EPMA Journal* 8 (1):23-33. doi: 10.1007/s13167-017-0081-y.

Baggiolini, Marco, and Ian Clark-Lewis. 1992. "Interleukin-8, a chemotactic and inflammatory cytokine." *FEBS letters* 307 (1):97-101.

Baker, M. 2010. "Screening: the age of fishes." *Screening: the age of fishes*. doi: 10.1038/nmeth0111-47.

Beek, J. F., P. Blokland, P. Posthumus, M. Aalders, J. W. Pickering, H. J. Sterenborg, and M. J. van Gemert. 1997. "In vitro double-integrating-sphere optical properties of tissues between 630 and 1064 nm." *Physics in medicine and biology* 42 (11):2255-2261. doi: 10.1088/0031-9155/42/11/017.

Belletti, Silvana, Jacopo Uggeri, Giovanni Mergoni, Paolo Vescovi, Elisabetta Merigo, Carlo Fornaini, Samir Nammour, Maddalena Manfredi, and Rita Gatti. 2015. "Effects of 915 nm GaAs diode laser on mitochondria of human dermal fibroblasts: analysis with confocal microscopy." *Lasers in Medical Science* 30 (1):375-381. doi: 10.1007/s10103-014-1651-z.

Bello, YM, and AF Falabella. 2002. "The role of graftskin (Apligraf) in difficult-to-heal venous leg ulcers." *Journal of wound care* 11 (5):182-183.

Beutler, B, Do Greenwald, JD Hulmes, M Chang, Y-CE Pan, J Mathison, R Ulevitch, and A Cerami. 1985. "Identity of tumour necrosis factor and the macrophage-secreted factor cachectin." *Nature* 316 (6028):552.

Beutler, BRUCE, VERONICA Tkacenko, I Milsark, NADIA Krochin, and ANTHONY Cerami. 1986. "Effect of gamma interferon on cachectin expression by mononuclear phagocytes. Reversal of the lpsd (endotoxin resistance) phenotype." *Journal of Experimental Medicine* 164 (5):1791-1796.

Bjordal, Jan, Mark I. Johnson, Vegard Iversen, Flavio Aimbire, and Rodrigo Lopes-Martins. 2006. "Low-Level Laser Therapy in Acute Pain: A Systematic Review of Possible Mechanisms of Action and Clinical Effects in Randomized Placebo-Controlled Trials." *Photomedicine and Laser Surgery* 24 (2):158-168. doi: 10.1089/pho.2006.24.158.

Black, Annie F, François Berthod, Nicolas L'heureux, Lucie Germain, and François A Auger. 1998. "In vitro reconstruction of a human capillary-like network in a tissue-engineered skin equivalent." *The FASEB Journal* 12 (13):1331-1340.

Boateng, Joshua S, Kerr H Matthews, Howard NE Stevens, and Gillian M Eccleston. 2008. "Wound healing dressings and drug delivery systems: a review." *Journal of pharmaceutical sciences* 97 (8):2892-2923.

Bolton, P. A., S. Young, and M. Dyson. 2004. "Macrophage responsiveness to light therapy-a dose response study." *Macrophage responsiveness to light therapy-a dose response study*.

Bolton, P., M. Dyson, and S. Young. 1992. "The effect of polarized light on the release of growth factors from the U-937 macrophage-like cell line." *The effect of polarized light on the release of growth factors from the U-937 macrophage-like cell line*.

Boring, Landin, Jennifa Gosling, Stephen W Chensue, Steven L Kunkel, Robert V Farese, Hal E Broxmeyer, and Israel F Charo. 1997. "Impaired monocyte migration and reduced type 1 (Th1) cytokine responses in CC chemokine receptor 2 knockout mice." *The Journal of clinical investigation* 100 (10):2552-2561.

Bossche, Jan den, Jeroen Baardman, Natasja A. Otto, Saskia Velden, Annette E. Neele, Susan Berg, Rosario Luque-Martin, Hung-Jen J. Chen, Marieke C. Boshuizen, Mohamed Ahmed, Marten A. Hoeksema, Alex Vos, and Menno Winther. 2016. "Mitochondrial Dysfunction Prevents Repolarization of Inflammatory Macrophages." *Cell reports* 17 (3):684-696. doi: 10.1016/j.celrep.2016.09.008.

Brown, Joanne R., David Goldblatt, Joanna Buddle, Louise Morton, and Adrian J. Thrasher. 2003. "Diminished production of anti-inflammatory mediators during neutrophil apoptosis and macrophage phagocytosis in chronic granulomatous disease (CGD)." *Journal of leukocyte biology* 73 (5):591-599. doi: 10.1189/jlb.1202599.

Buja, L Maximilian. 2005. "Myocardial ischemia and reperfusion injury." *Cardiovascular Pathology* 14 (4):170-175.

Byrnes, K. R., L. Barna, and V. M. Chenault. 2004. "Photobiomodulation improves cutaneous wound healing in an animal model of type II diabetes." *… and Laser Therapy*. doi: 10.1089/pho.2004.22.281.

Carver, N. 1991. "Acute rejection of cultured keratinocyte allografts in nonimmunosuppressed pigs." *Transplantation* 52:918-924.

Chawla, Ajay, Khoa D Nguyen, and YP Sharon Goh. 2011. "Macrophage-mediated inflammation in metabolic disease." *Nature Reviews Immunology* 11 (11):738-749.

Chen, A. C. H., P. R. Arany, and Y. Y. Huang. 2009. "Low level laser therapy activates NF-kB via generation of reactive oxygen species in mouse embryonic fibroblasts." *Low level laser therapy activates NF-kB via generation of reactive oxygen species in mouse embryonic fibroblasts*.

Chen, Aaron C., Praveen R. Arany, Ying-Ying Y. Huang, Elizabeth M. Tomkinson, Sulbha K. Sharma, Gitika B. Kharkwal, Taimur Saleem, David Mooney, Fiona E. Yull, Timothy S. Blackwell, and Michael R.

Hamblin. 2011. "Low-level laser therapy activates NF-kB via generation of reactive oxygen species in mouse embryonic fibroblasts." *PloS one* 6 (7). doi: 10.1371/journal.pone.0022453.

Cherry, Anne D, and Claude A Piantadosi. 2015. "Regulation of mitochondrial biogenesis and its intersection with inflammatory responses." *Antioxidants & redox signaling* 22 (12):965-976.

Chow, Roberta T., and Les Barnsley. 2005. "Systematic review of the literature of low-level laser therapy (LLLT) in the management of neck pain." *Lasers in surgery and medicine* 37 (1):46-52. doi: 10.1002/lsm.20193.

Cohen, I., P. Rider, Y. Carmi, and Braiman - A. of the …. 2010. "Differential release of chromatin-bound IL-1α discriminates between necrotic and apoptotic cell death by the ability to induce sterile inflammation." *Proceedings of the …*. doi: 10.1073/pnas.0915018107.

Colotta, F., F. Re, N. Polentarutti, S. Sozzani, and A. Mantovani. 1992. "Modulation of granulocyte survival and programmed cell death by cytokines and bacterial products." *Blood* 80 (8):2012-2020.

Colucci-Guyon, Emma, Jean-Yves Tinevez, Stephen A Renshaw, and Philippe Herbomel. 2011. "Strategies of professional phagocytes in vivo: unlike macrophages, neutrophils engulf only surface-associated microbes." *J Cell Sci* 124 (18):3053-3059.

Cvejic, Ana, Chris Hall, Magdalena Bak-Maier, Maria V. Flores, Phil Crosier, Michael J. Redd, and Paul Martin. 2008. "Analysis of WASp function during the wound inflammatory response--live-imaging studies in zebrafish larvae." *Journal of cell science* 121 (Pt 19). doi: 10.1242/jcs.032235.

Dawood, Munqith S., and Saif D. Salman. 2013. "Low level diode laser accelerates wound healing." *Lasers in medical science* 28 (3):941-945. doi: 10.1007/s10103-012-1182-4.

de Almeida, Patrícia, Rodrigo Lopes-Martins, Thiago Marchi, Shaiane Tomazoni, Regiane Albertini, João Corrêa, Rafael Rossi, Guilherme Machado, Daniela da Silva, Jan Bjordal, and Ernesto Junior. 2012. "Red (660 nm) and infrared (830 nm) low-level laser therapy in skeletal muscle fatigue in humans: what is better?" *Lasers in Medical Science* 27 (2):453-458. doi: 10.1007/s10103-011-0957-3.

de Lima, Fernando, Olavo de Neto, Fabiano Barbosa, Ailton do Galvão, Fernando Ramos, Christiane de Lima, and Célio de Rodrigues. 2016. "Is there a protocol in experimental skin wounds in rats using low-level diode laser therapy (LLDLT) combining or not red and infrared wavelengths? Systematic review." *Lasers in Medical Science* 31 (4):779-787. doi: 10.1007/s10103-016-1893-z.

de Medeiros, Melyssa, Irami Araújo-Filho, Efigênia da Silva, Wennye de Queiroz, Ciro Soares, Maria de Carvalho, and Maria Maciel. 2017. "Effect of low-level laser therapy on angiogenesis and matrix metalloproteinase-2 immunoexpression in wound repair." *Lasers in Medical Science* 32 (1):35-43. doi: 10.1007/s10103-016-2080-y.

de Oliveira, Sofia, Azucena López-Muñoz, Sergio Candel, Pablo Pelegrín, Ângelo Calado, and Victoriano Mulero. 2014. "ATP modulates acute inflammation in vivo through dual oxidase 1-derived H2O2 production and NF-κB activation." *Journal of immunology (Baltimore, Md. : 1950)* 192 (12):5710-5719. doi: 10.4049/jimmunol.1302902.

Deodhar, A.K., and RE Rana. 1997. "Surgical physiology of wound healing: a review." *Journal of postgraduate medicine* 43 (2):52.

Desmet, Kristina D, David A Paz, Jesse J Corry, Janis T Eells, Margaret TT Wong-Riley, Michele M Henry, Ellen V Buchmann, Mary P Connelly, Julia V Dovi, and Huan Ling Liang. 2006. "Clinical and experimental applications of NIR-LED photobiomodulation." *Photomedicine and Laser Therapy* 24 (2):121-128.

Dhivya, Selvaraj, Viswanadha Vijaya Padma, and Elango Santhini. 2015. "Wound dressings–a review." *Biomedicine* 5 (4).

Di Wang, Hui, Patrick J Pagano, Yue Du, Antonio J Cayatte, Mark T Quinn, Peter Brecher, and Richard A Cohen. 1998. "Superoxide anion from the adventitia of the rat thoracic aorta inactivates nitric oxide." *Circulation Research* 82 (7):810-818.

Doe, WILLIAM F, and PETER M Henson. 1978. "Macrophage stimulation by bacterial lipopolysaccharides. I. Cytolytic effect on tumor target cells." *Journal of Experimental Medicine* 148 (2):544-556.

Doroty, M. Dourado, Fávero Sílvio, Matias Rosemary, T. Carvalho Paulo de, and A. da Cruz-Höfling Maria. 2010. "Low-level laser therapy promotes vascular endothelial growth factor receptor-1 expression in endothelial and nonendothelial cells of mice gastrocnemius exposed to snake venom." *Photochemistry and Photobiology* 87 (2):418-426. doi: 10.1111/j.1751-1097.2010.00878.x.

Dube, A., H. Bansal, and P. K. Gupta. 2003. "Modulation of macrophage structure and function by low level He–Ne laser irradiation." *Modulation of macrophage structure and function by low level He–Ne laser irradiation*.

El Kabany, H. M., and S. S. Korraa. 2008. "Effect of He: Ne laser on neutrophils phagocytic activity." *Arab J. Biotech.* 11 (2):219-228.

Ellett, Felix, Luke Pase, John W Hayman, Alex Andrianopoulos, and Graham J Lieschke. 2011. "mpeg1 promoter transgenes direct macrophage-lineage expression in zebrafish." *Blood* 117 (4):e49-e56.

Ennis, William J., Claudia Lee, and Patricio Meneses. 2007. "A biochemical approach to wound healing through the use of modalities." *Clinics in Dermatology* 25 (1):63-72. doi: 10.1016/j.clindermatol.2006.09.008.

Ennis, William J., Claudia Lee, Malgorzata Plummer, and Patricio Meneses. 2011. "Current Status of the Use of Modalities in Wound Care: Electrical Stimulation and Ultrasound Therapy." *Plastic and Reconstructive Surgery* 127. doi: 10.1097/PRS.0b013e3181fbe2fd.

Enoch, Stuart, Joseph E Grey, and Keith G Harding. 2006. "ABC of wound healing: Recent advances and emerging treatments." *BMJ: British Medical Journal* 332 (7547):962.

Erdle, Brandon J, Sabine Brouxhon, Martin Kaplan, Joanne Vanbuskirk, and Alice P Pentland. 2008. "Effects of continuous-wave (670-nm) red light on wound healing." *Dermatologic Surgery* 34 (3):320-325.

Fabre, Hebert S. C., Ricardo L. Navarro, Paula Oltramari-Navarro, Rodrigo F. Oliveira, Deise A. A. Pires-Oliveira, Rodrigo A. C. Andraus, Nelson Fuirini, and Karen B. P. Fernandes. 2015. "Anti-inflammatory and analgesic effects of low-level laser therapy on the postoperative healing process." *Journal of Physical Therapy Science* 27 (6):1645-1648. doi: 10.1589/jpts.27.1645.

Fadok, Valerie A., Donna L. Bratton, Anatole Konowal, Peter W. Freed, Jay Y. Westcott, and Peter M. Henson. 1998. "Macrophages that have ingested apoptotic cells in vitro inhibit proinflammatory cytokine production through autocrine/paracrine mechanisms involving TGF-beta, PGE2, and PAF." *The Journal of clinical investigation* 101 (4):890-898. doi: 10.1172/JCI1112.

Fernandes, Kristianne, Nadhia Souza, Raquel Mesquita-Ferrari, Daniela de da Silva, Lilia Rocha, Agnelo Alves, Kaline de Sousa, Sandra Bussadori, Michael R. Hamblin, and Fábio Nunes. 2015. "Photobiomodulation with 660-nm and 780-nm laser on activated J774 macrophage-like cells: Effect on M1 inflammatory markers." *Journal of Photochemistry and Photobiology B: Biology* 153:344-351. doi: 10.1016/j.jphotobiol.2015.10.015.

Figurová, Mária, Valent Ledecký, Martina Karasová, Marián Hluchý, Alexandra Trbolová, Igor Capík, Slavomír Horňák, Peter Reichel, Jan M. Bjordal, and Peter Gál. 2016. "Histological Assessment of a Combined Low-Level Laser/Light-Emitting Diode Therapy (685 nm/470 nm) for Sutured Skin Incisions in a Porcine Model: A Short Report." *Photomedicine and laser surgery* 34 (2):53-55. doi: 10.1089/pho.2015.4013.

Filippo, Katia, Anne Dudeck, Mike Hasenberg, Emma Nye, Nico van Rooijen, Karin Hartmann, Matthias Gunzer, Axel Roers, and Nancy Hogg. 2013. "Mast cell and macrophage chemokines CXCL1/CXCL2 control the early stage of neutrophil recruitment during tissue inflammation." *Blood* 121 (24):4930-4937. doi: 10.1182/blood-2013-02-486217.

Flannagan, Ronald S., Gabriela Cosío, and Sergio Grinstein. 2009. "Antimicrobial mechanisms of phagocytes and bacterial evasion strategies." *Nature reviews. Microbiology* 7 (5):355-366. doi: 10.1038/nrmicro2128.

Forn-Cuní, G., M. Varela, P. Pereiro, B. Novoa, and A. Figueras. 2017. "Conserved gene regulation during acute inflammation between zebrafish and mammals." *Scientific Reports* 7:41905. doi: 10.1038/srep41905.

Frangez, Igor, Ksenija Cankar, Helena Frangez, and Dragica Smrke. 2017. "The effect of LED on blood microcirculation during chronic wound healing in diabetic and non-diabetic patients—a prospective, double-blind randomized study." *Lasers in Medical Science* 32 (4):887-894. doi: 10.1007/s10103-017-2189-7.

Frykberg, Robert G., and Jaminelli Banks. 2015. "Challenges in the Treatment of Chronic Wounds." *Advances in Wound Care* 4 (9):560-582. doi: 10.1089/wound.2015.0635.

Furukawa, Shigetada, Takuya Fujita, Michio Shimabukuro, Masanori Iwaki, Yukio Yamada, Yoshimitsu Nakajima, Osamu Nakayama, Makoto Makishima, Morihiro Matsuda, and Iichiro Shimomura. 2017. "Increased oxidative stress in obesity and its impact on metabolic syndrome." *The Journal of clinical investigation* 114 (12):1752-1761.

Gardai, Shyra, Ben B. Whitlock, Cheryl Helgason, Dan Ambruso, Valerie Fadok, Donna Bratton, and Peter M. Henson. 2002. "Activation of SHIP by NADPH oxidase-stimulated Lyn leads to enhanced apoptosis in neutrophils." *The Journal of biological chemistry* 277 (7):5236-5246. doi: 10.1074/jbc.M110005200.

Gauron, Carole, Christine Rampon, Mohamed Bouzaffour, Eliane Ipendey, Jérémie Teillon, Michel Volovitch, and Sophie Vriz. 2013. "Sustained production of ROS triggers compensatory proliferation and is required for regeneration to proceed." *Scientific reports* 3. doi: 10.1038/srep02084.

Gemert, M. J. C., and S. L. Jacques. 1989. "Skin optics." *IEEE Transactions …*.

Gigo-Benato, D., S. Geuna, A. de Castro Rodrigues, P. Tos, M. Fornaro, E. Boux, B. Battiston, and M. G. Giacobini-Robecchi. 2004. "Low-power laser biostimulation enhances nerve repair after end-to-side neurorrhaphy: a double-blind randomized study in the rat median nerve model." *Lasers in medical science* 19 (1):57-65. doi: 10.1007/s10103-004-0300-3.

Giorgio, Marco, Enrica Migliaccio, Francesca Orsini, Demis Paolucci, Maurizio Moroni, Cristina Contursi, Giovanni Pelliccia, Lucilla Luzi, Saverio Minucci, and Massimo Marcaccio. 2005. "Electron transfer between cytochrome c and p66 Shc generates reactive oxygen species that trigger mitochondrial apoptosis." *Cell* 122 (2):221-233.

Goren, Itamar, Nadine Allmann, Nir Yogev, Christoph Schürmann, Andreas Linke, Martin Holdener, Ari Waisman, Josef Pfeilschifter, and Stefan Frank. 2009. "A Transgenic Mouse Model of Inducible Macrophage Depletion : Effects of Diphtheria Toxin-Driven Lysozyme M-Specific Cell Lineage Ablation on Wound Inflammatory, Angiogenic, and Contractive Processes." *The American Journal of Pathology* 175 (1):132-147. doi: 10.2353/ajpath.2009.081002.

Gould, Lisa, Peter Abadir, Harold Brem, Marissa Carter, Teresa Conner-Kerr, Jeff Davidson, Luisa DiPietro, Vincent Falanga, Caroline Fife, and Sue Gardner. 2015. "Chronic wound repair and healing in older adults: current status and future research." *Wound Repair and Regeneration* 23 (1):1-13.

Gray, C., C. A. Loynes, M. Whyte, D. C. Crossman, S. A. Renshaw, and T. Chico. 2011. "Simultaneous intravital imaging of macrophage and neutrophil behaviour during inflammation using a novel transgenic zebrafish." *Thrombosis and haemostasis* 105 (5). doi: 10.1160/th10-08-0525.

Grigg, JM, M Silverman, JS Savill, C Sarraf, and C Haslett. 1991. "Neutrophil apoptosis and clearance from neonatal lungs." *The Lancet* 338 (8769):720-722.

Gur, Ali, Aysegul Jale Sarac, Remzi Cevik, Ozlem Altindag, and Serdar Sarac. 2004. "Efficacy of 904 nm gallium arsenide low level laser therapy in the management of chronic myofascial pain in the neck: A double-blind and randomize-controlled trial." *Lasers in Surgery and Medicine* 35 (3):229-235.

Hall, C., M. V. Flores, K. Crosier, and P. Crosier. 2009. "Live cell imaging of zebrafish leukocytes." *Live cell imaging of zebrafish leukocytes*.

Hamblin, M. R. 2017. "Mechanisms and applications of the anti-inflammatory effects of photobiomodulation." *AIMS Biophys* 4 (3):337-361. doi: 10.3934/biophy.2017.3.337.

Hamblin, Michael R. 2018. "Mechanisms and Mitochondrial Redox Signaling in Photobiomodulation." *Photochemistry and Photobiology* 94 (2):199-212. doi: 10.1111/php.12864.

Harvath, L., J. D. Robbins, and A. Russell. 1991. "cAMP and human neutrophil chemotaxis. Elevation of cAMP differentially affects chemotactic responsiveness." *The Journal of …*.

Hawkins, D., N. Houreld, and H. Abrahamse. 2005. "Low level laser therapy (LLLT) as an effective therapeutic modality for delayed wound healing." *Annals of the New York Academy of Sciences* 1056 (1):486-493.

Hawkins, Denise H., and Heidi Abrahamse. 2006. "The role of laser fluence in cell viability, proliferation, and membrane integrity of wounded human skin fibroblasts following helium-neon laser irradiation." *Lasers in Surgery and Medicine* 38 (1):74-83. doi: 10.1002/lsm.20271.

He, Li-Xia, Jun-Bo Wang, Bin Sun, Jian Zhao, Lin Li, Teng Xu, Hui Li, Jing-Qin Sun, Jinwei Ren, and Rui Liu. 2017. "Suppression of TNF-α and free radicals reduces systematic inflammatory and metabolic disorders: Radioprotective effects of ginseng oligopeptides on intestinal barrier function and antioxidant defense." *The Journal of nutritional biochemistry* 40:53-61.

Heidari, Mohadeseh, Mojgan Paknejad, Raika Jamali, Hanieh Nokhbatolfoghahaei, Reza Fekrazad, and Neda Moslemi. 2017. "Effect of laser photobiomodulation on wound healing and postoperative pain following free gingival graft: A split-mouth triple-blind randomized controlled clinical trial." *Journal of Photochemistry and Photobiology B: Biology* 172:109-114. doi: 10.1016/j.jphotobiol.2017.05.022.

Henry, J. Forman, and Torres Martine. 2002. "Reactive oxygen species and cell signaling: respiratory burst in macrophage signaling." *American journal of respiratory and critical care medicine* 166 (12 Pt 2):8. doi: 10.1164/rccm.2206007.

Henry, J. Forman, Maiorino Matilde, and Ursini Fulvio. 2010. "Signaling functions of reactive oxygen species." *Biochemistry* 49 (5):835-842. doi: 10.1021/bi9020378.

Henry, Katherine M, Luke Pase, Carlos Fernando Ramos-Lopez, Graham J Lieschke, Stephen A Renshaw, and Constantino Carlos Reyes-Aldasoro. 2013. "PhagoSight: an open-source MATLAB® package for the analysis of fluorescent neutrophil and macrophage migration in a zebrafish model." *PloS one* 8 (8):e72636.

Herbaczynska-Cedro, Krystyna, Krystyna Lembowicz, and Barbara Pytel. 1991. "NG-monomethyl-l-arginine increases platelet deposition on damaged endothelium in vivo. A scanning electron microscopic study." *Thrombosis research* 64 (1):1-9.

Hoeksema, M. A., J. L. Stöger, and M. P. J. de Winther. 2012. "Molecular pathways regulating macrophage polarization: implications for atherosclerosis." *Current atherosclerosis …*. doi: 10.1007/s11883-012-0240-5.

Honda, S., Y. Sasaki, K. Ohsawa, and Imai Y. of …. 2001a. "Extracellular ATP or ADP induce chemotaxis of cultured microglia through Gi/o-coupled P2Y receptors." *Extracellular ATP or ADP induce chemotaxis of cultured microglia through Gi/o-coupled P2Y receptors*. doi: 10.1523/JNEUROSCI.21-06-01975.2001.

Honda, S., Y. Sasaki, K. Ohsawa, and Imai - Y. of …. 2001b. "Extracellular ATP or ADP induce chemotaxis of cultured microglia through Gi/o-coupled P2Y receptors." *Journal of …*. doi: 10.1523/JNEUROSCI.21-06-01975.2001.

Hotamisligil, Gokhan S. 2006. "Inflammation and metabolic disorders." *Nature* 444 (7121):860-867.

Houreld, N., and Abrahamse H. Foot. 2005. "Low-level laser therapy for diabetic foot wound healing." *Low-level laser therapy for diabetic foot wound healing*.

Houreld, Nicolette N. 2014. "Irradiation at 660 nm modulates different genes central to wound healing in wounded and diabetic wounded cell models." *spie*. doi: 10.1117/12.2041430.

Hsieh, Yueh-Feng, Jui-Hsiang Hsieh, Eng-Kean Yeong, Wen-Tyng Li, Yu-Chi Chou, and Ruoh-Chyu Ruaan. 2012. "Effects of LED light irradiation on human foreskin fibroblasts and its implication to wound healing." *Journal of Medical and Biological Engineering* 33 (2):155-162.

Huang, Ying-Ying Y., Kazuya Nagata, Clark E. Tedford, Thomas McCarthy, and Michael R. Hamblin. 2013. "Low-level laser therapy (LLLT) reduces oxidative stress in primary cortical neurons in vitro." *Journal of biophotonics* 6 (10):829-838. doi: 10.1002/jbio.201200157.

Huang, Ying-Ying Y., Sulbha K. Sharma, James Carroll, and Michael R. Hamblin. 2010. "Biphasic dose response in low level light therapy - an update." *Dose-response : a publication of International Hormesis Society* 9 (4):602-618. doi: 10.2203/dose-response.11-009.Hamblin.

Idzko, Marco, Davide Ferrari, and Holger K Eltzschig. 2014. "Nucleotide signalling during inflammation." *Nature* 509 (7500):310.

Imai, Shin-ichiro, and Leonard Guarente. 2010. "Ten years of NAD-dependent SIR2 family deacetylases: implications for metabolic diseases." *Trends in pharmacological sciences* 31 (5):212-220.

Inaba, Kayo, Muneo Inaba, Nikolaus Romani, Hideki Aya, Masashi Deguchi, Susumu Ikehara, Shigeru Muramatsu, and RM Steinman. 1992. "Generation of large numbers of dendritic cells from mouse bone marrow cultures supplemented with granulocyte/macrophage colony-stimulating factor." *Journal of Experimental Medicine* 176 (6):1693-1702.

Ionin, AP, and EG Volkova. 1989. "Intravenous use of low-energy helium-neon laser irradiation in unstable angina." *Sovetskaia meditsina* (8):17-19.

Ishida, Takashi, Teruhiro Nakajima, Akira Kudo, and Atsushi Kawakami. 2010. "Phosphorylation of Junb family proteins by the Jun N-terminal kinase supports tissue regeneration in zebrafish." *Developmental biology* 340 (2):468-479.

Jelcic, M., B. Enyedi, J. B. Xavier, and P. Niethammer. 2017. "Image-Based Measurement of H 2 O 2 Reaction-Diffusion in Wounded Zebrafish Larvae." *Image-Based Measurement of H 2 O 2 Reaction-Diffusion in Wounded Zebrafish Larvae*.

Jiang, Fan, Yun Zhang, and Gregory J Dusting. 2011. "NADPH oxidase-mediated redox signaling: roles in cellular stress response, stress tolerance, and tissue repair." *Pharmacological reviews* 63 (1):218-242.

Joensen, Jon, Knut Øvsthus, Rolf K. Reed, Steinar Hummelsund, Vegard V. Iversen, Rodrigo Lopes-Martins, and Jan Bjordal. 2012. "Skin penetration time-profiles for continuous 810 nm and Superpulsed 904 nm lasers in a rat model." *Photomedicine and laser surgery* 30 (12):688-694. doi: 10.1089/pho.2012.3306.

Jones, Annie, and David Vaughan. 2005. "Hydrogel dressings in the management of a variety of wound types: A review." *Journal of Orthopaedic nursing* 9:S1-S11.

Jx, Jiang, and Török Nj. 2014. "NADPH Oxidases in Chronic Liver Diseases." *NADPH Oxidases in Chronic Liver Diseases.*

Kalyanaraman, Balaraman, Gang Cheng, Micael Hardy, Olivier Ouari, Marcos Lopez, Joy Joseph, Jacek Zielonka, and Michael B. Dwinell. 2017. "A review of the basics of mitochondrial bioenergetics, metabolism, and related signaling pathways in cancer cells: Therapeutic targeting of tumor mitochondria with lipophilic cationic compounds." *Redox Biology* 14. doi: 10.1016/j.redox.2017.09.020.

Karu, T, L Pyatibrat, and G Kalendo. 1995. "Irradiation with He・Ne laser increases ATP level in cells cultivated in vitro." *Journal of Photochemistry and Photobiology B: Biology* 27 (3):219-223.

Karu, T. 1987. "Photobiological fundamentals of low-power laser therapy." *IEEE Journal of Quantum Electronics* 23 (10):1703-1717. doi: 10.1109/jqe.1987.1073236.

Karu, T. I., L. V. Pyatibrat, S. F. Kolyakov, and N. I. Afanasyeva. 2008. "Relevant to Mechanisms of Laser Phototherapy: Reduction or Oxidation of Cytochrome c Oxidase Under Laser Radiation at 632.8 nm." *Relevant to Mechanisms of Laser Phototherapy: Reduction or Oxidation of Cytochrome c Oxidase Under Laser Radiation at 632.8 nm*.

Karu, T. I., T. P. Ryabykh, G. E. Fedoseyeva, and N. I. Puchkova. 1989. "Helium-neon laser-induced respiratory burst of phagocytic cells." *Lasers in surgery and medicine* 9 (6):585-588.

Karu, Tiina. 2010. "Mitochondrial Mechanisms of Photobiomodulation in Context of New Data About Multiple Roles of ATP." *Photomedicine and Laser Surgery* 28 (2):159-160. doi: 10.1089/pho.2010.2789.

Karu, Tiina. 2013. "Is It Time to Consider Photobiomodulation As a Drug Equivalent?" *Photomedicine and Laser Surgery* 31 (5):189-191. doi: 10.1089/pho.2013.3510.

Karu, Tiina I., Ludmila V. Pyatibrat, and Natalia I. Afanasyeva. 2004. "A Novel Mitochondrial Signaling Pathway Activated by Visible-to-near Infrared Radiation¶." *Photochemistry and Photobiology* 80 (2):366-372. doi: 10.1111/j.1751-1097.2004.tb00097.x.

Karu, Tiina I., Lydmila V. Pyatibrat, Sergei F. Kolyakov, and Natalya I. Afanasyeva. 2005. "Absorption measurements of a cell monolayer relevant to phototherapy: Reduction of cytochrome c oxidase under near IR radiation." *Journal of Photochemistry and Photobiology B: Biology* 81 (2). doi: 10.1016/j.jphotobiol.2005.07.002.

Katada, Sayako, Axel Imhof, and Paolo Sassone-Corsi. 2012. "Connecting threads: epigenetics and metabolism." *Cell* 148 (1-2):24-28.

Kato, Masru. 1981. "Cytochrome oxidase is a possible photoreceptor in mitochondria." *Photobiochem Photobiophys* 2:263-269.

Kato, Takayuki, Haruo Kutsuna, Nobuhide Oshitani, and Seiichi Kitagawa. 2006. "Cyclic AMP delays neutrophil apoptosis via stabilization of Mcl-1." *FEBS letters* 580 (19):4582-4586. doi: 10.1016/j.febslet.2006.07.034.

Kaviani, A., G. E. Djavid, and L. Ataie-Fashtami. 2011. "A randomized clinical trial on the effect of low-level laser therapy on chronic diabetic foot wound healing: a preliminary report." *A randomized clinical trial on the effect of low-level laser therapy on chronic diabetic foot wound healing: a preliminary report*. doi: 10.1089/pho.2009.2680.

Kazemi-Khoo, N. 2006. "Successful treatment of diabetic foot ulcers with low-level laser therapy." *The Foot* 16 (4):184-187. doi: 10.1016/j.foot.2006.05.004.

Keightley, Maria-Cristina, Chieh-Huei Wang, Vahid Pazhakh, and Graham J. Lieschke. 2014. "Delineating the roles of neutrophils and macrophages in zebrafish regeneration models." *The International Journal of Biochemistry & Cell Biology* 56:92-106. doi: 10.1016/j.biocel.2014.07.010.

Kelly, Beth, and Luke A. J. O'Neill. 2015. "Metabolic reprogramming in macrophages and dendritic cells in innate immunity." *Cell Research* 25 (7):771-784. doi: 10.1038/cr.2015.68.

Kennedy, A. D., and DeLeo - F. R. research. 2009. "Neutrophil apoptosis and the resolution of infection." *Immunologic research*. doi: 10.1007/s12026-008-8049-6.

Keuper, Michaela, Stephan Sachs, Ellen Walheim, Lucia Berti, Bernhard Raedle, Daniel Tews, Pamela Fischer-Posovszky, Martin Wabitsch, Martin Hrabě de Angelis, and Gabi Kastenmüller. 2017. "Activated macrophages control human adipocyte mitochondrial bioenergetics via secreted factors." *Molecular Metabolism*.

Khanna, Savita, Sabyasachi Biswas, Yingli Shang, Eric Collard, Ali Azad, Courtney Kauh, Vineet Bhasker, Gayle M. Gordillo, Chandan K. Sen, and Sashwati Roy. 2010. "Macrophage Dysfunction Impairs Resolution of Inflammation in the Wounds of Diabetic Mice." *PloS one* 5 (3):e9539. doi: 10.1371/journal.pone.0009539.

Kim, Soogeun, Sungho Shin, and Sungho Jeong. 2015. "Effects of tissue water content on the propagation of laser light during low-level laser therapy." *Journal of Biomedical Optics* 20 (5):051027.

Kobayashi, S. D., J. M. Voyich, and A. R. Whitney. 2005. "Spontaneous neutrophil apoptosis and regulation of cell survival by granulocyte macrophage-colony stimulating factor." *Journal of leukocyte …*. doi: 10.1189/jlb.0605289.

Kocsis, L, P Herman, and A Eke. 2006. "The modified Beer–Lambert law revisited." *Physics in Medicine & Biology* 51 (5):N91.

Koh, Timothy J., and Luisa DiPietro. 2015. "Inflammation and wound healing: the role of the macrophage." *Expert reviews in molecular medicine* 13. doi: 10.1017/S1462399411001943.

Konstantinovic, Ljubica M., Milisav R. Cutovic, Aleksandar N. Milovanovic, Stevan J. Jovic, Aleksandra S. Dragin, Milica Letic, and Vera M. Miler. 2010. "Low-Level Laser Therapy for Acute Neck Pain with Radiculopathy: A Double-Blind Placebo-Controlled Randomized Study." *Pain Medicine* 11 (8):1169-1178. doi: 10.1111/j.1526-4637.2010.00907.x.

Koopman, Werner J. H., Sjoerd Verkaart, Sjenet E. van Vries, Sander Grefte, Jan A. M. Smeitink, and Peter H. G. M. Willems. 2006. "Simultaneous quantification of oxidative stress and cell spreading using 5-(and-6)-chloromethyl-2',7'-dichlorofluorescein." *Cytometry Part A* 69A (12):1184-1192. doi: 10.1002/cyto.a.20348.

Kotwal, Girish J., and Sufan Chien. 2017. "Macrophage Differentiation in Normal and Accelerated Wound Healing." *Results and problems in cell differentiation* 62:353-364. doi: 10.1007/978-3-319-54090-0_14.

Kotwal, Girish J., Harshini Sarojini, and Sufan Chien. 2015. "Pivotal role of ATP in macrophages fast tracking wound repair and regeneration." *Wound Repair and Regeneration* 23 (5):724-727. doi: 10.1111/wrr.12323.

Kushibiki, Toshihiro, Takeshi Hirasawa, Shinpei Okawa, and Miya Ishihara. 2013. "Blue laser irradiation generates intracellular reactive oxygen species in various types of cells." *Photomedicine and Laser Surgery* 31 (3):95-104.

Kymplová, Jaroslava, Leoš Navrátil, and Jiří Knížek. 2003. "Contribution of phototherapy to the treatment of episiotomies." *Journal of clinical laser medicine & surgery* 21 (1):35-39.

Lambeth, J. David, Tsukasa Kawahara, and Becky Diebold. 2007. "Regulation of Nox and Duox Enzymatic Activity and Expression." *Free radical biology & medicine* 43 (3):319-331. doi: 10.1016/j.freeradbiomed.2007.03.028.

Lamy, M, M Mathy-Hartert, and G Deby-Dupont. 1996. "Neutrophil-induced oxidative stress." In *Yearbook of Intensive Care and Emergency Medicine*, 83-95. Springer.

Land, Walter G. 2015. "The role of damage-associated molecular patterns (DAMPs) in human diseases: part II: DAMPs as diagnostics, prognostics and therapeutics in clinical medicine." *Sultan Qaboos University Medical Journal* 15 (2):e157.

Lavine, WS, EG Maderazo, J Stolman, PA Ward, RB Cogen, I Greenblatt, and PB Robertson. 1979. "Impaired neutrophil chemotaxis in patients with juvenile and rapidly progessing periodontitis." *Journal of periodontal Research* 14 (1):10-19.

Leal Junior, Ernesto Cesar Pinto, Rodrigo Álvaro Brandão Lopes-Martins, Francis Dalan, Mauricio Ferrari, Fernando Montanari Sbabo, Rafael Abeche Generosi, Bruno Manfredini Baroni, Socrates Calvoso Penna, Vegard V Iversen, and Jan Magnus Bjordal. 2008. "Effect of 655-nm low-level laser therapy on exercise-induced skeletal muscle fatigue in humans." *Photomedicine and laser surgery* 26 (5):419-424.

Lee, S., E. Tak, J. Lee, M. A. Rashid, M. P. Murphy, and Ha - J. research. 2011. "Mitochondrial H2O2 generated from electron transport chain complex I stimulates muscle differentiation." *Cell research*.

Li, L., B. Yan, Y. Q. Shi, W. Q. Zhang, and Z. L. Wen. 2012a. "Live imaging reveals differing roles of macrophages and neutrophils during zebrafish tail fin regeneration." *Live imaging reveals differing roles of macrophages and neutrophils during zebrafish tail fin regeneration*. doi: 10.1074/jbc.M112.349126.

Li, Li, Bo Yan, Yu-Qian Shi, Wen-Qing Zhang, and Zi-Long Wen. 2012b. "Live imaging reveals differing roles of macrophages and neutrophils during zebrafish tail fin regeneration." *Journal of Biological Chemistry* 287 (30):25353-25360.

Li, Shasha, Ana Luiza Zaninotto, Iuri Santana Neville, Wellingson Silva Paiva, Danuza Nunn, and Felipe Fregni. 2015. "Clinical utility of brain stimulation modalities following traumatic brain injury: current evidence." *Neuropsychiatric Disease and Treatment* 11:1573-1586. doi: 10.2147/NDT.S65816.

Liepe, Juliane, Aaron Sim, Helen Weavers, Laura Ward, Paul Martin, and Michael Stumpf. 2016. "Accurate Reconstruction of Cell and Particle Tracks from 3D Live Imaging Data." *Cell Systems* 3 (1):102-107. doi: 10.1016/j.cels.2016.06.002.

Lima, F. Mafra de, A. Balbin Villaverde, R. Albertini, A. P. Ligeiro de Oliveira, H. C. Castro Faria Neto, and F. Aimbire. 2010. "Low-level laser therapy associated to N-acetylcysteine lowers macrophage inflammatory protein-2 (MIP-2) mRNA expression and generation of intracellular reactive oxygen species in alveolar macrophages." *Photomedicine and Laser Surgery* 28 (6):763-771. doi: 10.1089/pho.2009.2638.

Lin, Edith LC, Susan M Cormier, and Joni A Torsella. 1996. "Fish biliary polycyclic aromatic hydrocarbon metabolites estimated by fixed-wavelength fluorescence: comparison with HPLC-fluorescent detection." *Ecotoxicology and environmental safety* 35 (1):16-23.

Lisse, Thomas S., Benjamin L. King, and Sandra Rieger. 2016. "Comparative transcriptomic profiling of hydrogen peroxide signaling networks in zebrafish and human keratinocytes: Implications toward conservation, migration and wound healing." *Scientific Reports* 6 (1). doi: 10.1038/srep20328.

Liu, Jianhua, Adrian Ormsby, Nancy Oja-Tebbe, and Patrick J Pagano. 2004. "Gene transfer of NAD (P) H oxidase inhibitor to the vascular adventitia attenuates medial smooth muscle hypertrophy." *Circulation research* 95 (6):587-594.

Liu, Peng, Zhihong Deng, Shufang Han, Tao Liu, Ning Wen, Wei Lu, Xianhui Geng, Sha Huang, and Yan Jin. 2008. "Tissue-engineered skin containing mesenchymal stem cells improves burn wounds." *Artificial organs* 32 (12):925-931.

Loosley, Alex J., Xian M. O'Brien, Jonathan S. Reichner, and Jay X. Tang. 2015. "Describing directional cell migration with a characteristic directionality time." *PloS one* 10 (5). doi: 10.1371/journal.pone.0127425.

Lu, C., S. Song, Y. Tang, and F. Zhou. 2011. "Effect of low power laser irradiation on macrophage phagocytic capacity." *Biophotonics and Immune Responses*.

Lucas, T., A. Waisman, R. Ranjan, J. Roes, T. Krieg, W. Muller, A. Roers, and S. A. Eming. 2010. "Differential Roles of Macrophages in Diverse Phases of Skin Repair." *The Journal of Immunology* 184 (7):3964-3977. doi: 10.4049/jimmunol.0903356.

Lucas, Tina, Ari Waisman, Rajeev Ranjan, Jürgen Roes, Thomas Krieg, Werner Müller, Axel Roers, and Sabine A Eming. 2010. "Differential roles of macrophages in diverse phases of skin repair." *The Journal of Immunology* 184 (7):3964-3977.

Lumbroso, Delphine, Soaad Soboh, Avi Maimon, Sagie Schif-Zuck, Amiram Ariel, and Tal Burstyn-Cohen. 2018. "Macrophage-Derived Protein S Facilitates Apoptotic Polymorphonuclear Cell Clearance by Resolution Phase Macrophages and Supports Their Reprogramming." *Frontiers in Immunology* 9:358. doi: 10.3389/fimmu.2018.00358.

MacNeil, Sheila. 2007. "Progress and opportunities for tissue-engineered skin." *Nature* 445 (7130):874.

Mandrekar-Colucci, Shweta, J Colleen Karlo, and Gary E Landreth. 2012. "Mechanisms underlying the rapid peroxisome proliferator-activated receptor-γ-mediated amyloid clearance and reversal of cognitive deficits in a murine model of Alzheimer's disease." *Journal of Neuroscience* 32 (30):10117-10128.

Mantineo, Matias E, João Páscoa Pinheiro, and António Miguel Morgado. 2014. "Low-level laser therapy on skeletal muscle inflammation: evaluation of irradiation parameters." *Journal of biomedical optics* 19 (9):098002.

Mathias, Jonathan R., Benjamin J. Perrin, Ting-Xi Liu, John Kanki, Thomas A. Look, and Anna Huttenlocher. 2006. "Resolution of inflammation by retrograde chemotaxis of neutrophils in transgenic zebrafish." *Journal of Leukocyte Biology* 80 (6):1281-1288. doi: 10.1189/jlb.0506346.

Matsumoto, Brian. 2003. *Cell biological applications of confocal microscopy*. Vol. 70: Academic Press.

McCloy, Rachael A, Samuel Rogers, C Elizabeth Caldon, Thierry Lorca, Anna Castro, and Andrew Burgess. 2014. "Partial inhibition of Cdk1 in G2 phase overrides the SAC and decouples mitotic events." *Cell Cycle* 13 (9):1400-1412.

McDonald, B., K. Pittman, G. B. Menezes, and S. A. Hirota. 2010. "Intravascular danger signals guide neutrophils to sites of sterile inflammation." …. doi: 10.1126/science.1195491.

McDonald, Braedon, Keir Pittman, Gustavo B Menezes, Simon A Hirota, Ingrid Slaba, Christopher CM Waterhouse, Paul L Beck, Daniel A Muruve, and Paul Kubes. 2010. "Intravascular Danger Signals Guide Neutrophils to Sites of Sterile Inflammation." *science* 1195491 (362):330.

Mendez, Tatiana MTV, Antonio LB Pinheiro, Marcos TT Pacheco, Patricia M Nascimento, and Luciana MP Ramalho. 2004. "Dose and wavelength of laser light have influence on the repair of cutaneous wounds." *Journal of clinical laser medicine & surgery* 22 (1):19-25.

Meszaros, Adriana J, Jonathan S Reichner, and Jorge E Albina. 1999. "Macrophage phagocytosis of wound neutrophils." *Journal of leukocyte biology* 65 (1):35-42.

Meszaros, Adriana J, Jonathan S Reichner, and Jorge E Albina. 2000. "Macrophage-induced neutrophil apoptosis." *The Journal of Immunology* 165 (1):435-441.

Migliario, Mario, Pamela Pittarella, Matteo Fanuli, Manuela Rizzi, and Filippo Renò. 2014. "Laser-induced osteoblast proliferation is mediated by ROS production." *Lasers in Medical Science* 29 (4):1463-1467. doi: 10.1007/s10103-014-1556-x.

Mikut, Ralf, Thomas Dickmeis, Wolfgang Driever, Pierre Geurts, Fred A. Hamprecht, Bernhard X. Kausler, María J. Ledesma-Carbayo, Raphaël Marée, Karol Mikula, Periklis Pantazis, Olaf Ronneberger, Andres Santos, Rainer Stotzka, Uwe Strähle, and Nadine Peyriéras. 2013. "Automated Processing of Zebrafish Imaging Data: A Survey." *Zebrafish* 10 (3). doi: 10.1089/zeb.2013.0886.

Miller, Mark J, Sindy H Wei, Michael D Cahalan, and Ian Parker. 2003. "Autonomous T cell trafficking examined in vivo with intravital two-photon microscopy." *Proceedings of the National Academy of Sciences* 100 (5):2604-2609.

Minors, David S. 2007. "Haemostasis, blood platelets and coagulation." *Anaesthesia & Intensive Care Medicine* 8 (5):214-216.

Mirza, R., L.A. DiPietro, and T.J. Koh. 2009. "Selective and specific macrophage ablation is detrimental to wound healing in mice." *American Journal of Pathology* 175 (6):2454.

Mirza, Rita, and J. Timothy Koh. 2011. "Dysregulation of monocyte/macrophage phenotype in wounds of diabetic mice." *Cytokine* 56 (2):256-264. doi: 10.1016/j.cyto.2011.06.016.

Mittal, Rahul, Saroj Sharma, Sanjay Chhibber, and Kusum Harjai. 2005. "Effect of macrophage secretory products on elaboration of virulence factors by planktonic and biofilm cells of Pseudomonas aeruginosa." *Comparative immunology, microbiology and infectious diseases* 29 (1):12-26. doi: 10.1016/j.cimid.2005.11.002.

Moon, C. H., O. Kwon, C. H. Woo, and H. D. Ahn. 2014. "Therapeutic Effect of Irradiation of Magnetic Infrared Laser on Osteoarthritis Rat Model." *Photochemistry and …*. doi: 10.1111/php.12304.

Morimoto, Yuji, Tsunenori Aral, Makoto Kikuchi, Shinji Nakajima, and Haruo Nakamura. 1994. "Effect of low-intensity argon laser irradiation on mitochondrial respiration." *Lasers in surgery and medicine* 15 (2):191-199.

Moshakis, V, MJ Fordyce, JD Griffiths, and JA McKinna. 1984. "Tegadern versus gauze dressing in breast surgery." *The British journal of clinical practice* 38 (4):149.

Moshkovska, T. 2005. "It is time to test low level laser therapy in Great Britain." *Postgraduate Medical Journal* 81 (957):436-441. doi: 10.1136/pgmj.2004.027755.

Mugoni, Vera, Annalisa Camporeale, and Massimo M Santoro. 2014a. "Analysis of oxidative stress in zebrafish embryos." *JoVE (Journal of Visualized Experiments)* (89):e51328-e51328.

Mugoni, Vera, Annalisa Camporeale, and Massimo M. Santoro. 2014b. "Analysis of Oxidative Stress in Zebrafish Embryos." *JoVE (Journal of Visualized Experiments)* (89). doi: 10.3791/51328.

Murray, P. J., and T. A. Wynn. 2011. "Obstacles and opportunities for understanding macrophage polarization." *Journal of leukocyte biology*. doi: 10.1189/jlb.0710409.

Naderi, Mina, Mohammadreza Razzaghi, Gholamreza Djavid, and Zahra Hajebrahimi. 2017. "A Comparative Study of 660 nm Low-Level Laser and Light Emitted Diode in Proliferative Effects of Fibroblast Cells." *Journal of Lasers in Medical Sciences* 8 (Suppl 1). doi: 10.15171/jlms.2017.s9.

Nascimento, Silvia B, Romualdo B Sousa, Marcos Jullian B Martins, Antoniella Souza Gomes, Marcellus Henrique LP Souza, Richard L Guerrant, Fernando Q Cunha, Ronaldo A Ribeiro, and Gerly AC Brito. 2005. "Glutamine depletion potentiates leucocyte-dependent inflammatory events induced by carrageenan or Clostridium difficile toxin A in rats." *Immunology* 116 (3):328-336.

Nazarewicz, Rafal R, Alfiya Bikineyeva, and Sergey I Dikalov. 2013. "Rapid and specific measurements of superoxide using fluorescence spectroscopy." *Journal of biomolecular screening* 18 (4):498-503.

Nieminen, Julie, Christian St-Pierre, Pampa Bhaumik, Françoise Poirier, and Sachiko Sato. 2008. "Role of galectin-3 in leukocyte recruitment in a murine model of lung infection by Streptococcus pneumoniae." *The Journal of Immunology* 180 (4):2466-2473.

Niethammer, P., C. Grabher, A. T. Look, and Mitchison - T. J. Nature. 2009. "A tissue-scale gradient of hydrogen peroxide mediates rapid wound detection in zebrafish." *Nature*.

Niethammer, Philipp. 2016. "The early wound signals." *Current opinion in genetics & development* 40:17-22. doi: 10.1016/j.gde.2016.05.001.

Niethammer, Philipp, Clemens Grabher, A. T. Look, and Timothy J. Mitchison. 2009. "A tissue-scale gradient of hydrogen peroxide mediates rapid wound detection in zebrafish." *A tissue-scale gradient of hydrogen peroxide mediates rapid wound detection in zebrafish.* 459 (7249). doi: 10.1038/nature08119.

Novais, F. O., R. C. Santiago, and A. Báfica. 2009. "Neutrophils and macrophages cooperate in host resistance against Leishmania braziliensis infection." *The journal of …*.

Nunn, A. V. W., M. L. Barnard, K. Bhakoo, and Murray - J. Febs …. 1996. "Characterisation of secondary metabolites associated with neutrophil apoptosis." *FEBS …*. doi: 10.1016/0014-5793(96)00839-3.

Nussbaum, Samuel R., Marissa J. Carter, Caroline E. Fife, Joan DaVanzo, Randall Haught, Marcia Nusgart, and Donna Cartwright. 2018. "An Economic Evaluation of the Impact, Cost, and Medicare Policy

Implications of Chronic Nonhealing Wounds." *Value in Health* 21 (1):27-32. doi: 10.1016/j.jval.2017.07.007.

O'Neill, Luke AJ, and Charles A Dinarello. 2000. "The IL-1 receptor/toll-like receptor superfamily: crucial receptors for inflammation and host defense." *Immunology today* 21 (5):206-209.

Oliveira, Sofia de, Pierre Boudinot, Ângelo Calado, and Victoriano Mulero. 2015. "Duox1-derived H2O2 modulates Cxcl8 expression and neutrophil recruitment via JNK/c-JUN/AP-1 signaling and chromatin modifications." *Journal of immunology (Baltimore, Md. : 1950)* 194 (4). doi: 10.4049/jimmunol.1402386.

Oron, Uri, Tali Yaakobi, Amir Oron, Gal Hayam, Lior Gepstein, Ofer Rubin, Tamir Wolf, and Shlomo Ben Haim. 2001. "Attenuation of infarct size in rats and dogs after myocardial infarction by low-energy laser irradiation." *Lasers in surgery and medicine* 28 (3):204-211.

Oron, Uri, Tali Yaakobi, Amir Oron, Daniel Mordechovitz, Rona Shofti, Gal Hayam, Uzi Dror, Lior Gepstein, Tamir Wolf, and Christian Haudenschild. 2001. "Low-energy laser irradiation reduces formation of scar tissue after myocardial infarction in rats and dogs." *Circulation* 103 (2):296-301.

Owusu-Ansah, Edward, Amir Yavari, and Utpal Banerjee. 2008. "A protocol for _in vivo_ detection of reactive oxygen species." *Protocol Exchange*. doi: 10.1038/nprot.2008.23.

Palsson-McDermott, Eva M, and Luke Aj O'neill. 2013. "The Warburg effect then and now: from cancer to inflammatory diseases." *Bioessays* 35 (11):965-973.

Pase, L., J. E. Layton, C. Wittmann, F. Ellett, and C. J. Nowell…. 2012. "Neutrophil-delivered myeloperoxidase dampens the hydrogen peroxide burst after tissue wounding in zebrafish." *Neutrophil-delivered myeloperoxidase dampens the hydrogen peroxide burst after tissue wounding in zebrafish*.

Pase, L., C. J. Nowell, and G. J. Lieschke. 2012. "In Vivo Real-Time Visualization of Leukocytes and Intracellular Hydrogen Peroxide Levels During a Zebrafish Acute Inflammation Assay." *8 In Vivo Real-Time Visualization of Leukocytes and Intracellular Hydrogen Peroxide Levels During a Zebrafish Acute Inflammation Assay*.

Passarella, S, E Perlino, E Quagliariello, L Baldassarre, IM Catalano, and A Cingolani. 1983. "Evidence of changes, induced by HeNe laser irradiation, in the optical and biochemical properties of rat liver mitochondria." *Journal of Electroanalytical Chemistry and Interfacial Electrochemistry* 155:185-198.

Passarella, S., E. Casamassima, and S. Molinari. 1984. "Increase of proton electrochemical potential and ATP synthesis in rat liver mitochondria irradiated in vitro by helium-neon laser." *FEBS …*. doi: 10.1016/0014-5793(84)80577-3.

Passarella, Salvatore, Angela Ostuni, Anna Atlante, and Ernesto Quagliariello. 1988. "Increase in the ADP/ATP exchange in rat liver mitochondria irradiated in vitro by helium-neon laser." *Biochemical and biophysical research communications* 156 (2):978-986.

Pastore, M. Greco, S. Passarella, D. 2000. "Specific helium-neon laser sensitivity of the purified cytochrome c oxidase." *International journal of radiation biology* 76 (6):863-870.

Peplow, Philip V., Tzu-Yun Chung, Brigid Ryan, and David G. Baxter. 2011. "Laser photobiostimulation of wound healing: Reciprocity of irradiance and exposure time on energy density for splinted wounds in diabetic mice." *Lasers in Surgery and Medicine* 43 (8):843-850. doi: 10.1002/lsm.21094.

Pereira, Aymann N., Carlos de P. Eduardo, Edmir Matson, and Márcia M. Marques. 2002. "Effect of low-power laser irradiation on cell growth and procollagen synthesis of cultured fibroblasts." *Lasers in surgery and medicine* 31 (4):263-267. doi: 10.1002/lsm.10107.

Petrie, Timothy A., Nicholas S. Strand, Chao Tsung-Yang, Jeremy S. Rabinowitz, and Randall T. Moon. 2014. "Macrophages modulate adult zebrafish tail fin regeneration." *Development* 141 (13). doi: 10.1242/dev.098459.

Poiani, Guilherme da Cruz Ribeiro, Ana Luiza Zaninotto, Ana Maria Costa Carneiro, Renato Amaro Zangaro, Afonso Shiguemi Inoue Salgado, Rodolfo Borges Parreira, Almir Ferreira de Andrade, Manoel Jacobsen Teixeira, and Wellingson Silva Paiva. 2018. "Photobiomodulation using low-level laser therapy (LLLT) for patients with chronic traumatic brain injury: a randomized controlled trial study protocol." *Trials* 19 (1):17.

Quatromoni, J. G., and E. Eruslanov. 2012. "Tumor-associated macrophages: function, phenotype, and link to prognosis in human lung cancer." *American journal of translational …*.

Quirk, Brendan J, Purabi Sonowal, Mohammad-Ali Jazayeri, John E Baker, and Harry T Whelan. 2014. "Cardioprotection from ischemia-reperfusion injury by near-infrared light in rats." *Photomedicine and laser surgery* 32 (9):505-511.

Rajagopalan, Sanjay, Xiao Ping Meng, Santhini Ramasamy, David G Harrison, and Zorina S Galis. 1996. "Reactive oxygen species produced by macrophage-derived foam cells regulate the activity of vascular matrix metalloproteinases in vitro. Implications for atherosclerotic plaque stability." *The Journal of clinical investigation* 98 (11):2572-2579.

Rajaratnam, S., P. Bolton, and M. Dyson. 1994. "Macrophage responsiveness to laser therapy with varying pulsing frequencies." *Macrophage responsiveness to laser therapy with varying pulsing frequencies*.

Rajkumar, Vineeth S., Xu Shiwen, Maria Bostrom, Patricia Leoni, John Muddle, Mikael Ivarsson, Bengt Gerdin, Christopher P. Denton, George Bou-Gharios, Carol M. Black, and David J. Abraham. 2006. "Platelet-Derived Growth Factor-β Receptor Activation Is Essential for Fibroblast and Pericyte Recruitment during Cutaneous Wound Healing." *The American Journal of Pathology* 169 (6):2254-2265. doi: https://doi.org/10.2353/ajpath.2006.060196.

Renaud, Olivier, Philippe Herbomel, and Karima Kissa. 2011. "Studying cell behavior in whole zebrafish embryos by confocal live imaging: application to hematopoietic stem cells." *Nature protocols* 6 (12):1897-1904.

Renshaw, S. A., and N. S. Trede. 2012. "A model 450 million years in the making: zebrafish and vertebrate immunity." *A model 450 million years in the making: zebrafish and vertebrate immunity*.

Reyes-Aldasoro, Constantino C, S Akerman, and GM Tozer. 2008. "Measuring the velocity of fluorescently labelled red blood cells with a keyhole tracking algorithm." *Journal of microscopy* 229 (1):162-173.

Roach, Daniel R, Andrew GD Bean, Caroline Demangel, Malcolm P France, Helen Briscoe, and Warwick J Britton. 2002. "TNF regulates chemokine induction essential for cell recruitment, granuloma formation, and clearance of mycobacterial infection." *The Journal of immunology* 168 (9):4620-4627.

Robertson, A. L., and G. R. Holmes. 2014. "A zebrafish compound screen reveals modulation of neutrophil reverse migration as an anti-inflammatory mechanism." *A zebrafish compound screen reveals modulation of neutrophil reverse migration as an anti-inflammatory mechanism*.

Rodríguez, Norberto Santana, José Luis Martín Barrasa, Miguel Ángel Ponce González, Ana López García, José Antonio Ruiz Caballero, Antonio Torres García, and Jorge Freixinet Gilart. 2007. "Assessment of ischemia–reperfusion injury and early acute rejection in experimental lung transplantation after prolonged ischemia." *Archivos de Bronconeumología ((English Edition))* 43 (7):373-377.

Rong, Yuan, Dawn E Post, Russell O Pieper, Donald L Durden, Erwin G Van Meir, and Daniel J Brat. 2005. "PTEN and hypoxia regulate tissue factor expression and plasma coagulation by glioblastoma." *Cancer research* 65 (4):1406-1413.

Rosowski, Emily E, Qing Deng, Nancy P Keller, and Anna Huttenlocher. 2016a. "Rac2 Functions in Both Neutrophils and Macrophages To Mediate Motility and Host Defense in Larval Zebrafish." *The Journal of Immunology* 197 (12):4780-4790.

Rosowski, Emily E., Qing Deng, Nancy P. Keller, and Anna Huttenlocher. 2016b. "Rac2 Functions in Both Neutrophils and Macrophages To Mediate Motility and Host Defense in Larval Zebrafish." *J Immunol* 197 (12). doi: 10.4049/jimmunol.1600928.

Ross, Russell, and George Odland. 1968. "HUMAN WOUND REPAIR : II. Inflammatory Cells, Epithelial-Mesenchymal Interrelations, and Fibrogenesis." *The Journal of Cell Biology* 39 (1):152-168.

Rothe, Gregor, and Günter Valet. 1990. "Flow cytometric analysis of respiratory burst activity in phagocytes with hydroethidine and 2', 7'-dichlorofluorescin." *Journal of leukocyte biology* 47 (5):440-448.

Sáez, Pablo J, Pablo Vargas, Kenji F Shoji, Paloma A Harcha, Ana-María Lennon-Duménil, and Juan C Sáez. 2017a. "ATP promotes the fast migration of dendritic cells through the activity of pannexin 1 channels and P2X7 receptors." *Sci. Signal.* 10 (506):eaah7107.

Sáez, Pablo J., Pablo Vargas, Kenji F. Shoji, Paloma A. Harcha, Ana-María Lennon-Duménil, and Juan C. Sáez. 2017b. "ATP promotes the fast migration of dendritic cells through the activity of pannexin 1 channels and P2X7 receptors." *Sci. Signal.* 10 (506). doi: 10.1126/scisignal.aah7107.

Sanderson, Thomas H., Joseph M. Wider, Icksoo Lee, Christian A. Reynolds, Jenney Liu, Bradley Lepore, Reneé Tousignant, Melissa J. Bukowski, Hollie Johnston, Alemu Fite, Sarita Raghunayakula, John Kamholz, Lawrence I. Grossman, Karin Przyklenk, and Maik Hüttemann. 2018. "Inhibitory modulation of cytochrome c oxidase activity with specific near-infrared light wavelengths attenuates brain ischemia/reperfusion injury." *Scientific Reports* 8 (1):3481. doi: 10.1038/s41598-018-21869-x.

Sasada, Masataka, and Richard B. Johnston. 1980. "Macrophage microbicidal activity. Correlation between phagocytosis-associated oxidative metabolism and the killing of Candida by macrophages." *Journal of Experimental Medicine* 152 (1):85-98. doi: 10.1084/jem.152.1.85.

Sassone-Corsi, Paolo. 2013. "When metabolism and epigenetics converge." *Science* 339 (6116):148-150.

Savill, John, Nancy Hogg, Yi Ren, and Christopher Haslett. 1992. "Thrombospondin cooperates with CD36 and the vitronectin receptor in macrophage recognition of neutrophils undergoing apoptosis." *The Journal of clinical investigation* 90 (4):1513-1522.

Scaffidi, Paola, Tom Misteli, and Marco E. Bianchi. 2002. "Release of chromatin protein HMGB1 by necrotic cells triggers inflammation." *Nature* 418 (6894):191-195. doi: 10.1038/nature00858.

Scheiermann, Christoph, Yuya Kunisaki, and Paul S Frenette. 2013. "Circadian control of the immune system." *Nature Reviews Immunology* 13 (3):190.

Schindelin, Johannes, Ignacio Arganda-Carreras, Erwin Frise, Verena Kaynig, Mark Longair, Tobias Pietzsch, Stephan Preibisch, Curtis Rueden, Stephan Saalfeld, and Benjamin Schmid. 2012. "Fiji: an open-source platform for biological-image analysis." *Nature methods* 9 (7):676-682.

Schneider, Caroline A, Wayne S Rasband, and Kevin W Eliceiri. 2012. "NIH Image to ImageJ: 25 years of image analysis." *Nature methods* 9 (7):671.

Segal, Anthony W, Michael Geisow, Rodolfo Garcia, Angela Harper, and Robert Miller. 1981. "The respiratory burst of phagocytic cells is associated with a rise in vacuolar pH." *Nature* 290 (5805):406.

Sen, Chandan K. 2009. "Wound healing essentials: let there be oxygen." *Wound repair and regeneration : official publication of the Wound Healing Society [and] the European Tissue Repair Society* 17 (1):1-18. doi: 10.1111/j.1524-475X.2008.00436.x.

Shumilina, Ekaterina, Stephan M Huber, and Florian Lang. 2011. "Ca2+ signaling in the regulation of dendritic cell functions." *American Journal of Physiology-Cell Physiology* 300 (6):C1205-C1214.

Siegbahn, A., and A. Hammacher. 1990. "Differential effects of the various isoforms of platelet-derived growth factor on chemotaxis of fibroblasts, monocytes, and granulocytes." *The Journal of …*. doi: 10.1172/JCI114519.

Silva, Manuel T, M NazaréT Silva, and Rui Appelberg. 1989. "Neutrophil-macrophage cooperation in the host defence against mycobacterial infections." *Microbial pathogenesis* 6 (5):369-380.

Silva, Manuel T. 2011. "Macrophage phagocytosis of neutrophils at inflammatory/infectious foci: a cooperative mechanism in the control of infection and infectious inflammation." *Journal of leukocyte biology* 89 (5):675-683. doi: 10.1189/jlb.0910536.

Silveira, Paulo, Luciano da Silva, Daiane B. Fraga, Tiago P. Freitas, Emilio L. Streck, and Ricardo Pinho. 2009. "Evaluation of mitochondrial respiratory chain activity in muscle healing by low-level laser therapy." *Journal of Photochemistry and Photobiology B: Biology* 95 (2):89-92. doi: 10.1016/j.jphotobiol.2009.01.004.

Silveira, Paulo, Luciano da Silva, Daiane B. Fraga, Tiago P. Freitas, Emilio L. Streck, and Ricardo Pinho. 2009. "Evaluation of mitochondrial respiratory chain activity in muscle healing by low-level laser therapy." *Journal of Photochemistry and Photobiology B: Biology* 95 (2):89-92. doi: 10.1016/j.jphotobiol.2009.01.004.

Song, Ji Wei, Kun Li, Zhuo Wen Liang, Chen Dai, Xue Feng Shen, Yu Ze Gong, Shuang Wang, Xue Yu Hu, and Zhe Wang. 2017. "Low-level laser facilitates alternatively activated macrophage/microglia polarization and promotes functional recovery after crush spinal cord injury in rats." *Scientific Reports* 7 (1):620.

Song, Sheng, Feifan Zhou, and Wei R. Chen. 2012. "Low-level laser therapy regulates microglial function through Src-mediated signaling pathways: implications for neurodegenerative diseases." *Journal of Neuroinflammation* 9 (1):1-17. doi: 10.1186/1742-2094-9-219.

Souza, N. H. C., P. T. Marcondes, R. Albertini, R. A. Mesquita-Ferrari, K. P. S. Fernandes, and F. Aimbire. 2014. "Low-level laser therapy suppresses the oxidative stress-induced glucocorticoids resistance in U937 cells: Relevance to cytokine secretion and histone deacetylase in alveolar macrophages." *Journal of Photochemistry and Photobiology B: Biology* 130:327-336. doi: 10.1016/j.jphotobiol.2013.12.010.

Sun, Tao, Shaoming Mai, David Norton, John W Haycock, Anthony J Ryan, and Sheila Macneil. 2005. "Self-organization of skin cells in three-dimensional electrospun polystyrene scaffolds." *Tissue engineering* 11 (7-8):1023-1033.

Suzuki, Ryoichi, and Kazuo Takakuda. 2016. "Wound healing efficacy of a 660-nm diode laser in a rat incisional wound model." *Lasers in Medical Science* 31 (8):1683-1689. doi: 10.1007/s10103-016-2038-0.

Svensson, Carl-Magnus, Anna Medyukhina, Ivan Belyaev, Naim Al-Zaben, and Marc Figge. 2017. "Untangling cell tracks: Quantifying cell migration by time lapse image data analysis." *Cytometry Part A*. doi: 10.1002/cyto.a.23249.

Svensson, Carl-Magnus, Anna Medyukhina, Ivan Belyaev, Naim Al-Zaben, and Marc Figge. 2017. "Untangling cell tracks: Quantifying cell migration by time lapse image data analysis." *Cytometry Part A*. doi: 10.1002/cyto.a.23249.

Szeto, Hazel H, Shaoyi Liu, Yi Soong, Dunli Wu, Shaun F Darrah, Feng-Ying Cheng, Zhihong Zhao, Michael Ganger, Clara Y Tow, and Surya V Seshan. 2011. "Mitochondria-targeted peptide accelerates ATP recovery and reduces ischemic kidney injury." *Journal of the American Society of Nephrology* 22 (6):1041-1052.

Tan, B. H., C. Meinken, M. Bastian, and H. Bruns. 2006. "Macrophages acquire neutrophil granules for antimicrobial activity against intracellular pathogens." *The Journal of …*.

Taneja, Ravi, Jean Parodo, Song Hui Jia, Andras Kapus, Ori D Rotstein, and John C Marshall. 2004. "Delayed neutrophil apoptosis in sepsis is associated with maintenance of mitochondrial transmembrane potential and reduced caspase-9 activity." *Critical care medicine* 32 (7):1460-1469.

Tarlowe, Michael H, KB Kannan, Kiyoshi Itagaki, John M Adams, David H Livingston, and Carl J Hauser. 2003. "Inflammatory chemoreceptor cross-talk suppresses leukotriene B4 receptor 1-mediated neutrophil calcium mobilization and chemotaxis after trauma." *The Journal of Immunology* 171 (4):2066-2073.

Tchanque-Fossuo, Catherine N, Derek Ho, Sara E Dahle, Eugene Koo, Chin-Shang Li, R Rivkah Isseroff, and Jared Jagdeo. 2016. "A systematic review of low-level light therapy for treatment of diabetic foot ulcer." *Wound Repair and Regeneration* 24 (2):418-426.

Thomas, A, KG Harding, and K Moore. 2000. "Alginates from wound dressings activate human macrophages to secrete tumour necrosis factor-α." *Biomaterials* 21 (17):1797-1802.

Thompson, Robert W, Dennis R Holmes, Renato A Mertens, SHIXIONG Liao, MD Botney, RP Mecham, HG Welgus, and WC Parks. 1995. "Production and localization of 92-kilodalton gelatinase in abdominal aortic aneurysms. An elastolytic metalloproteinase expressed by aneurysm-infiltrating macrophages." *The Journal of clinical investigation* 96 (1):318-326.

Tunér, Jan. 2015. "The Laser Wound Healing Contradiction." *Photomedicine and laser surgery* 33 (6). doi: 10.1089/pho.2015.3905.

Tunér, Jan, and Lars Hode. 1998. "It's all in the parameters: a critical analysis of some well-known negative studies on low-level laser therapy." *Journal of clinical laser medicine & surgery* 16 (5):245-248.

Ushio-Fukai, Masuko. 2009. "Compartmentalization of redox signaling through NADPH oxidase–derived ROS." *Antioxidants & redox signaling* 11 (6):1289-1299.

Vaghardoost, Reza, Mahnoush Momeni, Nooshafarin Kazemikhoo, Soheila Mokmeli, Mostafa Dahmardehei, Fereshteh Ansari, Mohammad Nilforoushzadeh, Parisa joo, Sara Abadi, Soheila Gharagheshlagh, and Saeed Sassani. 2018. "Effect of low-level laser therapy on the healing process of donor site in patients with grade 3 burn ulcer after skin graft surgery (a randomized clinical trial)." *Lasers in Medical Science*:1-5. doi: 10.1007/s10103-017-2430-4.

van Breugel, Hans H. F. I., and Dop P. R. Bär. 1992. "Power density and exposure time of He-Ne laser irradiation are more important than total energy dose in photo-biomodulation of human fibroblasts in vitro." *Lasers in Surgery and Medicine* 12 (5):528-537. doi: 10.1002/lsm.1900120512.

Varga, Zoltan V, Csaba Matyas, Katalin Erdelyi, Resat Cinar, Daniela Nieri, Andrea Chicca, Balazs Tamas Nemeth, Janos Paloczi, Tamas Lajtos, and Lukas Corey. 2017. "β-Caryophyllene protects against alcoholic steatohepatitis by attenuating inflammation and metabolic dysregulation in mice." *British journal of pharmacology*.

Vasilenko, Tomáš, Martin Slezák, Ivan Kováč, Zuzana Bottková, Ján Jakubčo, Martina Kostelníková, Zoltán Tomori, and Peter Gál. 2010. "The effect of equal daily dose achieved by different power densities of low-level laser therapy at 635 and 670 nm on wound tensile strength in rats: a short report." *Photomedicine and laser surgery* 28 (2):281-283.

Vazquez, Alexei, Jiangxia Liu, Yi Zhou, and Zoltán N Oltvai. 2010. "Catabolic efficiency of aerobic glycolysis: the Warburg effect revisited." *BMC systems biology* 4 (1):58.

Vincent, William JB, Elizabeth A Harvie, John-Demian Sauer, and Anna Huttenlocher. 2017. "Neutrophil derived LTB4 induces macrophage aggregation in response to encapsulated Streptococcus iniae infection." *PloS one* 12 (6):e0179574.

Wahl, Sharon M, Denise A Hunt, Lalage M Wakefield, Nancy McCartney-Francis, Larry M Wahl, Anita B Roberts, and Michael B Sporn. 1987. "Transforming growth factor type beta induces monocyte

chemotaxis and growth factor production." *Proceedings of the National Academy of Sciences* 84 (16):5788-5792.

Walker, Steven L., Junko Ariga, Jonathan R. Mathias, Veena Coothankandaswamy, Xiayang Xie, Martin Distel, Reinhard W. Köster, Michael J. Parsons, Kapil N. Bhalla, Meera T. Saxena, and Jeff S. Mumm. 2012. "Automated Reporter Quantification In Vivo: High-Throughput Screening Method for Reporter-Based Assays in Zebrafish." *PloS one* 7 (1). doi: 10.1371/journal.pone.0029916.

Walters, Kevin B., Julie M. Green, Jill C. Surfus, Sa Yoo, and Anna Huttenlocher. 2010. "Live imaging of neutrophil motility in a zebrafish model of WHIM syndrome." *Blood* 116 (15). doi: 10.1182/blood-2010-03-276972.

Wang, Hong-Tao, Jin-Qiu Yuan, Bin Zhang, Mao-Long Dong, Chen Mao, and Dahai Hu. 2017. "Phototherapy for treating foot ulcers in people with diabetes." *wiley*. doi: 10.1002/14651858.CD011979.pub2.

Wang, Yijie, Mandy M. Zeigler, Gregory K. Lam, Melissa G. Hunter, Tim D. Eubank, Valery V. Khramtsov, Susheela Tridandapani, Chandan K. Sen, and Clay B. Marsh. 2007. "The Role of the NADPH Oxidase Complex, p38 MAPK, and Akt in Regulating Human Monocyte/Macrophage Survival." *American Journal of Respiratory Cell and Molecular Biology* 36 (1):68-77. doi: 10.1165/rcmb.2006-0165OC.

Wellen, Kathryn E, Georgia Hatzivassiliou, Uma M Sachdeva, Thi V Bui, Justin R Cross, and Craig B Thompson. 2009. "ATP-citrate lyase links cellular metabolism to histone acetylation." *Science* 324 (5930):1076-1080.

Wellen, Kathryn E, and Gökhan S Hotamisligil. 2005. "Inflammation, stress, and diabetes." *The Journal of clinical investigation* 115 (5):1111-1119.

West, A Phillip, Igor E Brodsky, Christoph Rahner, Dong Kyun Woo, Hediye Erdjument-Bromage, Paul Tempst, Matthew C Walsh, Yongwon Choi, Gerald S Shadel, and Sankar Ghosh. 2011. "TLR signalling augments macrophage bactericidal activity through mitochondrial ROS." *Nature* 472 (7344):476-480.

Wetzler, C., H. Kämpfer, B. Stallmeyer, J. Pfeilschifter, and S. Frank. 2000. "Large and sustained induction of chemokines during impaired wound healing in the genetically diabetic mouse: prolonged persistence of neutrophils and macrophages during the late phase of repair." *The Journal of investigative dermatology* 115 (2):245-253. doi: 10.1046/j.1523-1747.2000.00029.x.

Woodruff, L. D., and Bounkeo - J. M. laser surgery. 2004. "The efficacy of laser therapy in wound repair: a meta-analysis of the literature." *… and laser surgery*. doi: 10.1089/1549541041438623.

Wu, Shengnan, Da Xing, Xuejuan Gao, and Wei R. Chen. 2009. "High fluence low-power laser irradiation induces mitochondrial permeability transition mediated by reactive oxygen species." *Journal of Cellular Physiology* 218 (3):603-611. doi: 10.1002/jcp.21636.

Wu, Zu-Hui, Yu Zhou, Ji-Yao Chen, and Lu-Wei Zhou. 2010. "Mitochondrial signaling for histamine releases in laser-irradiated RBL-2H3 mast cells." *Lasers in Surgery and Medicine* 42 (6):503-509.

Wyllie, Andrew H, JF Ro Kerr, and AR Currie. 1980. "Cell death: the significance of apoptosis." In *International review of cytology*, 251-306. Elsevier.

Wynn, Thomas A., Ajay Chawla, and Jeffrey W. Pollard. 2013. "Macrophage biology in development, homeostasis and disease." *Nature* 496 (7446):445-455. doi: 10.1038/nature12034.

Yeo, Changmin, Heesung Kang, Hunjeong Park, and Byungjo Jung. 2011. "Comparison of various methods to enhance laser photon density in soft tissue: tissue temperature, laser pulse modulation, glycerol, and their combination." *spie*:788306. doi: 10.1117/12.874490.

Yoo, Sa, Taylor W. Starnes, Qing Deng, and Anna Huttenlocher. 2011. "Lyn is a redox sensor that mediates leukocyte wound attraction in vivo." *Nature* 480 (7375). doi: 10.1038/nature10632.

Young, Steve, Peter Bolton, Mary Dyson, Wil Harvey, and Costas Diamantopoulos. 1989. "Macrophage responsiveness to light therapy." *Lasers in Surgery and Medicine* 9 (5):497-505. doi: 10.1002/lsm.1900090513.

Yu, W., J. O. Naim, M. McGowan, and Ippolito - K. and …. 1997. "Photomodulation of oxidative metabolism and electron chain enzymes in rat liver mitochondria." *Photochemistry and …*. doi: 10.1111/j.1751-1097.1997.tb03239.x.

Zhang, Q., M. Raoof, Y. Chen, Y. Sumi, T. Sursal, and Junger - W. Nature. 2010. "Circulating mitochondrial DAMPs cause inflammatory responses to injury." *Nature*.

Zhang, Ruilong, Jun Zhao, Guangmei Han, Zhengjie Liu, Cui Liu, Cheng Zhang, Bianhua Liu, Changlong Jiang, Renyong Liu, Tingting Zhao, Ming-Yong Y. Han, and Zhongping Zhang. 2016. "Real-Time Discrimination and Versatile Profiling of Spontaneous Reactive Oxygen Species in Living Organisms with a Single Fluorescent Probe." *Journal of the American Chemical Society* 138 (11). doi: 10.1021/jacs.5b12848.

Zhang, Yan, Swati Choksi, Kun Chen, Yelena Pobezinskaya, Ilona Linnoila, and Zheng-Gang Liu. 2013. "ROS play a critical role in the differentiation of alternatively activated macrophages and the occurrence of tumor-associated macrophages." *Cell research* 23 (7):898-914.

Zhou, Rongbin, Amir S. Yazdi, Philippe Menu, and Jürg Tschopp. 2010. "A role for mitochondria in NLRP3 inflammasome activation." *Nature* 469 (7329):221. doi: 10.1038/nature09663.

Zorov, Dmitry B, Magdalena Juhaszova, and Steven J Sollott. 2006. "Mitochondrial ROS-induced ROS release: an update and review." *Biochimica et Biophysica Acta (BBA)-Bioenergetics* 1757 (5-6):509-517.

Zou, Kelly H., Simon K. Warfield, Aditya Bharatha, Clare M. C. Tempany, Michael R. Kaus, Steven J. Haker, William M. Wells, Ferenc A. Jolesz, and Ron Kikinis. 2004. "Statistical validation of image segmentation quality based on a spatial overlap index1 scientific reports." *Academic Radiology* 11 (2):178-189. doi: 10.1016/s1076-6332(03)00671-8.

APPENDICES

Appendix A

SUPPORTING TABLES & FIGURES

TABLE VII. USER-DEFINED PAREMETERS AND THEIR CORRESPONDING FUNCTIONALITIES IN ***ZIRMI*** TO EXECUTE AN IMAGE ANALYSIS

User Input	Default	Module	Functionality in *Zirmi*
Minutes Post Injury (MPI)	30 minutes	1	initial image time stamp in reference to injury; used to standardize time points across different imaging batches
Sampling Frequency	1 minute/frame	1	the rate at which images are taken; used to standardize time points across different imaging batches
Lateral Resolution	1.64 µm / pixel	1	used to compute quantitative measures
Z-stack resolution	10 µm	1	used to compute quantitative measures
Bits per pixel (BPP)	16	1	Bit depth; used to compute quantitative measures
Parameter 1	Otsu value	2	used to threshold pixel intensities for image segmentation
Parameter 2	NA	2	outline of wound perimeter
Parameter 3	65 µm	2	radial distance extends from wound perimeter; used to reproduce wound region of interest
Parameter 4	NA	2	outline of background regions
Parameter 5	70%	3	a percent used to select cell tracks based on distinguishable centroid positions relative to time domain
Parameter 6	0.9 µm		used to threshold cell

			movements as static
Parameter 7	NA	3	used to outline a zero position, S_o position; epicenter of wound
Parameter 8	NA	3	defines spatial domain, S1
Parameter 9	150 µm	3	defines the successive spatial domain radial extensions to define S2, S3, and S4
Parameter 10	NA	4	defines central directory used to save databases and visualizations
N/A, Not applicable		*Zirmi* is opensource permitting customization	

TABLE VIII. COMPARISION OF SINGLE WOUNDED ZEBRAFISH MACROPHAGE TEMPORAL SPEED AND STATIC RATIO AVERAGE

Time frame [min]	Velocity [µm /min]	Respective P value	Static Ratio (0 to 1)	Respective P value
	Interval		***Interval***	
Zirmi 30-59, (Interval 1, Z-I)	3.03 ± 1.2	*vs. Z-II, **p=0.009 vs. Z-III, ***p=0.0009*	0.43 ± 0.37	*vs. Z-II, n.s., p=0.14 vs. Z-III, *p=0.01*
Zirmi 60-89 (Interval II, Z-II)	4.00 ± 2	*vs. Z-III, *p=0.03,*	0.35 ± 0.35	*vs. Z-III, n.s. p=0.1*
Zirmi 90-120 (Interval III, Z-III)	5.08 ± 1.5	*vs. PhagoSight *p=0.01*	0.16 ± 0.13	*vs. PhagoSight 30-120 ***p=0.0004*
	Cumulative		***Cumulative***	
PhagoSight 30-120	4.01 ± 1.77	*vs. Z-I, **p=0.004 vs. Z-II, n.s, p=0.9*	0.40 ± 0.39	*vs. Z-I, n.s. p=0.96 vs. Z-II,n.s. p=0.6*
Zirmi 30-120 (Z -I,II,III)	4.02 ± 1.33	*vs. PhagoSight 30-120, n.s. p=0.34*	0.32 ± 0.26	*vs. PhagoSight t30-120, n.s. p=0.42*

Zirmi 30-59, data taken during the interval of 30-59 minutes, *Zirmi* 60-89 reflects the 60-89 minute interval, *Zirmi* 90-120 reflects 90-120 minute interval. *PhagoSight* 30-120 the 30-120 minute interval as determined by the *PhagoSight* software
n.s., Not Significant, Wilcoxon signed-rank test (*p<0.05,* *p<0.01, ***p<0.001, n.s. > 0.05);

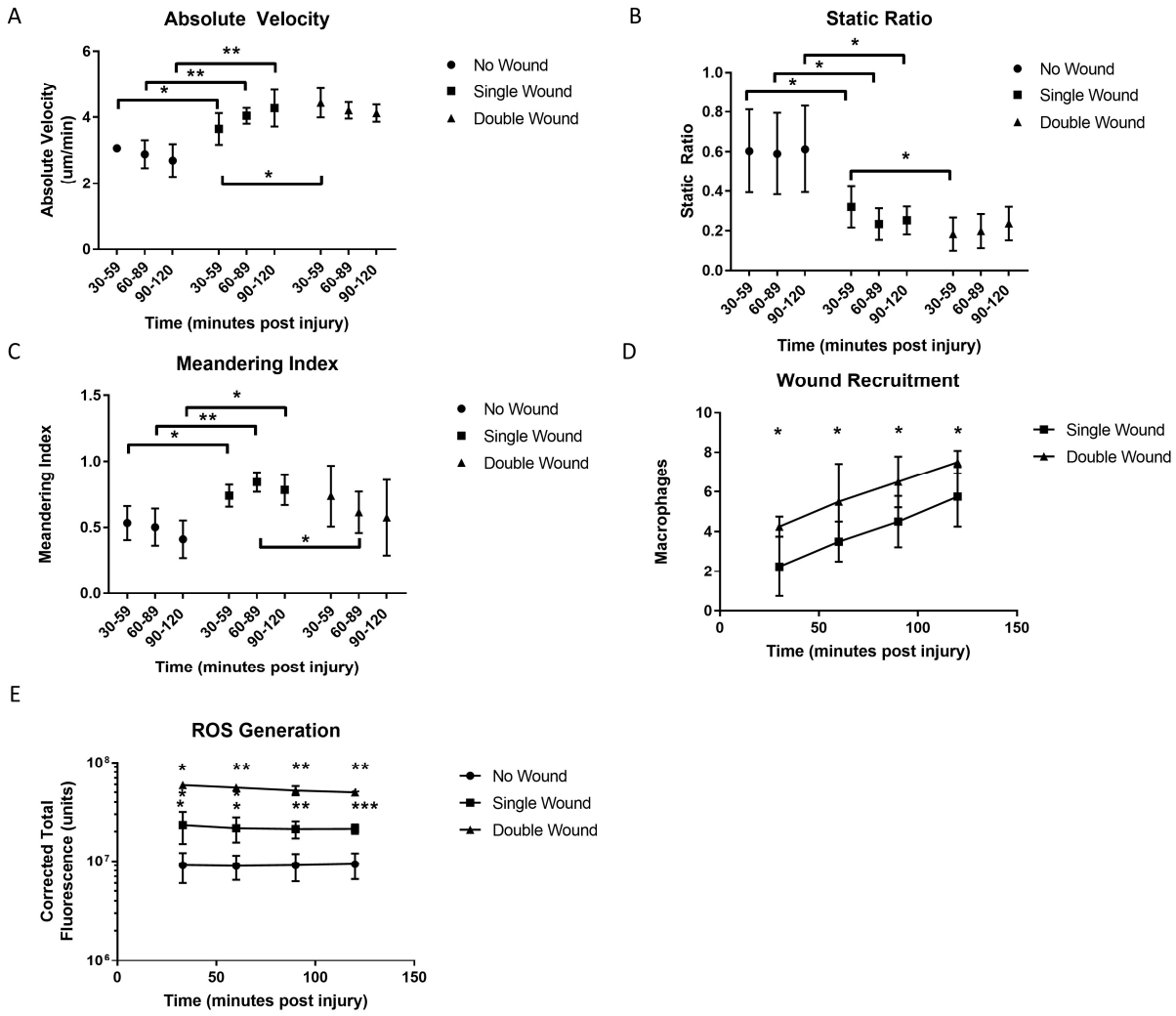

Figure 12. Wound severity comparative analysis. Macrophage velocities (A), static ratios (B), and meandering (C) at three intervals: 30-59, 60-89, and 90-120 minutes post injury in unwounded, singly wounded, and doubly wounded fins. Macrophage cumulative wound recruitment in fish with single wounds (D) was compared to those with double wounds; ROS generation shown as Corrected Total Fluorescence (CTF) in unwounded fish (n=4) was compared to singly wounded (n=4) fish, and singly wounded CTF was compared to doubly wounded (n=3) fish at user defined time points (E). All values are shown as mean ± SD in GraphPad, Prism.

Appendix B

SUPPORTING MATLAB SCRIPTS

SCRIPT 1

```
%   Zirmi Source Information can be found at:
%   <https://github.com/ADParedes/Zirmi>
%   Written By: Andre Daniel Paredes | email: andre.paredes@ymail.com
%   MATLAB Source Information can be found at:
%   <https://www.mathworks.com/help/images/image-analysis.html>
%   Description:  Single Image Processing Workflow commonly performed through available MATLAB tool. Requires %    manual modifications of thresholding and morphological function values per image.
Read Image
bytes = 2^8-1;
I = im2uint8(fluorescent_fish);
%Adjust Image to Prepare for Image Segmentation
background              = imopen(I,strel('disk',15));
I2                      = I - background;
I3                      = imadjust(I2);
figure                  ();imshow(I3);
%Binary Version
close all
% Step 2. Detect entire Fish Tail
[~, threshold]      = edge(I, 'sobel');
fudgeFactor         = .5;
BWs                 = edge(I,'sobel', threshold * fudgeFactor);
 figure(), imshow(BWs), title('binary gradient mask');
% Step 3. Dilate the Image
se90                = strel('line', 3, 90);
se0                 = strel('line', 3, 0);
BWsdil              = imdilate(BWs, [se90 se0]);
% figure(), imshow(BWsdil), title('dilated gradient mask');
% Step 4. Fill interior Gaps
BWdfill             = imfill(BWsdil,'holes');
% figure(), imshow(BWdfill);title('binary image with filled holes');
% Step 5. Close objects
BW2                 = bwareaopen(BWdfill, 1000);
% figure(), imshow(BW2), title('clear background objects');
% Step 6. Smoothen Objects
seD                 = strel('diamond',1);
BWfinal             = imerode(BW2,seD);
BWfinal             = imerode(BWfinal,seD);
BWfinal             = bwareaopen(BWfinal,1000);
figure, imshow(BWfinal), title('segmented fish image');
```

```
%Outline Original Image
BWoutline          = bwperim(BWfinal);
thickBWoutline     = bwmorph(BWoutline,'thicken',1);
Segout             = I;
Segout(thickBWoutline)   = bytes;
B                  = imoverlay(I,thickBWoutline,[1 1 0]);
figure, imshow(B), title('outlined original image');
%Analysis of Objects in Image
areaROI            = sum(sum(BWfinal));
MeanPixelIntensity  = sum(sum(uint8(BWfinal).*I))/areaROI;
cc                 = bwconncomp(BWfinal,4);
```

Script 1 Description: Example of a single image processing pipeline commonly performed through available MATLAB tools; Requires custom user-defined modifications of thresholding and morphological function values per image.

SCRIPT 2

```
%   Zirmi Source Information can be found at:
%   <https://github.com/ADParedes/Zirmi>
%   Written By: Andre Daniel Paredes | email: andre.paredes@ymail.com
%   Description: This uses “mindthegap” function incorporated into Zirmi as
%   a means to reproduce a wound region, acquire raw pixel intensity values, and eliminate
confounding
%   fluorescence within the wound gap that is difficult and time consuming
%   to perform manually.
Read Image
bytes = 2^8-1;
I = im2uint8(fluorescent_fish);
Adjust Image to Prepare for Image Segmentation
background              = imopen(I,strel('disk',15));
I2                      = I - background;
I3                      = imadjust(I2);
Binary Version
close all
% Step 2. Detect entire Fish Tail
[~, threshold]      = edge(I, 'sobel');
fudgeFactor         = .5;
BWs                 = edge(I,'sobel', threshold * fudgeFactor);
% Step 3. Dilate the Image
se90                = strel('line', 3, 90);
se0                 = strel('line', 3, 0);
BWsdil              = imdilate(BWs, [se90 se0]);
% Step 4. Fill interior Gaps
BWdfill             = imfill(BWsdil,'holes');
% Step 5. Close objects
BW2                 = bwareaopen(BWdfill, 1000);
% Step 6. Smoothen Objects
seD                 = strel('diamond',1);
BWfinal             = imerode(BW2,seD);
BWfinal             = imerode(BWfinal,seD);
BWfinal             = bwareaopen(BWfinal,1000);
Outline Original Image
BWoutline           = bwperim(BWfinal);
thickBWoutline      = bwmorph(BWoutline,'thicken',1);
Segout              = I;
Segout(thickBWoutline)   = bytes;
B                   = imoverlay(I,thickBWoutline,[1 1 0]);
% figure, imshow(B), title('outlined original image');
Clean and Define
bytes       = 2^8-1;
i           = 1;
[ix,iy]     = size(I);
```

```
diameter    = 30;
bw          = BWfinal;
Draw Circles
disp('Trace wound perimeter NOTE 1. Extend line to open water 2. Do not make a closed shape')
disp('Using "rice.png" example make a large open triangle in the middle of the figure to see how
this function works');
f=figure(1);imagesc(B); title('Trace Wound Perimeter');
[x, y]          = getline(f);
bw_woundgap     = poly2mask(x,y,ix,iy);
exist_woundgap  = sum(sum(bw_woundgap));
if exist_woundgap>0
   exist_woundgap          = 1;
   bw_woundgap_outline     = bwperim(bw_woundgap);
   figure(2);
   Segout_woundgap         = imoverlay(I,bw_woundgap,[1 0 0]);
   imshow(Segout_woundgap);
else
end;
Calculate the Metrics
%--find how many points have been established
num_points=length(x);
d       =(0);
n       =(0);
x1      = 0;
y1      = 0;
%-circle centers
Arr_xy  ={0};
Arr_x   ={0};
Arr_y   ={0};
%-masks
CMASK={0}; %  = combo;
RCMASK={0};%  = raw_combo;
for i=1:(num_points-1)
   xy          = 0; % saves two vertical arrays of centers of circles
   x1          = x(i);
   y1          = y(i);
   % Considering for loop condition this is impossible
   if i == num_points
      x2 = x(1);
      y2 = y(1);
   else
      x2 = x(i+1);
      y2 = y(i+1);
   end;
   f=figure(2+i);imagesc(I);
   hold on
```

```
plot(x,y,'LineWidth',2,'Color','r')
plot(x1,y1,'c*','LineWidth',2)
plot(x2,y2,'y*','LineWidth',2)
hold on
% calculate metrics
d(i)       = pdist([x1,y1;x2,y2]);
radius     = diameter/2;
n          = d(i);
num        = round(n); %number of circle points per line
%--figure out the line equation for the one drawn
coefficients= polyfit([x1, x2], [y1, y2], 1);
a          = coefficients (1);
b          = coefficients (2);
 xmin      = min(x(i:i+1));
 xmax      = max(x(i:i+1));
 ymin      = min(y(i:i+1));
 ymax      = max(y(i:i+1));
 funct     = linspace(xmin,xmax, num); % Adapt n for resolution of graph
fun_y      = a*funct+b;
xy         = [funct',fun_y'];
 Arr_xy{i}  = xy;
 Arr_x{i}   = funct;
 Arr_y{i}   = fun_y;
%--Presets for next for loop ------------------------------------%
 lens      = length(funct);
 Img_cmask  = {0};
 x_j       = 0;
 y_j       = 0;
%--For Loop for Establishing Circles ----------------------------%
 for j=1:lens
   %---showing purposes
   x_j              = funct(j);
   y_j              = fun_y(j);
   THETA              = linspace(0, 2 * pi, 1000);
   RHO              = ones(1, 1000) * radius;
   [X Y]            = pol2cart(THETA, RHO);
   xoc              = X + x_j;
   yoc              = Y + y_j;
   plot(xoc, yoc, '-','linewidth',2,'color','g')%'color',0.5.*rand(1,3));
   %---masking purposes
   cx               = x_j  ;
   cy               = y_j;
   r                = radius;
   [xm,ym]            = meshgrid(-(cx-1):(ix-cx),-(cy-1):(iy-cy));
   c_mask           =((xm.^2+ym.^2)<=r^2);
   cc_mask           = c_mask & bw; %corrected circle mask to be inside fish
```

```
        MaskPixelNum       = sum(sum(cc_mask));
        MaskPixelIntensity  = sum(sum(uint8(cc_mask).*I))/MaskPixelNum;
        mmpi(j)            = MaskPixelIntensity;
        Img_cmask{j}    = cc_mask;
        if j==1
           raw_combo   = c_mask
           combo       = cc_mask;
        else
           raw_combo   = raw_combo + c_mask;
           raw_combo   = im2bw(raw_combo);
           combo       = combo + cc_mask;
           combo       = im2bw(combo);
        end;
        Img_combomask{j}    = combo;
        hold on
    end;
    CMASK{i}    = combo;
    RCMASK{i}   = raw_combo;

end;
%Final Image
%After you found a, You can get b from your equation y=a*x+b
%Creating Circle Mask BW
%-Raw BW before filtering
raw_blank   = I;
blank       = BWfinal;
 for kk=1:i
     if kk==1
        %--ultimate combo
        ultimate_mask      = CMASK{kk};
        %--ultimate raw
        ultimateraw_mask   = RCMASK{kk};
     else
        %--ultimate combo
        ultimate_mask      = ultimate_mask + CMASK{kk};
        ultimate_mask      = im2bw(ultimate_mask);
        %--ultimate raw
        ultimateraw_mask   = ultimateraw_mask + RCMASK{kk};
        ultimateraw_mask   = im2bw(ultimateraw_mask);
     end;
     blank      = imoverlay(blank,bwperim(CMASK{kk}),0.3.*rand(1,3));
     raw_blank  = imoverlay(raw_blank,bwperim(RCMASK{kk}),0.6.*rand(1,3));
 end;
RUSegout    = imoverlay(I,bwperim(ultimateraw_mask),[1 1 1]);
USegout     = imoverlay(I,bwperim(ultimate_mask),[1 1 0]);
figure(); imshow(RUSegout); title('Raw Mask'); hold on
```

```
plot(x,y,'LineWidth',2,'Color','r')
hold off
figure(); imshow(USegout); title('Fish Mask'); hold on
plot(x,y,'LineWidth',2,'Color','r')
hold off
Mind the Wound Gap
disp('This is where we need to eliminate fluorescence debris in the wound gap')
   if exist_woundgap>0
      exist_woundgap         = 1;
      bwfinal = ~ultimate_mask | bw_woundgap;
      bwfinal = ~bwfinal;
   else
   end;
FinalSegout     = imoverlay(BWfinal,bwperim(bwfinal),[1 0 1]);
figure(); imshow(FinalSegout); title('Fish Mask'); hold on
plot(x,y,'LineWidth',2,'Color','r')
hold off
figure(); imshow(bwfinal); title('only regions of interest'); hold on
Analysis of Objects in Image
areaROI            = sum(sum(bwfinal));
MeanPixelIntensity  = sum(sum(uint8(bwfinal).*I))/areaROI;
```

Script S2 Description: Demonstrates the V-shaped image segmentation functionality within *Zirmi* as a reproducible means to reproduce acquire raw pixel intensity values and eliminate confounding fluorescence automatically within the wound gap. This is difficult and time consuming to perform manually.

SCRIPT 3

```
%  Zirmi Source Information can be found at:
%  <https://github.com/ADParedes/Zirmi>
%  Written By: Andre Daniel Paredes | email: andre.paredes@ymail.com
%  Matlab Source Information can be found at:
%  <https://www.mathworks.com/help/images/image-analysis.html>
%  Description:  Manual tracing technique to image segment wound region and acquire
%  raw pixel intensity
Read Image
bytes = 2^8-1;
I = im2uint8(fluorescent_fish);
Manually Image Segment Wound Region
disp          ('Outline the Wound Region')
close all; imagesc(I); colormap('gray'); movegui('northeast');title('ROS REGION');
RosRegion      = roipoly();
imshow(RosRegion)
MaskPixelNum       = sum(sum(RosRegion));
MaskPixelIntensity = sum(sum(uint8(RosRegion).*I))/MaskPixelNum;
display(strcat('Raw Pixel Intensity (abu):',num2str(MaskPixelIntensity)))
display(strcat('Region area (pixel^2):',num2str(MaskPixelNum)));
```

Script S3 Description: Manual tracing technique to image segment wound region and acquire raw pixel intensity

VITA

NAME:

ANDRE DANIEL PAREDES

EDUCATION:

University of Illinois-Chicago, IL (UIC) **2018 (anticipated)**
Ph.D. Richard and Loan Hill Department of Bioengineering

University of California-Irvine, CA (UCIrvine) **2010**
B.S. in Biomedical Engineering

RESEARCH EXPERIENCE:

Ph.D. Thesis-Studies of Electromagnetic Waves in Zebrafish **2016-2018**
Division of Translational Research, Transplant Biology Laboratory, UIC
Mentor and chair, Amelia Bartholomew, MD, MPH, FACS

- Developed and tested hypotheses for multiple projects on *in vivo (danio rerio)* transgenic zebrafish animal model, including: (1) 3D + t confocal imaging (2) soluble probe loading, (3) caudal fin wound assay, and (4) 635 nm CW HeNelaser irradiation
- Applied Data Vision and Data Science approaches in MATLAB to pipeline fluorescent and physical quantitative evaluations
- Established zebrafish model of single and dual tail fin wounding and reactive oxygen species quantification in real time
- Trained in the rabbit and murine models of electromagnetic radiation delivered by a LINAC source
- Applied Data Science approaches in MATLAB and R to establish predictors on whole blood evaluations of 48 hematopoietic, coagulopathic, and biochemical parameters following 6,7,8,8.5,9 and 10Gy total body radiation
- Performed quality control and assurance in key analytics, including plasma derived coagulation factors (II,V,VII,VIII,IX,X,XI, and XII) analytics and whole 4-color flow cytometric analyses of peripheral blood

Ph.D. Thesis-Studies of Live-cell Imaging **2010- 2016**
Bioengineering, Laboratory of Live-cell Imaging & Ultrafast Laser Microsurgery, UIC
Co-Mentor, Jun Cheng, Ph.D.

- Developed and tested hypotheses for multiple projects on *in vitro* J774A.1 macrophages, and *in vivo (danio rerio)* transgenic zebrafish after 1035 nm ultrafast pulse ND:YAG laser irradiation, including: (1) *vitro* phagocytosis kinetics, (2) *in vitro* and in *in vivo* oxidative stress, (3) *in vivo* wound leukocyte recruitment kinetics
- Performed laser to microscope unique set-up for 1035 nm ultrafast laser radiation, including automatically configuring robotic stage movements, 3D + t epifluorescence imaging, and laser energy deliverance via developed LabView and Visual Basic original scripts.
- Used developed digital image processing approaches for quantitative evaluations

Biophotonics Research Program - Beckman Laser Institute, CA **2009-2010**

- Developed experience with *in vitro* cell techniques including routine culturing,

transfections and fluorescent imaging
- Assisted in experimentation of cell mechanotransduction endocytosis force (pN) measurements, using 1035 nm ND:YAG laser tweezer and quad photodiode.

Undergraduate Research Program - Botvinick Laboratory, UCIrvine
2008-2009
- Developed vaterite crystals and evaluated its ability to deform and flow a material
- Tested vaterite microrheology based viscous structural rearrangements

Undergraduate Researcher -Integrated Nanosystem Research Facility, UCIrvine
2007-2008
- Performed polydimethylsiloxane PDMS synthesis and curing via photolithography etched silicon wafer.
- Performed positive pressure experiments to test microflow regulators of different conformations and consistencies to optimize a microvalve for cellular based evaluations

CONFERENCE PROCEEDINGS:

2018 RADRES, Radiation Research Society Annual Conference - *Chicago, IL*
Oral: "*Electromagnetic radiation of 3,9, or 18 Joule/cm2 fluences demonstrate a dose response effect on macrophage recruitment, directionality, tissue injury, and reduction of oxidative stress"*

2017 MHSRS, Military Health System Research Symposium - *Kissimmee, FL*
Poster: "*Low Level Light Laser Treatment Reduces Macrophage Retention and Reactive Oxygen Species Levels accelerating wound regeneration"*

2017 ATC, American Transplant Congress - *Chicago, IL*
Poster: "*Low Level Light Laser Treatment Reduces Macrophage retention and ROS Levels Following Tissue Injury"*

2016 BMES, Biomedical Engineering Society - *Minneapolis, MN*
Accepted Abstract: "*An Automated Real-time Approach for Quantifying Phagocytosis and Reactive Oxygen Species Levels*"

2015 UIC College of Medicine Research Forum - *Chicago, IL*
Poster: "*In vivo Imaging of Leukocyte Inflammatory Migration Response to Caudal Fin Wound in Larval Zebrafish* "

2014 AAAS, American Association for Advancement in Science National Conference - *Chicago, IL*
Poster: "*Macrophage photobiomodulated inflammatory activity via NIR ultrafast laser irradiation*"

2010 AAAS, American Association for Advancement in Science National Conference – *San Diego, CA*
Poster: "*Evaluation of mechanic transduction in the adhesion forces between Notch and Delta Lateral inhibition*"

2008 Society of Advancement of Hispanic/Chicano & Native Americans Science National Conference - *Salt Lake City, UT*
Poster: "*Vaterite Crystal Formation for Microrheometry with Laser Tweezers*"

2008 AAAS, American Association for Advancement in Science National Conference – *Boston, MA*,
Poster: "*Novel Polymer Based Microflow Regulator: Lab-on-a-Chip Application*"

MANUSCRIPTS:

Andre D. Paredes, David Benavidez, Jun Cheng, Steve Mango, Michael Donoghue, Amelia Bartholomew, Zebrafish automated and quantitative image analysis of in vivo macrophage kinetics and oxidative stress time-lapse images. Submitted to J Biological Methods, 2018

*Andre D. Paredes, David Benavidez, Jun Cheng, Steve Mangos, Rachana Patil, Michael Donoghue, Enrico Benedetti, Amelia Bartholomew***,** *In vivo detection of photobiomodulated macrophage kinetics, oxidative stress, and wound closure within Zebrafish. Submitted to J. Photomedicine and Laser Surgery, 2018.*